Institut für Neurale Signalverarbeitung

Zentrum für Molekulare Neurobiologie Hamburg

Falkenried 94, 20251 Hamburg

Structural requirements and role of oxidoreductase features for Kvβ-mediated potassium channel inactivation

Dissertation

Zur Erlangung des Doktorgrades
des Fachbereiches Biologie
der Universität Hamburg

Vorgelegt von

Vitya Andranic VARDANYAN

Hamburg 2003

Genehmigt vom
Fachbereich Biologie der
Universität Hamburg
auf Antrag von Herrn Prof. Dr. O. PONGS
Weitere Gutachter der Dissertation:
Herr Professor Dr. M. BÖTTGER

Tag der Disputation: 24. Oktober 2003

Hamburg, den 10. Oktober 2003

Professor Dr. A. Frühwald
Dekan

TABLE OF CONTENTS

3. Results

4. Discussion

Introduction

The physiological functions of ion channels are as diverse as their kinetic properties and expression patterns in different cells and tissues (Hille 2001). In excitable cells they are responsible for the generation and propagation of action potentials (Hodgkin and Huxley 1952), for the initiation and modulation of neurotransmitter release (Meir et al., 1999) and for the excitation-contraction coupling (Nerbonne 2000). In non-excitable cells they may regulate cell volume (Niemeyer et al., 2001, Noulin et al. 2001), intracellular ionic homeostasis, cell proliferation and immune-activation (Cahalan et al., 2001).

Ion channels allow ions to cross an impermeable lipid membrane along their electrochemical gradients. The electrochemical gradient for a particular ion is a result of the non-equal distribution of this ion between intra- and extracellular medium, which is maintained by active transport mechanisms, and of the actual membrane potential. Ion channels, under certain circumstances, open their specific permissive pathway - a process known as gating (Larsson 2002, Horn 2002). Binding of ligands, like neurotransmitters, nucleotides, hormones or even ions to a specific site of the protein may cause gating.

Voltage-gated ion channels have the unique property to sense changes in membrane potential. These proteins, responsible for membrane voltage controlled electric signaling, include voltage-gated potassium (Kv, Eag, BK, KCNQ), sodium (Nav), calcium (Cav) and chloride (ClC) channels. In addition to biophysical and structural similarities within the family, all family members are highly selective to K^+, Na^+, Ca^{2+} and Cl^-, respectively.

Potassium channels are a vast group of proteins (Jan and Jan 1997) conducting potassium ions across the membrane essentially barrierless, at rates of about 10^8 ions per second and with selectivity of 10^4 times preferring K^+ over Na^+ (Berneche and Roux 2001). They play a crucial role in excitable cells by determining the resting membrane potential, slope and duration of action

potentials as well as their frequencies and propagation patterns in neurons (Hille 2001, Pongs 1996). Potassium channels are also essential for modulation of neurotransmitter release and synaptic plasticity (Johnson et al., 2000, Watanabe et al., 2002) and for excitation-contraction coupling in heart (Nerbonne 2000) and vascular smooth muscle (Plüger et al., 2000,). They modulate exocytosis (Kurachi and Ishii 2003), cell proliferation and cell volume (Dubois and Rouzaire-Dubois 1993). Mutations in potassium channels, leading to their malfunctions, are usually associated with diseases in human brain, heart, pancreas and kidney (Weinreich and Jentsch 2000, Cooper and Jan 1999).

More than 66 different genes have been identified, which code for potassium channel proteins. It is assumed, that most of them are able to form functional potassium channels (Packer et al., 2000). Functional diversity of potassium channels is enhanced further by heteromultimerization, by association with their auxiliary subunits and modulation by different intracellular factors (Pongs 1999).

1.1 Structure of potassium channels

Voltage-gated K^+ (Kv) channels are multimeric protein complexes consisting of principal α subunits associated with auxiliary β or γ subunits. Four Kvα subunits, each consisting of 6 putative transmembrane domains (S1 to S6), tetramerise to form a functional channel (MacKinnon 1991, Li et al., 1994). Crystallization of the bacterial potassium channel KcsA revolutionized our understanding of potassium channel structure (Doyle et al., 1998). It revealed basic structural principles for selectivity and conductivity of all potassium channels. The crystal structure of KcsA has revealed, that the ion conducting pathway (pore) is formed by four S6 domains from different subunits, cradling a highly conserved sequence motif TVG(Y/F)G, the "signature sequence" (Heginbotham et al., 1992) of the potassium channel, at the outer part of the pore. The pore at the

center of the channel becomes wider (cavity), then it narrows again at the structure called “bundle crossing” (Figure 1) at the cytoplasmic side. Due to sequence similarity, it is assumed, that all potassium channels share a similar structure of the pore. In Shaker-related potassium channels, it is assumed, that S6 α-helix is interrupted by a conserved glycine residue, which makes the structure the wider in cytoplasmic side than in KcsA (del Camino et al., 2000). The crystal structure of a K+ channel from *Methanobacter thermoautotrophicum* MthK in its open state suggests, that another conserved glycine residue serves as a hinge to open the channel (Jiang et al., 2002a).

The first four transmembrane segments S1-S4 are thought to function as a membrane voltage sensor (Seoh et.al., 1996, Horn 2002). The S4 transmembrane domain contains conserved positively charged residues, which move in the membrane electric field upon depolarization, leading to a series of conformational changes and opening of the channel gate (Lu et al., 2002, Yifrach and MacKinnon 2002, Bezanilla 2002). The role of the segments S1-S3 is still controversial (Sato et al., 2003). They do contain conserved acidic residues (Keynes and Elider 1999) that might interact with basic residues in S4 and play a role in the channel activation process (Papazian et al., 1995).

Binding studies of the N-terminal domains of Kv1, Kv2, Kv3 and Kv4 α subunits determined a region known as NAB domain (Xu et al., 1995), named also T1 or tetramerization domain (Shen et al., 1993). Being highly conserved in a subfamily-specific manner, the T1 domain restricts the channel diversity by allowing heteromerization only within subfamilies. It prevents the formation of heteromeric channels between different subfamilies (Yu et al., 1996). The crystal structure of the Kv1.1 tetramerization domain revealed basic principles of tetramer formation in Kv channels (Kreusch et al., 1998).

The carboxy terminus is the most variable region of potassium channels. In KvLQT channels a carboxy terminal region serves as a multimerization domain (Schmitt et al., 2000). In inward rectifier channels (Kir) it compiles a bowl-like structure - a receptor site for binding of polyamines

and Mg^{2+} ions (Nishida and MacKinnon 2003). In large-conductance calcium-activated potassium channels (BK_{Ca}), which connect the calcium signaling pathways to membrane excitability, the carboxy-terminus is thought to mediate Ca^{2+} binding (Vergara 1998; Jiang et al., 2001b).

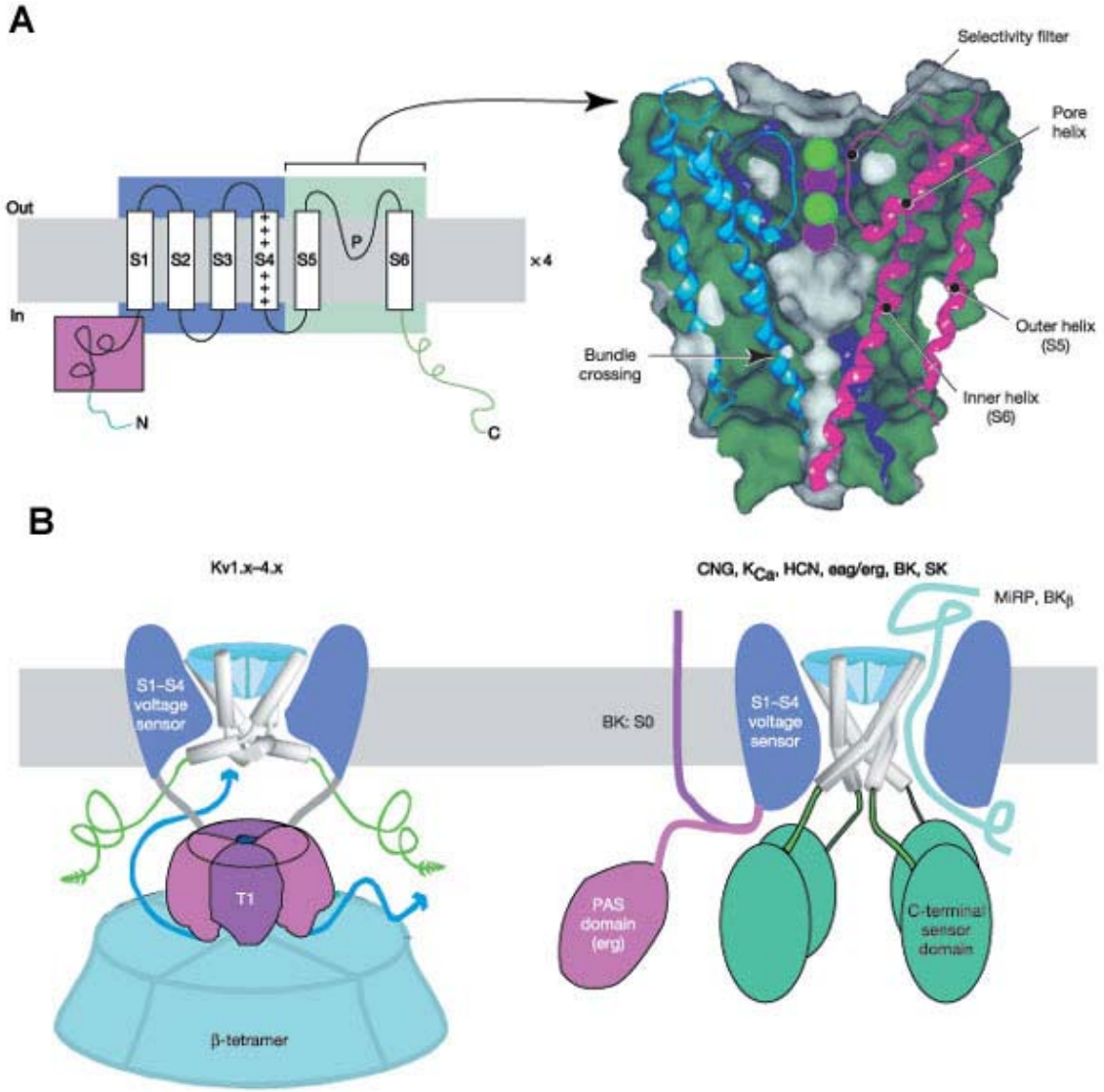

Figure 1. Summary of structural components of voltage-gated potassium channels (from Yellen, 2002).

A) Simple 2D diagram of voltage-gated potassium channels. Red coloured box shows the tetramerization domain of Kv1-Kv4 channels. The blue box marks transmembrane domains S1-S4. With the green box are indicated the pore-forming domains S5–P-loop–S6. The 3D crystal structure of KcsA, thought to be a main structural motif for all potassium channels, is shown on the right. The fourth subunit is omitted from the structure for simplicity.
B) Topological diagram of Kv channels with Kvβ subunit, represented at bottom of transmembrane domains (cyan). The structure of the C-terminus of Kv channels is largely unknown. The C-terminal regions of the channels are represented in green, S1-S4 transmembrane segments in blue. On the right a topological model of other voltage-gated potassium channels (BK, eag/erg, HCN) and their β-subunits is shown.

1.2 Inactivation of Shaker-related potassium channels

Many potassium channels have the property to enter a non-conducting state after channel activation. This process is called "inactivation". The inactivated state is different from the resting closed state of the channel in that, the channels main gate is no more a barrier for ionic flux, but the other structural elements inhibit the current flow. It is caused by at least two different mechanisms. In one case the inactivating domain plugs the ion permeation pathway by the distal N-terminus of the channel protein (Hoshi et al., 1990) or by a similar structure at the N-terminus of Kvβ subunits (Rettig et al., 1994). This process, known as a "N-type" inactivation, follows a “ball and chain” mechanism, where several amino acids from the N-terminus bind to a receptor site in the pore of the open channel (Zhou et al., 2001). In second case the channel can also enter a C-type inactivated state, usually characterized by slower kinetics of current decay in comparison to N-type inactivation. The name "C-type" inactivation originally came from C-terminal splice variants of *Shaker* channels being studied (Hoshi et al., 1991). Lately, this C-type inactivation was referred to as slow inactivation, associated with the shifting of gating charge (Loots and Isacoff 1998, Larsson and Elinder 2000). The slow inactivation of channels involving the pore region (selectivity filter) is known as P-type inactivation (Yang et al., 1997, Loots and Isacoff 1998).

N-type inactivation is characterized by following 5 main features: 1) Enzymatic or genetic removal of the N-terminus of particular Kvα (Hoshi et al., 1990) or N-terminus of associated β subunits (Rettig et al., 1994) eliminate the fast inactivation. 2) Application of peptides, corresponding to the mentioned N-terminal sequences restores the disrupted fast inactivation (Zagotta et al., 1990). 3) These synthetic peptides compete for the binding sites in the pore of channel (Murrell-Langnado and Aldrich 1993). 4) Increase of external K^+ concentration accelerates the recovery of channels from N-type inactivation (Demo and Yellen 1991). 5) N-type

inactivated channels reopen during recovery from inactivation (Ruppersberg et al., 1991, Demo and Yellen 1991).

1.3 Beta subunits of Shaker-related potassium channels

β subunits of potassium channels do not form functional channels by themselves but play an important regulatory role for Kvα subunits. Beta subunits of the Shaker-related potassium channels (Kvβ) were isolated by the sequence similarity to the protein associated with cloned α-dendrotoxin-sensitive K^+ channel from the rat brain (Scott et al., 1990, Scott et al., 1994). All presently known Kvβ subunits have a highly conserved core region, showing 62-78% primary sequence identity in this region and a variable N-terminus (Hanlon and Wallace 2002). Three different genes code Kvβ subunits. Some of these genes can be alternatively spliced, resulting Kvβ1.2 (McCormack et al., 1995) and Kvβ1.3 (England et al., 1995) splice variants. Hydropathy analysis of Kvβ subunits have shown, that they do not possess transmembrane segments, and there is no evidence for glycosilation of the protein (Scott., 1990, Rettig et al., 1994). It was proposed, that Kvβ subunits association with Kvα subunits forms an octameric channel complex with a 4α/4β stoichiometry (Parcej et al., 1992, Orlova et al., 2003), assembly of which, takes place early in biosynthesis (Nagaya and Papazian., 1997, Papazian 1999). *In vitro* expression of Kvβ subunits shows that they can form also heteromers (Xu and Li 1997).

The Kvβ interaction site in Kvα subunits was mapped to be the C-terminal part of the tetramerization domain (Sewing et al., 1996), but the details of the interaction site became only clear after co-crystallization of N-terminally truncated Kvβ2 with the T1 domain of Kv1.1. (Gulbis et al., 2000). The analysis of the Kvβ2 crystal structure has confirmed the earlier hypothesis, that Kvβ subunits are members of the oxidoreductase superfamily of enzymes, which had been

proposed previously on the basis of primary structure analysis of Kvβ subunits and Drosophila homologue, Hyperkinetic (McCormack and McCormack 1994). The structure of Kvβ2 resembles a TIM barrel motif with bound $NADP^+$ (Gulbis et al., 1999). The catalytic site, composed of conserved tyrosine, aspartic acid and lysine residues, is configured in a way, that it may allow a hydrate transfer reaction, like in other oxidoreductases. However, as yet there is no evidence for Kvβ oxidoreductase activity, and a substrate has not been yes identified either. Although abundantly expressed in the mammalian nervous system (Heinemann et al., 1995, Rhodes et al., 1997), the physiological role of Kvβ subunits is not yet clear. It was shown, that co-expression of some Kvβ subunits with certain Kv1 channels can increase the expression level of Kv1 channels (Accili et al., 1997). In addition, co-expression of Kvβ subunits may change the midpoint of voltage-dependent activation of Kv1 channels (Heinemann et al., 1996). Moreover, the association of Kvβ1 (Rettig et al., 1994) or Kvβ3 (Leicher et al., 1998) subunits with delayed rectifier Kv1 channels may produce rapidly inactivating A-type channels.

Like a Kv1.4 N-terminus, N-termini of these subunits can serve as a "ball" domain, plugging the pore of the open channel (Lee et al 1996, Morales et al; 1995, Castellino et al., 1995).

However, under certain conditions the presence of inactivating domain and its receptor site in S6 may not be sufficient to get an N-type inactivating. Kvβ-mediated inactivation may be dependent on structural determinants of Kv channels. For example, Kv1.6 possesses a small domain preventing Kvβ1.1-mediated inactivation (Röper et al., 1998). Similarly, Kv1.3 does not show fast N-type inactivation when co-expressed with Kvβ1.1 either. Kvβ-mediated N-type inactivation can be also physiologically regulated. The state of the distal N-terminal cysteine residue (C7 in Kvβ1.1) in oxidizing conditions prevents fast inactivation of Kvα (Rettig et al., 1994), whereas it allows fast inactivation in reducing conditions. The phosphorylation of the "ball"-domain may also regulate N-type inactivation of A-type channel (Antz et al., 1999).

The role of putative oxidoreductase features of Kvβ subunits in modulating the biophysical properties of Kvα/Kvβ channel complexes has been investigated.

The structural determinants for Kvα to allow Kvβ-mediated inactivation are also studied with chimeric channels composed from Kv1.2, which allows fast inactivation, and from Kv2.1, which do not interact with Kvβ subunits.

2. Materials and Methods

2.1 Molecular biology

2.1.1 Clones and vectors

All clones encoding rat Kv1α and Kvβ subunits were available at laboratory collection of clones. cDNA fragments coding for α and β subunit of channels were cloned into pcDNA3 (Invitrogen) vectors.Transient transfected of CHO and HEK 293 cells with appropriate plasmids is described below. For cRNA synthesis, corresponding clones in pAKS (Invitrogen) or pGEM-HE-Juel vectors were used. The complete sequences of used genes could be found at the NLM site with appropriate GenBank™ accession numbers shown in Table 1.

Gene name	Accession number
Rat Kv1.1	X12589
Rat Kv1.2	X17621
Rat Kv1.3	X16001
Rat Kv1.4	X16002
Rat Kv1.5	X16003
Rat Kv1.6	AJ276137
Rat Kvβ1.1	NM017303
Rat Kvβ2	NM017304
Rat Kvβ3.1	X76723

Table 1 Used clones with GenBank™ accession numbers.

2.1.2 *In Vitro* Mutagenesis

Turbo Pfu DANN proof-reading polymerase (Stratagene) was used to introduce mutations in Kvβ and Kvα subunits with PCR technique. PCR products were isolated using GFX^{TM} PCR DNA and Gel Band purification kit (Amersham Biosciences). Appropriate fragments of PCR products were cloned into corresponding vectors by restriction enzymes and T4-DNA ligase (Fermentas). Mutated channels and subunits were sequenced at the sense and anti-sense DNA strains using BigDye terminator cycle sequencing kit.

2.1.3 Kv1.2/Kv2.1 and Kvβ1.1/Kvβ3 chimeras

The overlap-PCR mutagenesis technique was used to construct the chimeric cDNA, encoding chimeric channels between rat Kv1.2 (GenBank^{TM} accession numberm X16003) and human Kv2.1 (GenBank^{TM} accession number X68302) exploring appropriate restriction sites. The chimeric channels were cloned into the pGem-He-Juel vector. cDNA sequences of the chimeric channels use are followings (numbers refer to the appropriate nucleotides in ORF of DNA encoding the channel): ChimA, 1-492 Kv1.2/570-2577Kv2.1, ChimB, 1-489 Kv1.2 / 567-1181 Kv2.1 / 1176-1254 Kv1.2 / 1266-2577 Kv2.1, ChimC, 1-843 Kv1.2 / 861- 2577 Kv2.1, ChimD, 1-1173 Kv1.2 / 1185-2577 Kv2.1, ChimE, 1-1215 Kv1.2 / 1227-2577 Kv2.1, ChimF, 1-1254 Kv1.2 / 1266-2577 Kv2.1, ChimG, 1-492 Kv1.2 / 570-954 Kv2.1 / 948-978 Kv1.2 / 990-2577 Kv2.1. Appropriate channels are illustrated in Figures 4, 5 and 7).

Kvβ1.1/Kvβ3 chimeras were made from Kvβ1.1 and Kvβ3, which were available as clones in pAKS vector. The cDNAs for the Kvβ chimeras between rat Kvβ1.1 (GenBankTM accession number X70662) and rat Kvβ3 (GenBankTM accession number X76723) were obtained

exploiting appropriate restriction enzyme sites and/or using an overlap polymerase chain reaction. The chimeric cDNAs were cloned into the pAKS vector. For the construction of the different chimeras, the following DNA fragments were joined together (note that numbers in parentheses refer to cDNA nucleotides): KvβchiA, Kvβ3.1-(1-1080) and Kvβ1.1-(1000-1546); KvβchiArev Kvβ1.1-(1-997) and Kvβ3.1-(1075-1599); KvβchiB, Kvβ3.1-(390-1260) and Kvβ1.1-(1180-1534); KvchiC, Kvβ3.1-(390-1260) and Kvβ1.1-(1180-1534); KvβchiD Kvβ3.1-(390-1380) and Kvβ1.1-(1300-1534); KvβchiE, Kvβ3.1-(390-1534) and Kvβ1.1-(1453-1534); KvβchiF, Kvβ3.1-(390-1450), Kvβ1.1-(1370-1453), and Kvβ3.1-(1535-1606); KvβchiG, Kvβ3.1-(390-1376), Kvβ1.1-(1304-1385), and Kvβ3.1-(1457-1606); KvβchiH, Kv3.1-(390-1222), Kvβ1.1-(1142-1237), Kvβ3.1-(1318-1440), Kvβ1.1-(1370-1453), Kvβ3.1-(1535-1606); KvβchiI, Kvβ3.1-(390-1222), Kvβ1.1-(1142-1270), Kvβ3.1-(1285-1440), Kvβ1.1-(1370-1453), Kvβ3.1-(1535-1606). Clone-cards of the chimeric cDNAs are attached at the end of work. The sequences of the amplified PCR fragments were verified by sequencing using BigDye terminator cycle sequencing kit (PerkinElmer life sciences), and ABI automated sequencer (PerkinElmer life sciences).

2.1.4 *In vitro* cRNA synthesis

cRNA synthesis was performed using the AMBION cRNA synthesis kit (Ambion). pcDNA3 and pGEM-He-Juel vectors possess a T7 promoter site, suitable for using the appropriate kit. AMBION cRNA synthesis kit for SP6 promoter was used to produce cRNA from genes cloned in pAKS vectors. Double stranded cDNA was linearized at 3´linearization site with appropriate restriction sites, and were purified according phenol-acetate precipitation protocol. The synthesis was done following the manufacturer's manual.

2.2 Functional expression of proteins

For patch-clamp experiments two different cell-lines were used in this work - Chinese Hamster Ovary (CHO) and Human Embryonic Kidney (HEK) 293. Xenopus oocytes were used mainly for two electrode voltage-clamp experiments. For application of synthetic peptides we used Xenopus oocytes to obtain giant patches.

2.2.1 Oocytes from *Xenopus laevis*

2.2.1.1 Isolation and maintenance of oocytes

Xenopus oocytes were first used to express the membrane receptors and channels almost two decades ago. The oocytes from Xenopus frogs are big and viable, suitable for injection of foreign cRNA and cDNA. They possess endogenous calcium sensitive chloride channels, which mediate currents in the 100-200 nA range, negligible, when Kv channels were heterologously expressed. South African clawed female frogs - *Xenopus laevis,* were purchased from NASCO (Tennessee, USA) and Kähler, (Hamburg). Only sexually mature GSH-tested females (9-14 cm) were operated to obtain oocytes. Under sterile conditions ovarian lobe of one side was surgically removed. The oocytes were washed with OR2 solution (see below). The oocyte-preparation was later incubated 4-5 hours in OR2 solution containing 3-4 mg/ml collagenase and was gently shaked. After the collagenase treatment, oocytes were carefully washed several times with OR2 solution. Stage VI and stage VII oocytes were selected and incubated in gentamicin containing solution overnight at 18^{o}C without $CO_{2.}$. cRNA injections were performed the next day.

2.2.1.2 cRNA injection into oocytes

3.5 mm capillary glass (WPI) was used to fabricate cRNA injection pipettes, using a PB-7 puller (Narishige, Japan). The pipette-tips were broken at the diameter of 10-14 μm using a MF-900 microforge (Narishige, Japan). Pipettes were "backed" for 3h at 250^{o}C. A micro-injector (manual Drummond microinjector or Nanoliter-2000) was adjusted to the micromanipulator. Pipettes were first back-filled with mineral oil, followed by back filling of cRNA up into the rest of the glass-pipette volume (3-4μl). Injections were performed in a sterile injection-chamber with grooves cut at one side at 90^{o}, at the other side 45^{o}, respectively. From the 45^{o} side of chamber the micropipette was adjusted for injection, the 90^{o} wall served as mechanical resistance for oocytes. The chamber was filled with OR2 solution during injection. Injection volumes ranged between 50-75 nl per oocyte, depending on experiment. Injected oocytes were incubated in the gentamicine containing incubation-medium (see solutions) at 18^{o}C. Incubation solution was changed several times upon need. Electrophysiological recordings were performed during the next 1-7 days.

2.2.2 Tissue cell culture.

2.2.2.1 Trypsination and maintenance of the cells.

As a mammalian expression system for potassium channels and their β subunits CHO and HEK 293 cells were used. In the DUKX-mutant of CHO cells the activity of dehydrofolatereductase was suppressed (Urlaub and Chasin 1980). These cells were kept in a sterile incubator and the

plating was performed under the sterile conditions (werkbank SterilGARD II, Type A/B3; Baker, Stanford, ME). Cells were cultivated under the standard conditions, +37^{o}C, 95% relative atmospheric humidity and 5% CO_2. As culture-medium MEM Alpha-based solutions was used. 50 ml heat-inactivated serum albumin was added to 500 ml MEM Alpha (Seromed, Biochrom). We also added 5 ml Penicillin-Streptomycin-Glutamine solution (100x; Pen.:10000U/ml, Strep.: 10000μg/ml, Glut.: 29.2 mg/ml) to the medium.

Cells were seeded in culture standard flasks (Nun-clone). After reaching a phase of 50-70% confluence, medium was removed and the cells were washed with PBS solution (Gibco BRL). Cells were then incubated approximately 5 min in 5 ml trypsine-EDTA solution containing tubes. Loss of cell adherence was checked under the HBO 50 microscope (Zeise). The reaction was stopped by adding of 5 ml serum containing medium. Cells were harvested and centrifuged in a 15 ml petri tube. The sediment was re-suspended in fresh medium. After counting the cells in a counting-chamber and appropriate dilution, they were re-plated in flasks or 35 mm standard at the density 2-5x10^4 dishes for electrophysiological experiments.

2.2.2.2 Transfection of cells.

Transient transfection of cells with cDNA was performed using LipofectAMINE reagent (Invitrogen). The LipofectAMINE reagent was aliquoted and stored at +4^{o}C. LIPOFECT AMINE Reagent is a 3:1 (w/w) liposome formulation of the polycationic lipid (2,3-dioleyloxy-N-[2(sperminecarboxamido)-ethyl]-N, N-dimethyl-1-propanaminium trifluoroacetate (DOSPA)) and the neutral lipid dioleoyl phosphatidylethanole-amine (DOPE) in membrane-filtered water. The transient transfection of HEK 293 and CHO cells was performed according to the manufacturers` protocol. The cells were incubated at 37^{o}C in a CO_2 – incubator and the next two days electrophysiological recordings were performed.

2.3 Electrophysiology.

2.3.1 Two-electrode voltage-clamp set up.

The two microelectrode voltage-camp technique was used to record currents from Xenopus oocytes expressing channels. In some experiments the inside-out configuration of the patch-clamp method was used. Currents from CHO and HEK 293 cells were recorded using the patch-clamp technique in the whole-cell and perforated-patch configuration. The Xenopus oocyte heterologous expression system is widely used for the electrophysiological characterisation of ion channels. It has several advantages over the other expression systems. Xenopus oocytes could be obtained easily and they are viable under appropriate conditions for 2-3 weeks. The cells are big, allowing easy injection with foreign cRNA or cDNA. Xenopus oocytes have only a few endogenous channels, which usually mediate a small fraction of the unspecific currents. They are very stable during recording, making it possible to apply long-lasting protocols. To obtain voltage-clamp conditions two glass-microelectrodes, filled with 3M KCl solution are impaled oocyte. The voltage electrode measures the membrane voltage, transmitting the signal to a feedback amplifier, which injects appropriate amounts of current through the current electrode (second electrode) to keep the membrane potential at a given value (Figure 2). The speed of the voltage-clamp (voltage clamp gain) is depending on the frequency of the feedback-circuit. Due to the capacitance of the membrane a transient capacitive current component will flow during the voltage-clamp step charge, which is given by following equation:

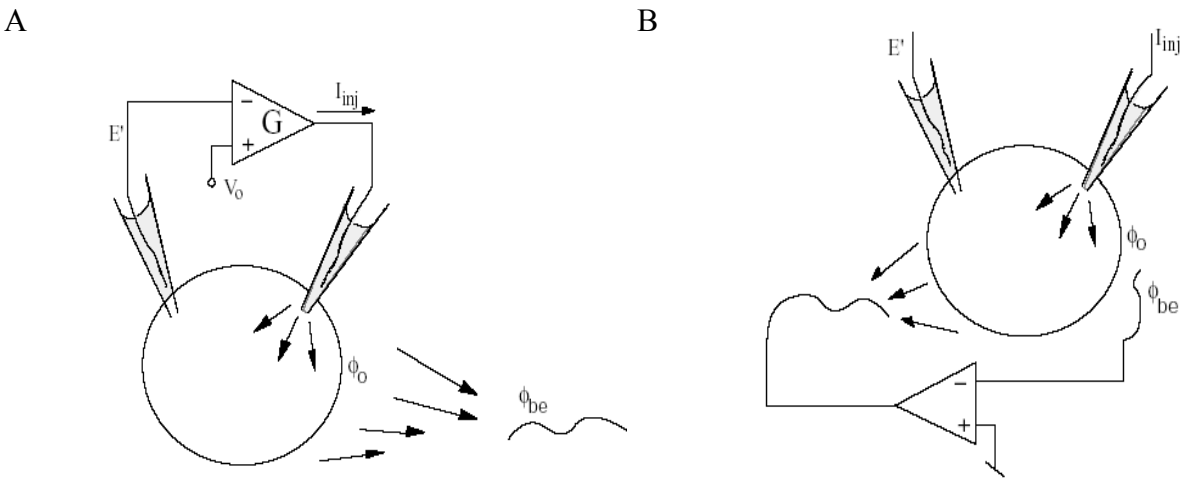

Figure 2. Simplified scheme of the two-microelectrode voltage-clamp technique. A – The principle of voltage-clamping with simple feedback-amplifier. E-voltage electrode, G- feed-back amplifier, I_{inj}-amount and direction of injected current, Vo-given voltage, ϕ_o- potential at close proximity to the membrane, ϕ_{be}– ground potential. B – the role of Bath-clamp circuit. In operational amplifiers a new voltage-clamp circuit (bath-clamp) is added to the feed-back amplifier, which clamps ϕ_o-potential to 0 mV value. In this way series resistance (Rs) is largely decreased.

$$\mathbf{I_{cap} = C}\, d\mathbf{V}/d\mathbf{t}$$

Where; $\mathbf{I_{cap}}$ is the capacitive current, **C**-is the capacitance of the membrane, **V** is the membrane potential. In Figure 2 the current $\mathbf{I_{inj}}$ is being applied to clamp the membrane at a given voltage. $\boldsymbol{\phi_o}$, the potential at the outside surface of the cell membrane, will be different from the potential $\boldsymbol{\phi_{be}}$ at the bath electrode (taken as zero in the situation diagrammed above). The measured potential V would not be the exact membrane potential but the sum of V and ϕ_o. The discrepancy is given by the equation

$$\phi_o = R_s / I_{inj}$$

Where; R_s is the "series resistance", the electric resistance of the path through the bath solution from the membrane surface to the bath electrode. This effect becomes critical when I_{inj} is large.

To decrease this effect, the ϕ_o is clamped at 0 mV which is achieved in operational amplifiers by a second voltage-clamp circuit (Figure 2B).

OOCYTE CLAMP 720 C (Warner Instruments, Inc) is an operational amplifier, which function is based on the described principle. The amplifier was synchronized with a Mac G 3 computer through an ITC-16 interface (Instrutech, USA). The "Pulse" program (HEKA electronics) was used for the control of parameters and for application of voltage protocols.

The oocyte was positioned in a special recording chamber, which can be perfused by various solutions. Agar-bridges provided electrical connection between the bath-clamp circuit and the chamber-perfusing solution. Microelectrodes were pulled from borosilicate glass in a vertical puller PB-7 (Narishige, Japan). The tips of electrodes were broken to get an inner opening diameter of 4-8 μm. Electrodes were filled with 3M KCl solution using capillary glass-pipettes. Such electrodes were "leaky" and could not be used for experiments unless the tip is plugged by Agar-KCl solution using a suction syringe (1g agar in 50 ml 3M KCl boiled 2 minutes). The agar-bridges were filled with the same high-conductive Agar-KCL solution. The electrical resistance of the electrodes was checked after immersing them into the chamber filled with bath solution. The resistances were 0.2-0.8 MΩ for voltage electrodes, and 0.1-0.4 MΩ for current electrodes.

To avoid voltage-clamp artifacts due to remaining Rs, only currents below 10-15 μA were recorded and analyzed. The voltage-clamp gain and the scale of the measured currents were controlled by the amplifier. The membrane capacitance was not compensated.

2.3.2 The patch-clamp technique

The patch-clamp technique developed by Neher and Sakmann is the most important tool for studies of ion channels (Neher and Sakmann 1999). The membrane potential of a small piece of

the cell membrane is clamped to a given potential and the current through this tiny membrane can be measured. The glass pipette (patch pipette), is approached towards the membrane surface and by application of a small negative pressure in the pipette, a very tight seal between the membrane and the pipette is created. The resistance between the two surfaces can be as high as 10^9-10^{12} Ohm, which is called the Giga-seal. From this initial situation, different recording configurations of patch-clamp technique can be obtained, which allow diverse ways to investigate of ion channels. In the whole-cell configuration a negative pressure is applied, in order to rupture the patch membrane. This procedure allows to get an electrical access to the cell interior. In perforated patch configuration the inclusion of antibiotics in the pipette solution make the membrane under the pipette electrically conductive. Furthermore, the whole cell configuration allows measurement of the current under defined intra-and extracellular conditions. The measurable current under these conditions usually varies between some tens of pA and a couple of nA. In our experiments an EPC-9 patch clamp commercial amplifier (HEKA Elektronik) was used to record the macroscopic whole-cell currents from CHO and HEK 293 cells. The principal scheme for electrical circuit of the whole cell patch-clamp is shown in Figure 3. The patch-clamp recording set-up was consisting of: a Faraday cage, a pneumatic vibration isolation table, a Zeiss Axiovert inverted microscope (Axiovert 405M) a Patchman micromanipulator (Eppendorf).

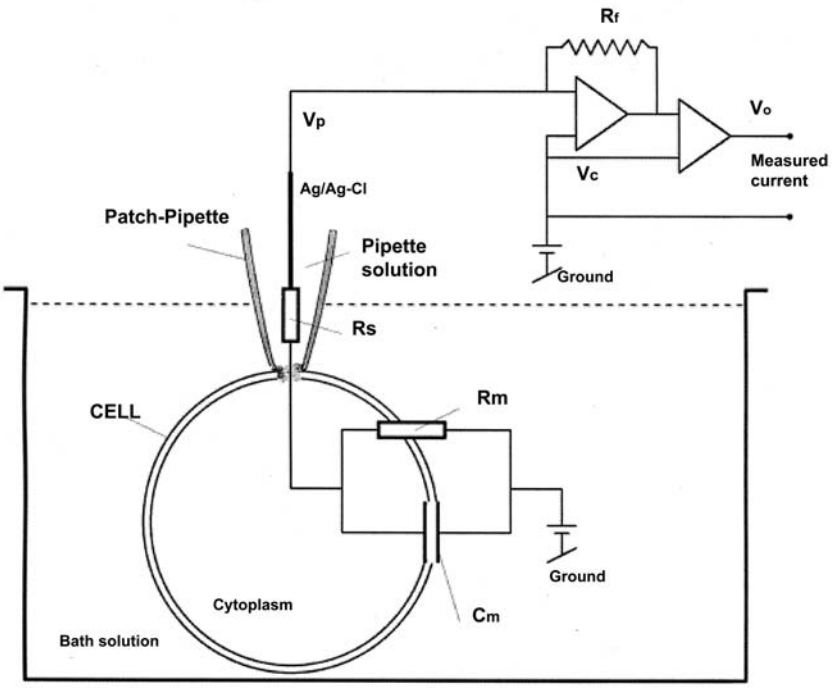

Figure 3. Simplified diagram of patch-clamp technique. In whole-cell configuration the membrane under the patch-pipette is ruptured to get electrical access to the cell cytoplasm. In perforated-patch configuration a porous antibiotic molecules incorporated in the membrane provide access to the cell interior. **Rs**-series resistance, Rm-membrane resistance**, Rf**-feedback resistance, **Cm**-membrane capacitance, **Vp**-pipette potential, **Vo**-output potential.

2.3.3 Giant oocyte patches

cRNA encoding Kv2.1 channel was injected into the oocytes at concentrations of 0.25-0.5µg/µl, 50nl per oocyte and in 2-5 days the whole-oocyte currents were recorded using two electrode voltage-clamp. The amplitude of currents ranged 35 - 60 µA upon depolarizing the oocyte membranes from -80 mV to +60 mV. It was possible to pull inside-out patches from oocytes already being recorded by two-electrode voltage-clamp. For this purpose, the vitalline membrane of the oocyte under the study was manually removed using Dumont number 5 or 55 forceps. Usually, to facilitate this process, it is recommended to expose the oocytes to hyperosmotic depolarizing solution (Sackmann and Neher 1999). However, in our experiments it was easier to get oocyte giant patches when the vitelline membrane was removed in bath solution for (see

Solutions). Manually pulled glass-pipettes were used for application of synthetic peptides. The application-pipettes had opening diameters of 20-30 μM. At the beginning of the application, the tip of the patch-pipette, which contained the giant membrane patch, was adjusted in close proximity of the application-pipette. Multi-channel application system Valvebank 8 II (AutoMate scientific, Inc) was used for switching between appropriate solutions.

2.3.4 Solutions

2.3.4.1 Solutions for two-electrode voltage clamp

The following solutions were used for two-electrode voltage-clamp experiments:

Oocyte Ringer 2 (OR2)	82.5	mM	NaCl
	2.0	mM	KCl
	1.0	mM	$MgCl_2$
	5.0	mM	HEPES
	pH was adjusted to 7.5 with NaOH		
	and the solution was stored at 4° C no longer than 2 weeks.		

For collagenase solutions 3-4μg/μl Collagenase was added to this solution (0.06 g in 15-20ml)

Gentamicin - Solution	75.0	mM	NaCl
(Incubation solution)	2.0	mM	KCl
	2.0	mM	$CaCl_2$
	1.0	mM	$MgCl_2$
	5.0	mM	Na-Pyruvate
	5.0	mM	HEPES
	pH was adjusted to 7.5 with NaOH, 50 μg/ml gentamicin was		
	added and the solution was stored 4° C.		

Measuring solutions	79.5	mM	NaCl
(ND96)	2.0	mM	KCl
	2.0	mM	$CaCl_2$
	1.0	mM	$MgCl_2$
	5.0	mM	HEPES

pH was adjusted to 7.5 with NaOH, the solution was sterile filtered and stored at 4° C.

Tricain-solution: 0.6 g in 500 ml tab-water

Agar- Plug for electrodes:

1.0g Agar was added to 50 ml 3 M KCl solution and boiled at +60° C.

2.3.4.2 Solutions for Patch-clamp experiments

Extracellular solution

135	mM	NaCl
5.0	mM	KCl
2.0	mM	$CaCl_2$
2.0	mM	$MgCl_2$
5.0	mM	HEPES
10	mM	sucrose

Phenol-red 0.01mg/ml was added. The pH was adjusted to 7.4 with NaOH. Osmolarity was 300-320 mOsm. After sterile filtration the solution was stored at 4^oC.

Intracellular solution

125	mM	KCl
11	mM	EGTA
1	mM	$CaCl_2$
1	mM	$MgCl_2$
10	mM	HEPES

pH was adjusted to 7.2 with 1M KOH, sterile-filtered and stored at 4^{o}C. Before usage the following components were added:

2	mM	Glutathione
2	mM	K_2ATP

pH was adjusted to 7.2 with KOH, and solution was kept on ice for several hours. For the perforated patch experiments the same solution was used additionally containing 0.2 mM Amphotericin B. The pH and osmolality of solutions were checked after Amphotericin B addition. Amphotericin B stock solution was made in dimethylsulphoxide (DMSO) at the concentration of 40 mg/ml. Control solutions for Amphotericin B experiments contained the same concentration of DMSO.

2.3.4.3 Solutions for giant oocyte patches

Bath-solution for patches

(to remove the oocyte vitelline membrane)

100	mM	K-aspartate
20	mM	KCl
2	mM	EGTA
4	mM	$MgCl_2$
10	mM	HEPES

pH was adjusted to 7.2 with 1M KOH, sterilely filtered and stored at 4°C (Sackman and Neher 1997).

Giant oocytes patch pipette solution

115	mM	NaCl
2.5	mM	KCl
1.8	mM	$Ca\ Cl_2$
10	mM	HEPES

pH was adjusted to 7.2with 1M NaOH

2.3.5 Data acquisition and analysis

Currents were recorded and stored on a G3 Mac computer using "PULS"-software (HEKA elektronics). Voltage protocols from holding potential of –80 mV to +60 mV were applied at 1s and 15 s durations. Data were filtered at 10 kHz.. Current traces were analyzed with "PULS-FIT" (HEKA). Obtained data were further processed with the programs IGOR (Wavemetrics) and Kaleidagraph (Sinergy Software). Current inactivation traces were fitted by exponential functions of the following forms:

for single-exponential kinetics;

$$I(t) = I_0 + I_1 exp(-t/\tau_1)$$

for three exponential kinetics;

$$I(t) = I_0 + I_1 exp(-t/\tau_1) + I_2 exp(-t/\tau_2) + I_3 exp(-t/\tau_3)$$

Were **I(t)** is the current amplitude **I** at the **t** time, **Io** is the current amplitude at the beginning. $\mathbf{I_1}$ is amplitude accounted for by $\boldsymbol{\tau_1}$ rate. $\mathbf{I_2}$ and $\mathbf{I_3}$ are amplitudes of accounted by τ_2 and τ_3,

respectively. τ_1, τ_2 and τ_3 are time constants of the exponential decays with their corresponding amplitudes.

The curves defining the voltage-dependence of activation and the voltage-dependence of steady-state inactivation were obtained by fitting to the Boltzman functions to the data. If the data were not adequately fitted by a first order of Botlzman-function, fourth order form of it was used. Conductance was calculated from peak current amplitudes. In whole-cell patch-clamp measurements, at the defined intracellular and extracellular potassium concentrations, the reversal-potential for potassium ions was calculated. In two-electrode voltage clamp measurements, the K^+ - tail current reversal potential was measured. The conductance values were normalized to value obtained at +80 mV. Normalized conductance plots were fitted by the following functions:

$$G_{norm} = G / G_{max} = 1/\{1 + \exp [(V_m - V_{1/2}) / Ks]\} \text{ (first order boltzman),}$$

$$G_{norm} = G / G_{max} = 1/\{1 + \exp [(V_m - V_{1/2}) / Ks]\}^4 \text{(fourth order boltzman)}$$

Where $\mathbf{G_{norm}}$ is the normalized conductance, $\mathbf{G_{max}}$ is the maximal conductance at +80 mV, **Vm** is the membrane potential, $\mathbf{V_{1/2}}$ is the voltage of half-maximal activation, **Ks** is the slope factor for GV curve. Protocols for determination of the voltage-dependent activation covered the voltage range from -60 mV to +80 mV in 10 mV increments.

Recovery of the channels from steady-state inactivation was determined by double-pulse protocols according following scheme:

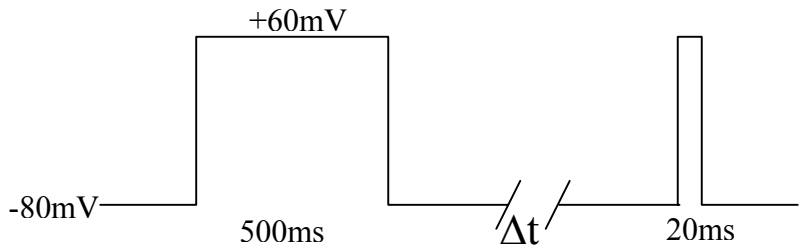

All data are given as mean ± SEM. Statistical analysis was performed with Kaleidagraph software (Synergy) and with IGOR (Wavemetrics). When necessary, Student´s T-test was applied to compare obtained set of data.

3. Results

3.1 Structural determinants of Kvβ-mediated inactivation

3.1.1 Chimeric replacement of Kv2.1 cytoplasmic N-terminus is not sufficient to induce the inactivating activity of Kvβ1.1.

In contrast to Kv1 channels, Kv2.1 does not functionally interact with Kvβ subunits in heterologous expression systems (Nakahira et al., 1996). Our experimental data with Kv2.1 and Kv1.2 co-expressed with Kvβ1.1 in Xenopus oocytes confirmed these results (Figure 4A, B). Tail current recordings indicated that in the presence of Kvβ1.1, Kv1.2 deactivation was biphasic (Figure 4A). A fast component of deactivation was followed by slower component, presumably due to the recovery of Kv1.2/Kvβ1.1 channels from N-type inactivation. The slower current kinetics were not observed when Kv2.1 was co-expressed with Kvβ1.1 (Figure 4b). A possible reason for the lack of functional interaction between Kv2.1 and Kvβ1.1 were, that the Kv2.1 T1-domain is not suitable for Kvβ association. Thus, to allow Kvβ–binding, the complete cytoplasmic N-terminus of Kv2.1, up to the S1 transmembrane segment was replaced by the corresponding part of Kv1.2. (ChimA, Figure 4C). Functional expression in Xenopus oocytes showed, that ChimA channels have different gating properties in comparison with respective parental channels (Figure 4C). ChimA showed slower activation, inactivation and deactivation kinetics. We were particularly interested in the inactivation of the ChimA channels upon co-expression with Kvβ1.1. As judged by accelerated slow inactivation kinetics in the presence of Kvβ1.1 (Figure 4C), ChimA apparently interacted with Kvβ1.1, but this interaction did not result in rapidly inactivating currents as observed for Kv1.2/Kvβ1.1 channels. No difference

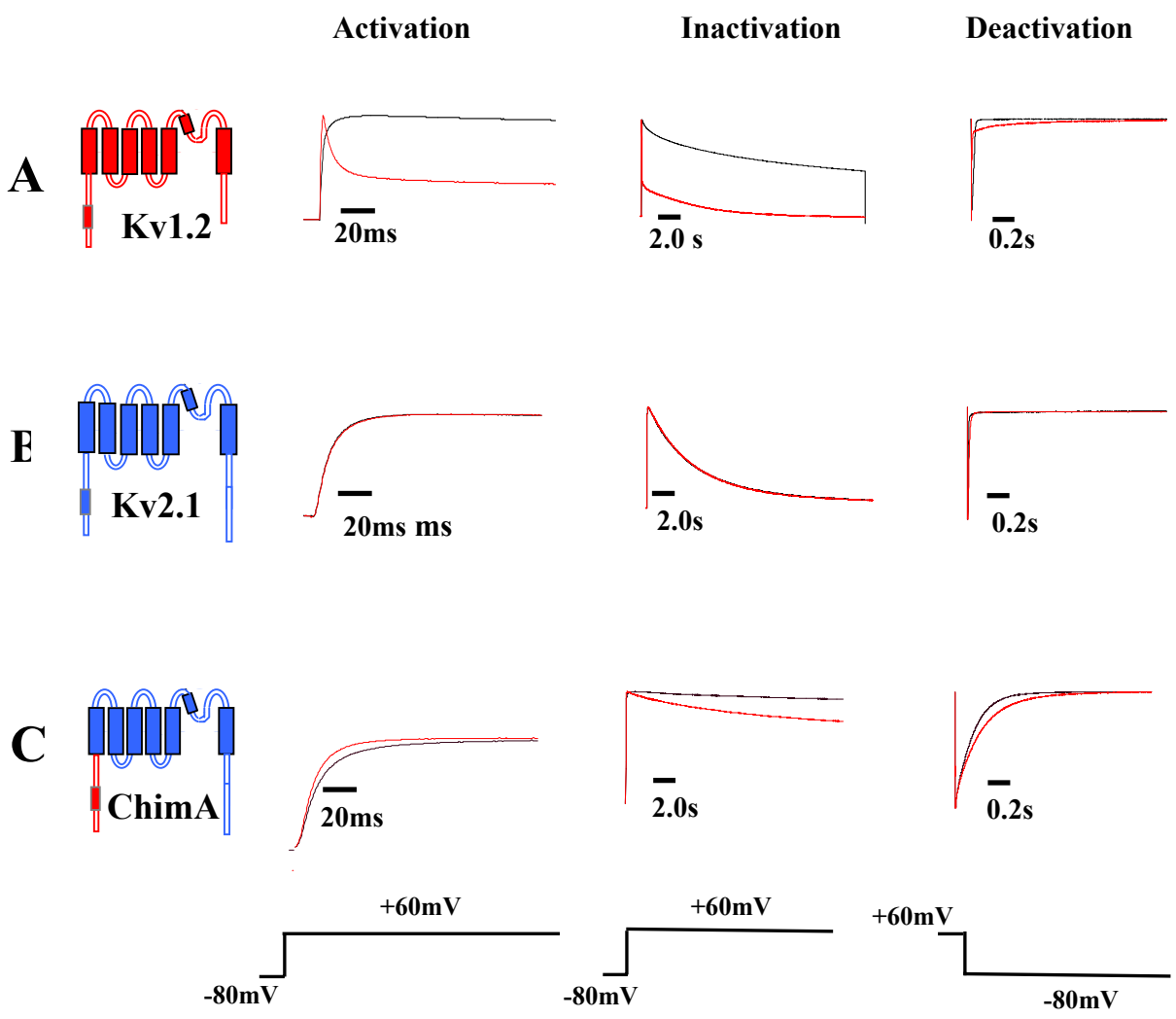

Figure 4. Examples of current traces of Kv1.2, Kv2.1 and ChimA alone and co-expression with Kvβ1.1. The activation, inactivation and deactivation of the channels are shown in different time scales. The S5-Ploop-S6 regions, shown in cartoons were defined by sequence alignment of Kv2.1 with KcsA and subsequent comparison of amino acids corresponding to the known crystal structure of KcsA (Doyle et al., 1998). Kv1.2 and its fragments in chimeric channels are shown in red. Kv2.1 is shown in blue. Traces are normalized to peak currents. Bars indicated the time calibration. Kvβ1.1 coexpression trace is shown in red.

in deactivation kinetics of ChimA tail current was observed in the presence of Kvβ1.1 (Figure 4C). Kinetic parameters are summarized in Table 2.

3.1.2 Kv2.1 channels possess a receptor site for the Kvβ1.1 N-terminal inactivating domain

Primary sequence analysis of Kv2.1 and Kv1.2 proteins showed differences at several amino acids residues in S6 segments. In particular, the V407 position of Kv1.2 which was shown to

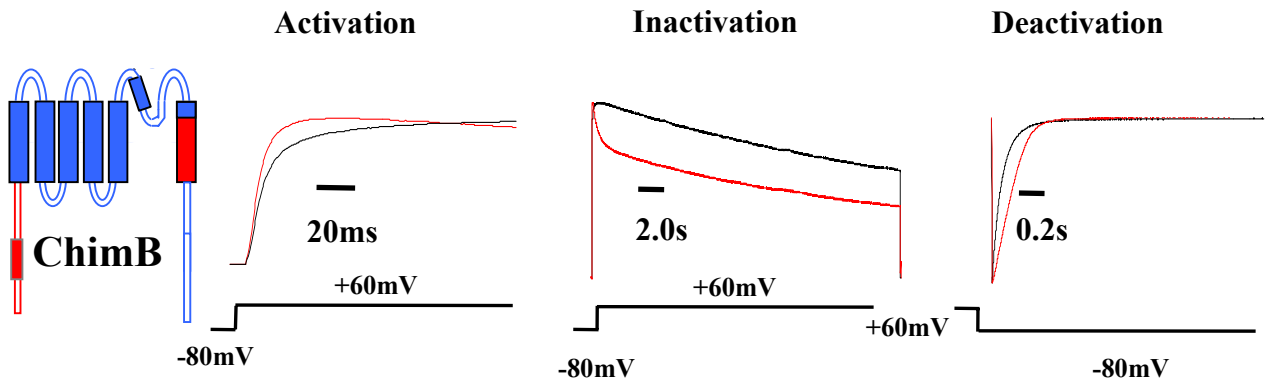

Figure 5. Replacement of putative Kv2.1 receptor site for Kvβ1.1 inactivating domain by homologue region of Kv1.2 in ChimA induced partial inactivation. The fast inactivating component is seen co-expressing ChimB with Kvβ1.1 (red trace). This fast decaying component is absent in ChimB and is much slower than Kv1.2/Kvβ1.1 (see Figure 4A). The deactivation kinetics of ChimB alone and in presence of Kvβ1.1 was measured in 70mM K^+. Leak currents are subtracted. Bars show time calibration.

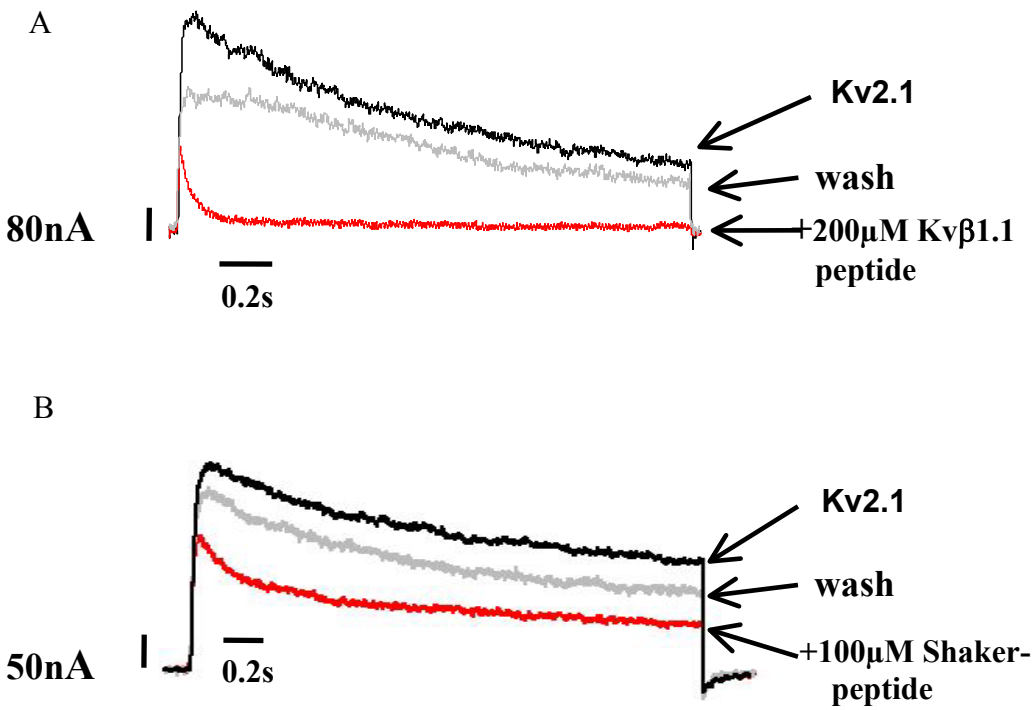

Figure 6. Application of synthetic inactivating peptides on the inside-out patches of Xenopus oocytes expressing Kv2.1. Both Kvβ1.1 and Shaker B peptides were dissolved in bath solution used for the inside-out patch perfusion and were applied to giant oocyte patches. Kv2.1 currents were elicited upon depolarization of membrane from -80 mV - to +60 mV.

make direct contact with V3 of the Kvβ1.1 "ball"-domain (Zhou et al., 2001), is homologous to I409 in Kv2.1. To investigate whether amino acid sequence differences in S6 are responsible for the lack of Kvβ1.1-mediated fast inactivation in ChimA, a large part of S6 in ChimA was replaced by the corresponding fragment of Kv1.2 (ChimB; Figure 5). ChimB/Kvβ1.1 clearly showed a fast inactivating component. ChimB/Kvβ1.1 channels showed biphasic kinetics of inactivation during the longer depolarizing pulses (15s). However, Kvβ1.1 did not induce the same effect as it did upon coexpresion with Kv1.2 wild type (Figure 4A). These experimental results did not support the idea, that sequence differences in S6 and lack of a receptor site for the Kvβ1.1 inactivating domain are the only reason for suppressed inactivating activity in ChimA/Kvβ1.1. Kv2.1, apparently, possesses a receptor site for N-terminal inactivation domains, as it has been demonstrated by Isacoff´s group, showing that the application of the Shaker B peptide to Kv2.1-containing inside-out patches did confer rapid inactivation on channel (Isacoff et al., 1991). To test if this applies also to the Kvβ1.1 N-terminal inactivating domain, we applied a synthetic peptide corresponding to the first 26 amino acids of Kvβ1.1 to inside-out macropatches excised from Xenopus oocytes expressing Kv2.1 wild type (Figure 6A). As a control, we also applied the Shaker B synthetic peptide (Figure 6B). The results obtained with Shaker B synthetic peptide corresponded well to the ones obtained by Isacoff et al. (1991). Furthermore, as the figure 6 shows, similar to Shaker B, the Kvβ1.1 inactivating domain was able to block the Kv2.1 channel. The application of Kvβ1.1 inactivating peptide caused a rapid decay of Kv2.1-mediated currents, which was reversible upon washout of the peptide.

3.1.3 Transmembrane segments play a role in Kvβ1.1-mediated rapid inactivation.

I further investigated Kvβ1.1-mediated inactivation in Kv2.1 by constructing 5 more chimeras (ChimC, ChimD, ChimE, ChimF, ChimG) between Kv1.2 and Kv2.1. Membrane topology

cartoons of these chimeric channels as well as their gating properties in the absence and presence of Kvβ1.1 are shown in Figure 7. ChimC, composed from a Kv1.2 N-terminus, extending up to

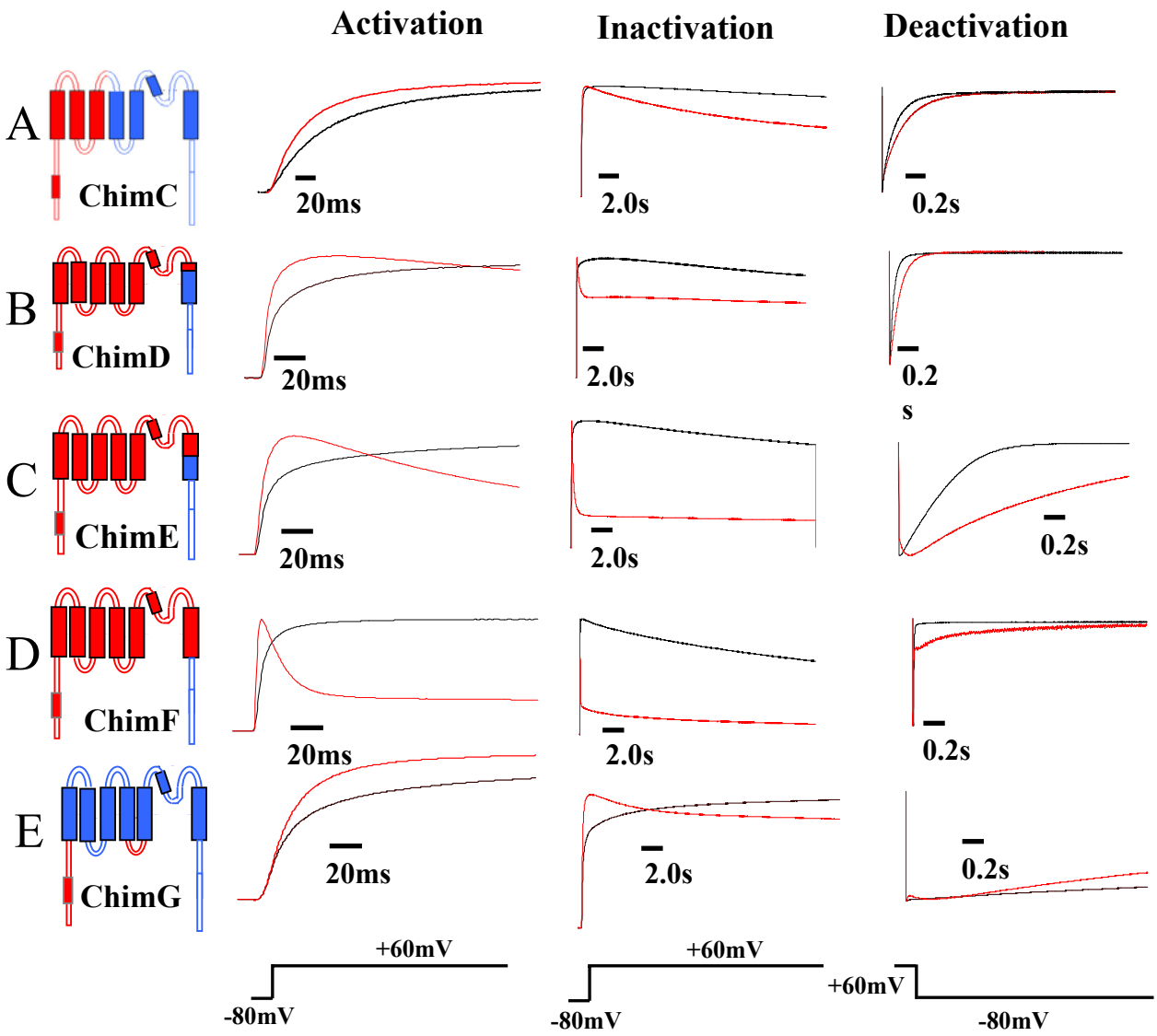

Figure 7. Replacement of all transmembrane domains from the Kv1.2 rescues fast inactivation of Kv2.1. Chimeric channels showed different inactivation kinetics when co-expressed with Kvβ1.1. The first column (150ms) shows activation the second one inactivation (15s). Deactivation kinetic of the channels alone and in presence of Kvβ1.1 were measured in 70mM K^+ shown in third column. The S5-Ploop-S6 region in cartoons was defined by comparison of corresponding regions in KcsA and Kv2.1. Red current traces correspond to the co-expression Kvβ1.1. Kv1.2 in chimeric channels is shown in red, correspondingly, Kv2.1 regions are shown in blue. Traces are normalised to peak current. Leak currents are subtracted: Bars indicate the time calibration.

the middle of the S3-S4 linker and from the appropriate C-terminal part of the Kv2.1 showed modestly accelerated inactivation in the presence of Kvβ1.1, similar to ChimA/Kvβ1.1. Further

extension of the Kv1.2 N-terminal part yielded ChimD, which included S4, S5 and the P-loop segments from Kv1.2. Co-expression of ChimD with Kvβ1.1 resulted in fast inactivation, however, this rapid inactivation was still much slower (τ was ten times larger) than Kv1.2/Kvβ1.1 inactivation (Figure 7B). Furthermore, the ChimD/Kvβ1.1 inactivation was incomplete, and the inactivating current component produced only 18.6 % decay during a 15 s depolarizing pulse (Figure 7B). ChimE, which contained the N-terminal sequence of Kv1.2 up to the PVP motif in S6, also showed a rapid inactivation with Kvβ1.1 (Figure 7C), but, similar to ChimD/Kvβ1.1, the fast component of ChimE/Kvβ1.1 inactivation was almost ten times slower than the one of Kv1.2 with Kvβ1.1. However, the fast inactivating component of ChimE/Kvβ1.1 produced around 81 % of total current decay (Table 2). Faster Kvβ1.1-mediated inactivation of chimeric channels could only be obtained by an entire exchange of all transmembrane domains including the linkers connecting them (ChimF; Figure 7D). Co-expression of ChimF with Kvβ1.1 resulted in currents with kinetic parameters of inactivation identical to the ones obtained for Kv1.2/Kvβ1.1 (Figure 4A, 7D). We considered the possibility, that the cytoplasmic linkers segments S2/3 and S4/5 may prevent rapid and complete inactivation. Based on experimental results with ChimC/Kvβ1.1 it seemes likely that the S2/3 linker played minor role. Thus, in ChimG the cytoplasmic linker S4-S5 of Kv2.1 was replaced by the corresponding region of Kv1.2 (Figure 7E). ChimG did not show fast inactivation when co-expressed with Kvβ1.1. Both in the absence and presence of Kvβ1.1 the deactivation kinetics of ChimG were extremely slow (Figure7E). Possibly, the coupling between voltage sensor and the gate was modified in ChimG.

Channel	τ_1 (ms)	$RA_{(\tau 1)}$	τ_2 (ms)	τ_{deact} (ms)	I_{peak} /I_{15s} (%)
Kv1.2	592 ± 72 (n=3)	31,2 (n=3)	12300±4600 (n=3)	6.4±3,7 (n=3)	62.7±7.1 (n=3)
Kv2.1	2130 ± 1212 (n=4)	31,4 (n=4)	5780±2451 (n=4)	7.12±2.43 (n=4)	6.2±4.91 (n=3)
ChimA	21800 ± 2210 (n=5)	-	-	157 ± 36.8 (n=3)	89.1±6.35 (n=4)
ChimB	14700± 1100 (n=3)	-	-	67.8 ± 24.0 (n=3)	65.5±5.35 (n=3)
ChimC	24800±6400 (n=5)	-	-	146 ± 48 (n=4)	91.2±6.2 (n=3)
ChimD	27300±2320 (n=4)	-	-	127±18 (n=4)	87.4±6.8 (n=4)
ChimE	22400±4600 (n=4)	-	-	313 ±103 (n=3)	80.9±2.2 (n=4)
ChimF	672 ± 72 (n=4)	34,6 (n=4)	14700±3600 (n=4)	5.03±2.2 (n=4)	67.9±9.1 (n=3)
ChimG	-	-	-	8400±2100 (n=3)	-
Kv1.2+ Kvβ1.1*	14.7±3.9 (n=4)	92±5 (n=4)	645±140 (n=4)	4.21±4.3 **ii** τ_2 1500±1030 $RA(\tau_1)$ 74.5±14% (n=3)	n.d.
Kv2.1+ Kvβ1.1	2040 ± 1410 (n=3)	29 ± 6 (n=4)	5290± 2330 (n=4)	6.81 ± 4.8 (n=4)	7.1±4.9 (n=4)
ChimA+ Kvβ1.1	8990 ± 660 (n=5)	-	- -	205.7±26.3 (n=4)	87.3±7.3 (n=3)
ChimB+Kvβ1.1	244±14 (n=5)	51±7.2 (n=5)	10740 ±2050 (n=5)	64.3±12.4 (n=4)	36.1±6.3 (n=4)
ChimC+Kvβ1.1	8300±1180 (n=4)	-	-	168.3±56,9 (n=4)	67.5±11 (n=4)
ChimD+Kvβ1.1	153±16,9 (n=7)	-	-	96.7±41.4 (n=4)	81,4±6.1 (n=4)
ChimE+Kvβ1.1	105±21 (n=5)	81±1.5 (n=5)	13000± 15200 (n=3)	397±197 **ii** τ_2 1.793±683 $RA(\tau_1)$ 71±13% (n=4)	28.2 ±7.3 (n=5)
ChimF+Kvβ1.1*	13.4±1.37 (n=4)	94±2 (n=3)	904±210 (n=4)	4.21±4.3 **ii** τ_2 793±883 $RA(\tau_1)$ 80±24% (n=3)	n.d.
ChimG+Kvβ1.1	573±245 (n=4)	51±8.1 (n=3)	17500±3840 (n=2)	n.d.	61.7±4.8 (n=3)

Table 2. Inactivation and deactivation kinetics of different channels in presence and absence of Kvβ1.1 Decaying components of channels were fitted with two exponential functions. Example of corresponding traces are shown in Figure 4, 5 and 7. With asterisks are indicated fits to 1s current traces of corresponding channels. **ii-** indicates that tail currents could be only adequately fitted with two exponential function. τ_2 and $RA(\tau_1)$ are showing the second time constant and amplitude of first component correspondingly.

3.2 Oxidoreductase features of Kvβ subunits determine their inactivating activity.

3.2.1 Gain of inactivating function in Kvβ3.

3.2.1.1 C-terminal domains of Kvβ3 are responsible for the lack of inactivating function.

Previously, it has been shown, that association of Kvβ1.1 and Kvβ3 potassium channel beta subunits with Kv1.5 α subunits gives rise to rapidly inactivating A-type currents in a mammalian cell-line (Leicher et al., 1998). In the Xenopus oocyte expression system, however, rapid inactivation is observed only in the case of Kv1.5 co-expressed with Kvβ1.1 (Heinemann et al., 1996). Even co-injection of 25 times higher amounts of Kvβ3 than Kv1.5 cRNA did not confer a rapid inactivation to Kv1.5 (data are not shown). To identify the structural correlates of this phenomenon, chimeric Kvβ1.1/Kvβ3 subunits were constructed and were functionally co-expressed with Kv1.5 in Xenopus oocytes. The constructs showed, that both Kvβ1.1 and Kvβ3 possess a functional N-terminal "ball" domain. The chimera KvβchiA possesses the same sequence at the N-terminus as Kvβ3, but C-terminal domain of Kvβ1.1. In contrast to Kvβ3, co-expression of KvβchiA confers fast inactivation to Kv1.5 (Figure 8). Hence, prevention of inactivation could *not* be explained by properties of the Kvβ3 "ball" domain, but rather by the properties of its C-terminal part. Figure 8 shows a summary of experiments performed with chimeric beta subunits. Some chimeric beta subunits changed the mid-point of the half maximal activation of Kv1.5 channels. In addition, some of them significantly changed the slope factor of Kv1.5 GV-curve (Table 3). A modulation of GV curves suggest that those chimeric subunits, which do not show a complete fast inactivating activity, were nevertheless, associated with alpha subunits. Since N-type inactivation itself is nearly voltage-independent (Hoshi et al., 1990, Zhou et al., 2001), I investigated Kvβ-mediated rapid inactivation of Kv1 channels only at positive potentials (+60 mV and +80 mV) to obtain maximal number of open channels. In the table 3

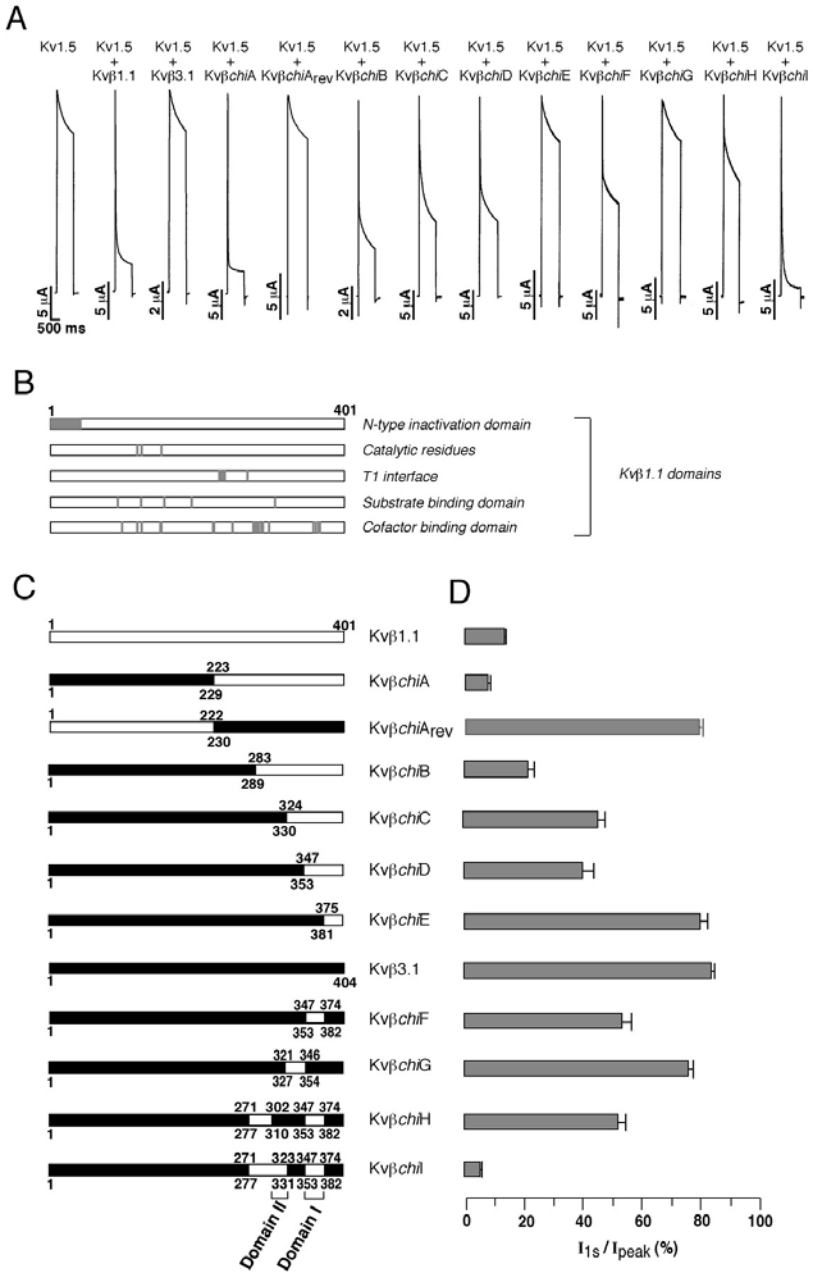

Figure 8. Inactivating activity of Kvβ1.1, Kvβ3.1, and the chimeric Kvβ subunits, when coexpressed with Kv1.5. **A**, currents were elicited in Xenopus oocytes expressing Kv1.5/Kvβ combinations indicated on top of each trace. The current traces were recorded using depolarizing steps from a holding potential of -80mV to a test potential of +80 mV of 1 s. Leak currents have been subtracted. Bars show current and time calibrations. **B**, bar diagrams show (in gray) relative positions of domains and amino acid residues in Kvβ1.1, which form the N-type inactivation domain, Kvβ oxidoreductase active site and the interface for assembly with Kvα subunits. **C**, bar diagrams of chimeric constructs KvβchiA - I (open bars, Kvβ1.1; filled bars, Kvβ3.1). Numbers on top refer to first and last Kvβ1.1 amino acid residue; numbers at bottom refer to first and last Kvβ3.1 amino acid residue in each construct. **D**, mean percentage (I_{1s}/I_{peak}) of peak current (I_{peak}) remaining after 1 s of inactivation (I_{1s}) for Kv1.5 co-expressed with Kvβ1.1, Kvβ3.1, and each of the constructs as indicated (experimental protocol as in A; n = 9-20).

is summarizes the kinetic parameters of inactivation and voltage-dependent activation of Kv1.5 alone and co-expressed with wild type and chimeric Kvβ subunts in Xenopus oocytes.

Subunits	τ_1 (ms)	$RA_{(\tau1)}$ %	τ_2 (ms)	I_{1s}/I_{peak} %	$V_{1/2}$ (mV)	K_s (mV)	N
Kv1.5	608±21	22±2	12486±49	85±1	11.2±1.1	15.1±0.2	4
Kv1.5 + Kv3	306 ± 55	39 ± 5	1341 ± 44	84 ± 2	21.6 ± 2.7	18.9 ± 1.3	11
Kv1.5 + Kv*chi*A	22 ± 1	90 ± 4	45 ± 6	7 ± 1	17.4 ± 2.0	19.7 ± 0.6	17
Kv1.5 + Kv*chi*A$_{rev}$	260 ± 30	18 ± 2	1063 ± 40	80 ± 1	17.9 ± 0.9	17.6 ± 0.1	9
Kv1.5 + Kv*chi*B	14 ± 1	72 ± 11	386 ± 16	22 ± 2	36.3 ± 1.7	20.2 ± 0.5	25
Kv1.5 + Kv*chi*C	24 ± 2	44 ± 7	362 ± 19	46 ± 3	38.1 ± 2.1	19.7 ± 0.5	11
Kv1.5 + Kv*chi*D	23 ± 3	75 ± 16	647 ± 70	41 ± 3	20.1 ± 0.9	21.2 ± 0.7	9
Kv1.5 + Kv*chi*E	210 ± 49	37 ± 6	590 ± 100	81 ± 3	17.1 ± 1.2	24.1 ± 0.8	20
Kv1.5 + Kv*chi*F	17 ± 1	22 ± 7	644 ± 20	53 ± 4	27.4 ± 1.4	27.3 ± 0.8	10
Kv1.5 + Kv*chi*G	398 ± 31	46 ± 7	1346 ± 90	77 ± 1	17.1 ± 1.1	19.8 ± 0.7	13
Kv1.5 + Kv*chi*H	25 ± 4	40 ± 6	667 ± 29	52 ± 3	22.1 ± 1.6	27.2 ± 1.1	10
Kv1.5 + Kv*chi*I	30 ± 4	67 ± 16	291 ± 27	6 ± 1	22.4 ± 1.1	18.0 ± 0.5	9
Kv1.5 + Kvβ1.1wt	13 ± 1	90 ± 10	75 ± 0.5	13 ± 1	17.2 ± 1.5	21.9 ± 0.3	14

Table 3. Gating parameters for wild type Kvβ3 and Kvβ1.1 as well as for chimeric Kvβ3/Kvβ1.1 subunits co-expressed with Kv1.5 in Xenopus oocytes. The decay phase of current traces elicited by depolarizing pulses from –80 to +80mV during the 1s pulse was fitted with single and double exponential functions. τ_1 is fast inactivation time constant, $RA_{(\tau1)}$ is the relative amplitude of the fast component of inactivation, τ_2 is slow inactivation time constant. I_{1s}/I_{peak} is the percentage of current amplitude relative to peak remaining after 1s depolarizing pulse to +80mV. $V_{0.5}$ is the voltage of half-maximal activation, and **Ks** is the slope factor of voltage-dependent activation.

3.2.1.2 Putative oxidoreductase domains of Kvβ subunits connected to inactivating function?

The co-expression of the chimeric β subunits Kvβ*chiA and* Kvβ*chiArev* with Kv1.5 showed, that C-terminal domain of Kvβ3.1 may be involved in regulation of its fast inactivating activity. Transferring Domain I and Domain II (Figure 9) from Kvβ1.1 to Kvβ3 resulted in Kvβ*chiI*, that conferred rapid inactivation to Kv1.5. Domain I corresponds to the residues 353-382 in Kvβ3. Domain II includes amino acids 277-331 of Kvβ3. In the 3D model of Kvβ2, position of the Domain I covers the putative catalytic as well as NADPH binding sites of Kvβ3. Seven residues of Domain I cover the adenosine binding pocket (Figure 9B, C). Ser-366, Gln-370, Glu-373 and His-374 in Kvβ3 contribute to cofactor binding. Residues in Domain II (310- 330 in Kvβ3) have

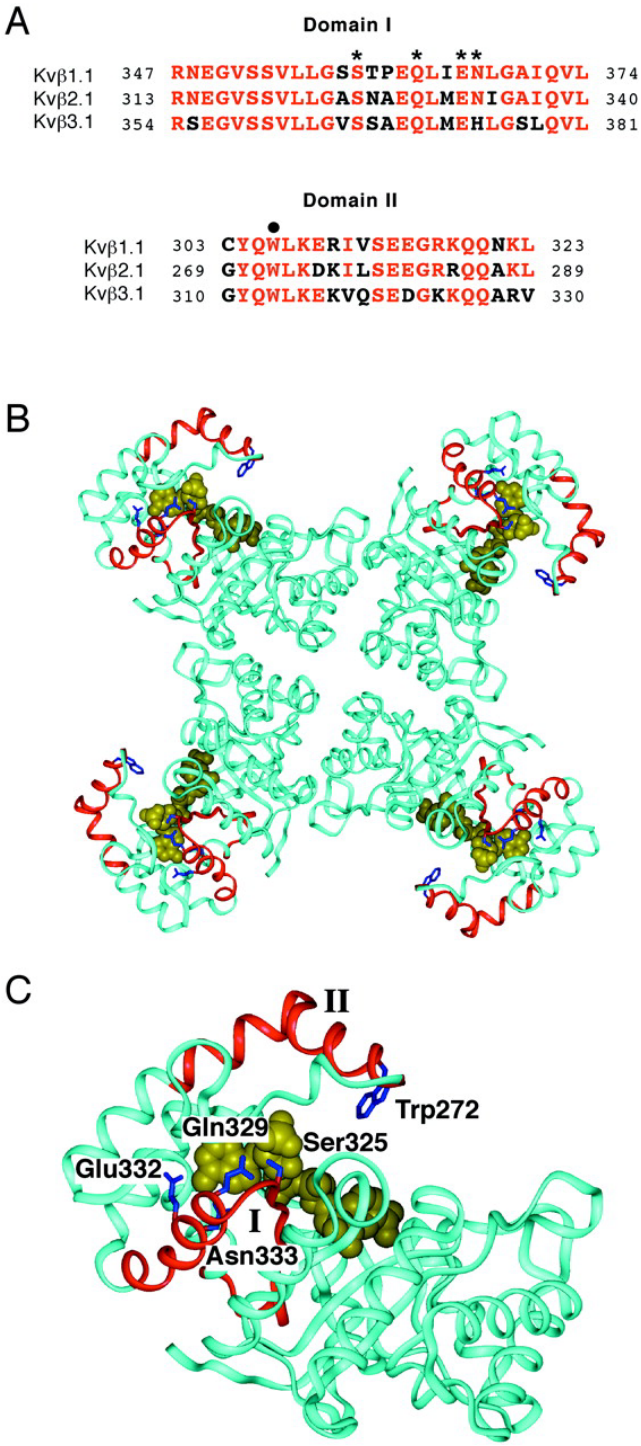

Figure 9. Localization of domains I and II in the Kvβ2 crystal structure. ***A*** - alignment of Domain I and Domain II sequences of Kvβ1.1, Kvβ2.1, and Kvβ3. Numbers at *right* and *left* refer to first and last amino acid residue shown. ***Asterisks*** indicate amino acid residues that are in close contact with the adenosine moiety of the NADPH cofactor bound in the Kvβ2 active site. A ***Black dot*** **marks** -Kvβ2 amino acid residue proposed to contribute to the substrate-binding site. Identical amino acid residues are in **red**. Amino acid residues are given in the single letter code. ***B***-ribbon diagram of the three-dimensional structure of Kvβ2 tetramer according to Guilbis at al. 1999. Domains I and Domain II, defined in ***C,*** are coloured **red**. NADPH cofactor **(*green*)** is shown as Corey-Pauling-Koltun model. Domain I residues 325, 329, 332, and 333 and domain II residue 272 are labelled. Side-chains are in *stick representation* and have been coloured ***magenta***. ***C*** **-** Kvβ monomer to illustrate domain I side-chains in NADPH binding pocket and domain II side-chain in substrate binding site. Model was prepared with the program INSIGHT (Molecular Simulations Inc., San Diego, CA) and based on the Kvβ2 structure as available in the Protein Database accession number 1 QRQ.

been proposed to participate in substrate binding, according to analogies to closely related oxidoreductases. Overlapping of these two domains with cofactor binding site and substrate binding domain of related oxidoreductases lead us to the conclusion, that the absence of inactivating activity of the Kvβ3 can be determined by its oxidoreductase activity.

3.2.2 Loss of inactivating activity in Kvβ1.1.

3.2.2.1 Pyridine nucleotide binding affinity of Kvβ1.1 is correlated with its fast inactivation activity

Although the substrate(s) of Kvβ subunits is not known, the crystal structure of the conserved core-domain of the Kvβ2 shows $NADP^+$ bound at the putative active site (Gulbis et a., 1999). Enzymes that are closely related to Kvβ subunits usually do not show catalytic activity if they fail to bind pyridine nucleotide coenzymes (Vartanov et al., 1992, Sanli and Blaber 2001). In order to disrupt the nucleotide coenzyme binding of Kvβ1.1 point mutations were introduced at the sites, which according the crystal structure of Kvβ2, have direct contacts with $NADP^+$ (Kvβ1.1Q248R, Kvβ1.1R298E). Before the effect of point mutations Kvβ1.1Q248R and Kvβ1.1R298E on the inactivating activity of Kvβ1.1 was studied in coexpression experiments with Kv1.5, the effect of these mutations on the nucleotide coenzyme binding affinity of Kvβ1.1 was biochemically examined. It has been shown previously, that an N-terminal truncation of Kvβ2 did not affect its coenzyme binding properties (Liu et al., 2001). For this reason 39 amino acids were deleted from the N-terminus of Kvβ1.1wt, Kvβ1.1Q284R and Kvβ1.1R298E. These N-terminally truncated constructs could be expressed in E.coli. Freshly purified proteins showed the absorbance peak at 275 nm and an additional absorbance at 310 - 450 nm range, indicating that NADPH was bound to the purified protein. When excited with 290 nm, wild type protein

showed two emission bands with peaks at 335 and 450 nm. With extensive dialysis (2 weeks), the 450 nm band disappeared and the 335 nm band increased in size. This means that the freshly purified enzyme had bound NADPH, which, however gradually unbound (or oxidized to NADP+) during dialysis. NADPH affinity of dialyzed protein (having bound NADP+) could be measured by titration with freshly prepared NADPH buffer. In this case, the absorbance peak at 335 nm decreased and a new peak appeared at 450 nm. The peak at the 450 nm is indicative of bound NADPH. At some concentration of NADPH this process reached saturation. The wild type Kvβ1.1 showed a relative high affinity to nucleotide coenzymes, whereas Kvβ1.1Q284R showed a 10 times lower affinity for both $NADP^+$ and NADPH. The mutant Kvβ1.1R298E did not show binding of nucleotide coenzymes (Table 4). These findings indicate, that corresponding residues of Kvβ1.1 and Kvβ2 are critical for nucleotide coenzyme binding. Both β subunits coud bind also other pyridine nucleotides such as $NADP^+$, NADH and NAD^+ with lower affinity.

Protein	ΔNKv1βwt	ΔNKv2βwt*	ΔNKv1Q248R	ΔNKv1R298E
NADPH	0.13±0.03	012±0.01	1.7±0.15	ND
NADH	1.84±0.36	1.23±0.16	9.95±1.9	ND
$NADP^+$	0.26±0.02	0.36±0.02	3.42±0.16	ND
NAD^+	3.17±0.26	3.61±0.4	26.8±7.0	ND

Table 4. K_d values of pyridine nucleotide bindng to different Kvβ subunits. Values are mean ± standard deviation. Proteins were expressed in E.coli. Dissociation constants are given in μM units.
*** -** data are taken from Liu et al., 2001 for comparison.

For electrophysiological experiments corresponding cRNA, encoding for non-truncated Kvβ1.1Q248R or Kvβ1.1R298E proteins, were co-injected into Xenopus oocytes with Kv1.5 cRNA. No fast inactivation was observed at α:β cRNA ratio of 1:1, and the slow inactivation of Kv1.5/Kvβ1.1Q284R and Kv1.5/Kvβ1.1R298E channels, respectively, was not significantly different from the once for homomeric Kv1.5 (Figure 10A, B). Neither Kv1.5/Kvβ1.1Q284R nor

Kv1.5/Kvβ1.1R298E channels showed fast inactivation even if the α:β cRNA injection ratio was decreased down to 1:25, albeit Kv1.5/Kvβ1.1R298E channels showed slight changes in inactivation kinetics with lower amounts of Kvβ1.1 cRNA. Both mutant beta subunits *did* change slow-inactivation kinetics of K1.5 channel, indicating that these mutant subunits were associated with the channel's alpha subunits. This low C-type inactivation of Kv1.5/Kvβ1.1Q284R channels was accelerated, which could be better observed during 15s depolarizing pulses to +60 mV (Figure 10C, D). The GV curves (Figure 11) of Kvβ1.1Q248R and Kvβ1.1R298E co-expressed with Kv1.5 did not change significantly,

Subunits (ratio)	τ_1 (ms)	**RA** (τ_1) %	τ_2 (ms)	**RA**$_{(2)}$ %	τ_3**(ms)** (ms)	I_{1s}/I_{peak} %	I_{15s}/I_{peak} %	**n**
Kv1.5	583±86	24±1.2	10177±496	-	-	82.9±1.3	37.2±1.3	5
Kv1.5+Kvβ1.1wt(1:1)	6.8±0.7	92±1	172±8	-	-	10±1	-	17
(1:25)	5.4±0.3	95.5	299±19.4	-	-	13.0±2.9	-	5
Kv1.5+Kvβ1.1Q248R	650±92.2	35±5.2	5418±833	-	-	66.7±3.8	19.2±6.09	6
(1:25)	76.1±9.4	19±2.6	6771±20.2	56±3	4212±295	49.4±1.5	10.9±2.7	5
Kv1.5+Kvβ1.1R298E	24.4±15.9	33.6±13	622±92	48±4	2378±470	77.4±3.7	36.2±3.0	9
(1:25)	85.0±39.8	21.8±4.8	892±101	30.1±4	6632±1117	75.5±3.0	36.4±2.64	8

Table 5. Parameters of inactivation kinetics of Kv1.5 alone, and when co-expressed with wild type and NADPH binding mutant Kvβ1.1 subunits. Curves (1s, +60 mV) were fitted double and, where necessary, tripl-exponential functions. τ_1, τ_2 and τ_3 are time constant of exponential decays, **RA**$_{(\tau_1)}$ is the relative amplitude of fast component in percentage. τ_2 is the time constant of second component, **RA**$_{(\tau_2)}$ is the relative amplitude of second component in percentage, I_{1s}/I_{peak} , I_{15s}/I_{peak} are the percentage current amplitudes remaining after 1 and 15 second depolarizing pulse to +60 mV.

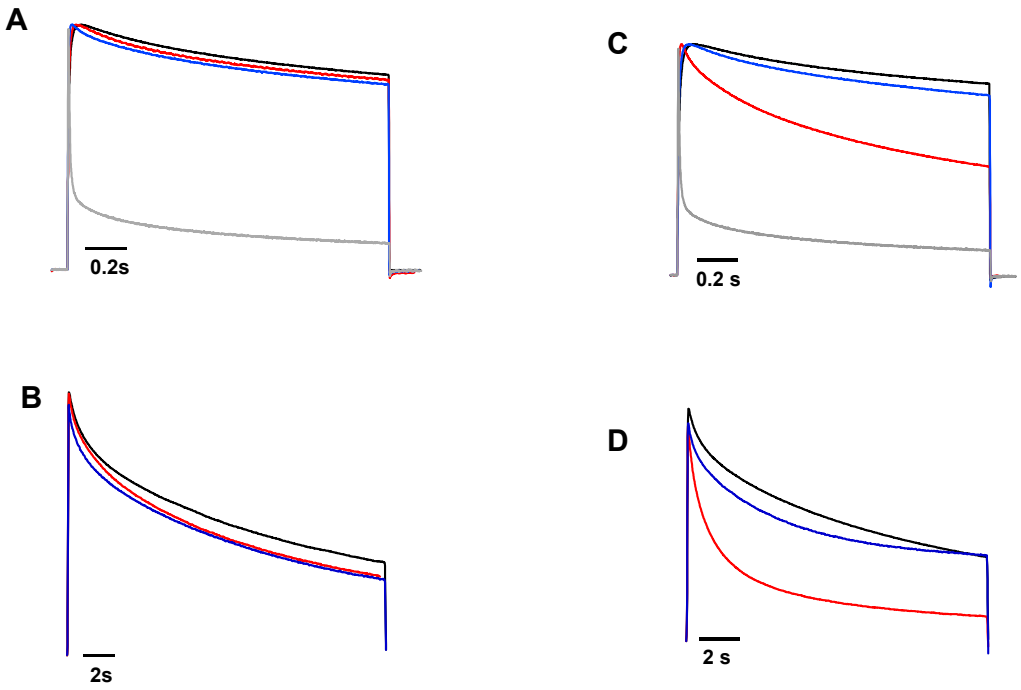

Figure 10. Normalized outward currents mediated through Kv1.5, and by its co-expression with Kvβ1.1wt and mutant subunits. Kv1.5 (black), Kv1.5/Kvβ1.1wt (gray), Kv1.5/Kvβ1.1R298E (blue), Kv1.5/Kvβ1.1Q248R (red). Currents were elicited in Xenopus oocytes using depolarizing pulses from a holding potential of -80 mV to +60 mV. ***A*** *and* ***B*** show the co-expression of channel subunits at a ratio of cRNA 1:1. ***D*** *and* ***C*** show co-injection cRNA at the α:β ratio of 1:25. Leak currents are subtracted. ***Bars*** indicate time calibrations. Recordings in *A* and *B* are from oocytes injected with 1 ng of both Kv1.5 and Kvβ cRNA, whereas in *C* and *D* 1 ng of Kv1.5 and 25 ng of Kvβ cRNA were injected.

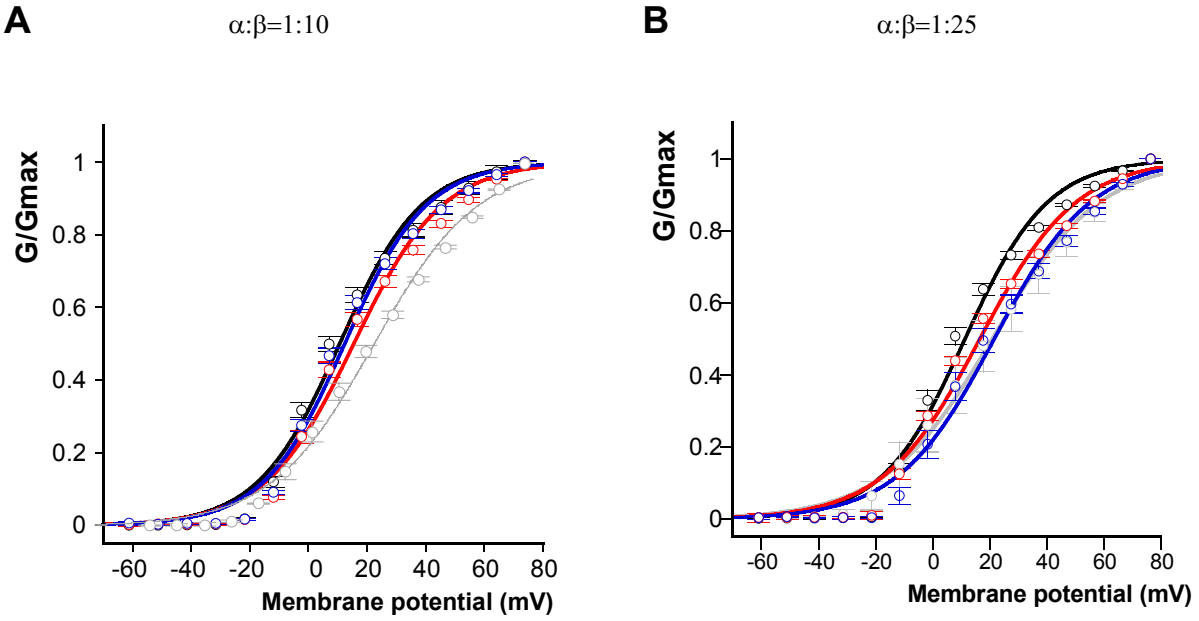

Figure 11. Normalized GV curves for Kv1.5, in absence and presence of different β subunits. Kv1.5 (black), Kv1.5/Kvβ1.1wt (gray), Kv1.5/Kvβ1.1R298E (blue) and Kv1.5/Kvβ1.1Q248R (red). Conductance-voltage relationships were calculated from peak currents. Reversal potentials for potassium currents were determined by tail current measurements. Depolarising pulses from –60 mV to +80 mV in 10mV increments were applied from holding potential of -80 mV. Channel subunits were co-expressed using two different α:β cRNA ratios, 1:1 in ***A***, and 1:25 in ***B***.

as compared to Kvβ1.1wt. A summary of kinetic parameters obtained with co-expression of mentioned Kvβ1.1 NADPH binding mutants with Kv1.5 are shown in Table 5. The slow inactivation kinetics of Kv1.5 co-expressed with mutant Kvβ1.1 channels showed dependence on the α:β cRNA injected ratio at the range 1:25 (Figure 11). To investigate the cRNA dose-dependence of the Kvβ1.1-mediated inactivation activity, a wide range of α:β cRNA ratios were tested. We considered the possibility that the effect of NADPH binding mutations could be simply caused by inefficient expression or membrane trafficking of the β subunits. If this was true, increasing the amounts of mutant beta subunits cRNA and keeping Kv1.5 cRNA constant should lead to the expression of current with increasingly fast inactivation. If inactivating

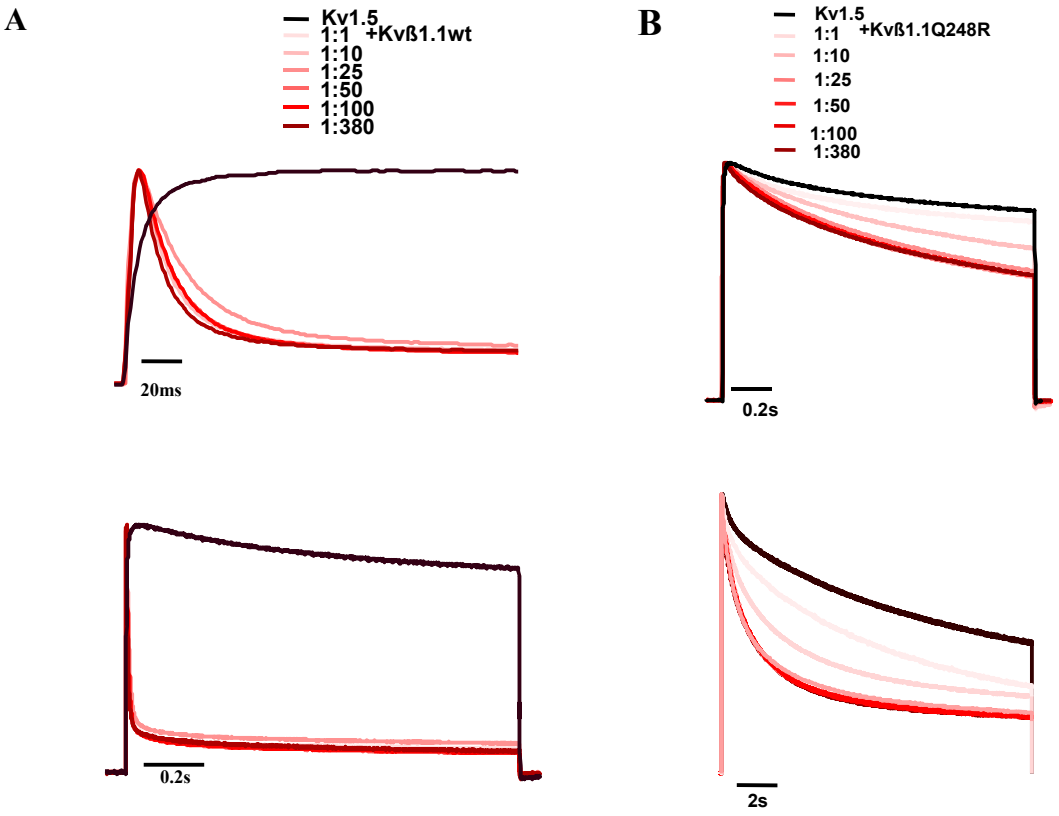

Figure 12. Effect of injected α:β cRNA ratio on current inactivation tested for Kv1.5/Kvβ1.1 and Kv1.5/Kvβ1.1Q248R co-expression. Outward potassium currents were normalized and presented at two different time scales. Kv1.5 cRNA (2 ng/oocyte) alone or corresponding amounts of Kvβ subunits cRNA were co-injected to cover α:β ratios from 1:1 to 1:380. ***A-*** Kv1.5 and Kv1.5/Kvβ1.1wt control, ***B-*** Kv1.5 and Kv1.5/Kvβ1.1Q248R. Homeomeric currents mediated by Kv1.5 are represented in **black**, currents obtained by cRNA injection of wild type and mutant Kvβ1.1 with Kv1.5 are shown colour-coded (**red**). Currents were elicited by depolarizing the oocyte membrane from a holding potential of -80 mV to +60 mV. Leak currents have been subtracted. **Bars** indicate time calibrations.

Kv1.5/Kvβ1.1Q248R channels were trapped in intercellular compartments recorded current amplitudes should be lower than those with Kv1.5/Kvβ1.1wt. Figure 12 shows typical normalized current traces for Kv1.5 with Kvβ1.1wt (as a control) and for Kv1.5 with Kvβ1.1Q248R at different ratios of injected cRNAs in Xenopus oocytes. As summarized in figure 13 the amount of Kvβ1.1Q248R cRNA influenced the kinetics of the current obtained. This effect was not seen with Kvβ1.1wild type. The effect of beta subunits was saturated at the ratio 1:25 (also see Figure 10). No further change in inactivation properties of Kv1.5 channels is achieved by injecting even higher amounts of wild type and mutant beta subunit cRNA.

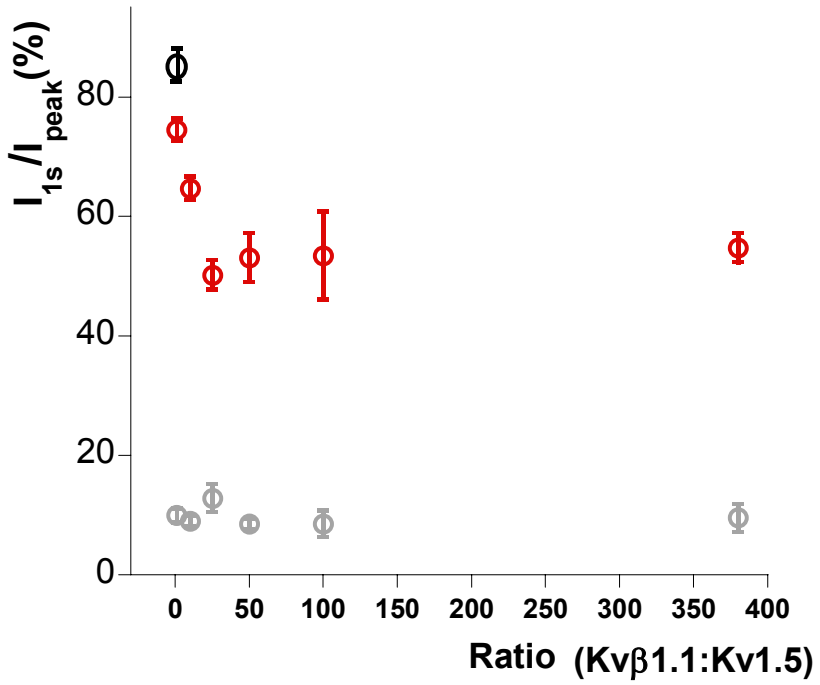

Figure 13. Current decay after 1s pulse for Kv1.5 (black), Kv1.5+Kvβ1.1wt (gray) and Kv1.5+Kvβ1.1Q248R (red) injected at different cRNA ratios in Xenopus oocytes. Currents were elicited by depolarizing pulses from -80 mV to +60 mV by 1s duration. Injected amounts of Kv1.5 cRNA was kept constant (2ng/oocyte) and Kvβ1.1 cRNA amount was appropriately increased to get β:α ratios indicated at the X-axe.

The expression level of Kv1.5 was not different from the expression level of Kv.5/Kvβ1.1Q248R and Kv1.5/Kvβ1.1wt, as was judged from the peak amplitudes of the recorded currents (Figure 14).

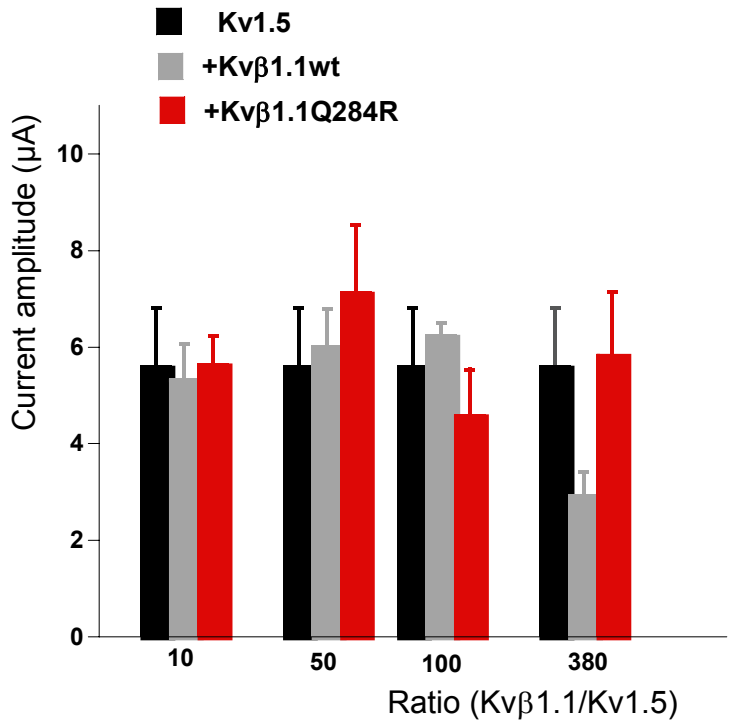

Figure 14. Peak current amplitude of oocytes injected by different ratio of Kvβ:Kvα cRNA. Outward potassium currents were recorded at the potential +60 mV. Injection amounts were 2ng/oocyte for Kv1.5, and 20, 100, 200, 640 - ng/oocyte for appropriate Kvβ subunits, correspondingly.

3.2.2.2 Mutations at the putative catalytic residues in Kvβ1.1 attenuate its inactivating activity

Based on the results from experiments with Kvβ1.1/Kvβ3 chimeric subunits, it is likely that differences in the putative oxidoreductase active sites between the Kvβ1.1 and Kvβ3, respectvly, are responsible for the observed discrepancies between inactivating activities. In enzymes, structurally related to Kvβ subunits (e.g. 3α-Hydroxisteroid dehydrogenase, aldose reductase or aldedyd reductase), it has been shown, that mutating residues responsible for hydride transfer, decreases or abolishes their catalytic activity (Schlegel et al., 1998a, Tarle et al., 1993, Schlegel et al., 1998b). Corresponding residues of Kvβ subunits, potentially capable of catalyzing the transfer of the hydride from nicotinamide ring to the substrate, are conserved (Gulbis et al.,

1999). Corresponding residues in Kvβ1.1 wild type for hydride transfer are D119, Y124 and K152. Accordingly, three point mutations D119A, Y124F and K152A were introduced in Kvβ1.1 subunit designated "catalytic site mutations". Co-expression of Kvβ1.1Y124F or Kvβ1.1K152A with Kv1.5 attenuated the fast inactivation normally observed with Kvβ1.1 wild type co-expression. The Kv1.5/Kvβ1.1D119A channel did not show fast inactivation (Figure 6) at both ratios of tested cRNA 1:1 and 1:5. However during a longer (15s) depolarizing pulses Kv1.5/Kvβ1.1D119A channels showed accelerated C-type inactivation, when compared to Kv1.5 alone. Decrease of α:β cRNA injection ratio lead to a more pronounced effect of the

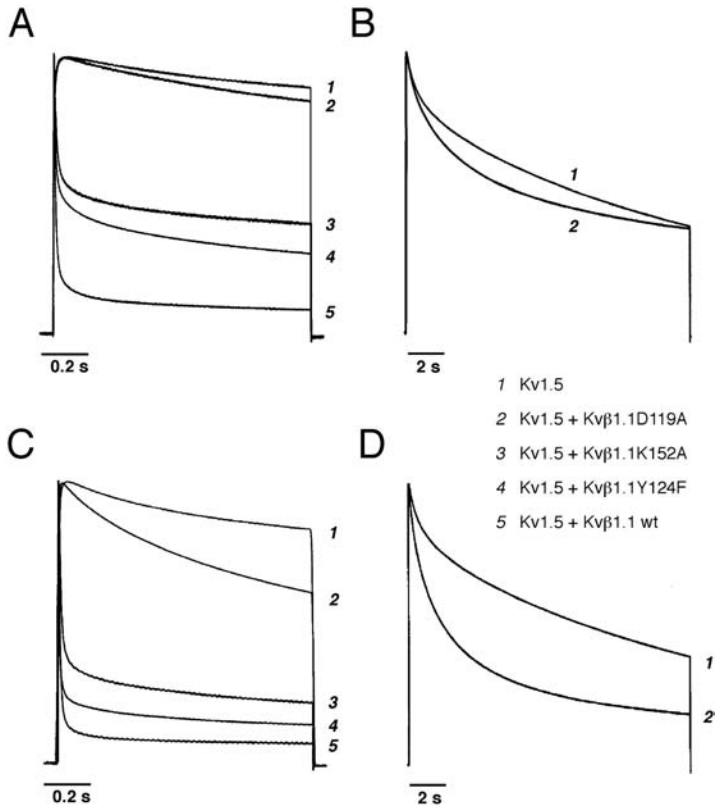

Figure 15. Examples of normalized outward currents mediated by Kv1.5 alone or co-expressed with wild-type Kvβ1.1 (Kv1.1wt) or with mutants Kvβ1.1D119A, Kvβ1.1Y124F, and Kvβ1.1K152A subunits, respectively. Currents were elicited in *Xenopus* oocytes using depolarizing steps from a holding potential of -80 mV to a test potential of +60 mV. ***A*** and ***B*** - the ratio α:β is 1:1, ***C*** and ***D*** – the ratio is 1:5. Leak currents have been subtracted. *Bars* indicate time calibrations. Recordings in ***A*** and ***B*** are from oocytes co-injected with 3 ng for both Kv1.5 and different Kvβ1.1 cRNA, whereas in ***C*** and ***D*** 3 ng of Kv1.5 and 15 ng of Kvβ1.1 cRNA were injected.

mutation D119A. Kinetic parameters obtained for Kvβ1.1 catalytic point mutation when co-expressed with Kv1.5 in Xenopus oocytes are shown in Table 6.

Subunits (ratio)	τ_1 (ms)	$RA_{(\tau1)}$ %	τ_2 (ms)	I_{1s}/I_{peak} %	$V_{1/5}$ (mV)	K_s (mV)	n
Kv1.5	608±21	22±2	12486±49	85±1	11.2±1.1	15.1±0.2	4
Kv1.5+Kvβ1.1wt(1:1)	6.8±0.7	92±1	172±8	10±1	17.4±2.0	19.7±0.6	17
(1:5)	5.4±0.5	96±1	104±7	5±1	17.9±0.9	17.6±0.1	9
Kv1.5+Kvβ1.1D119A	860±86	35±2	7313±521	81±3	36.3±1.7	20.2±0.5	25
(1:5)	627±28	48±1	4371±71	67±1	38.1±2.1	19.7±0.5	11
Kv1.5+Kvβ1.1Y124F	10.3±1.6	77±3	355±14	31±4	20.1±0.9	21.2±0.7	9
(1:5)	7.9±0.2	91±1	310±4	16±1	17.1±1.2	24.1±0.8	20
Kv1.5+Kvβ1.1K152A	11.1±1.0	74±2	354±6	36±1	27.4±1.4	27.3±0.8	10
(1:5)	8.2 ± 0.4	82 ± 3	311±19	30 ± 2	17.1±1.1	19.8±0.7	13

Table 6. Catalytic site mutant β subunits were co-expressed with Kv1.5 in Xenopus oocytes. Parameters of inactivation of channels are represented. Decaying phase of the current traces was fitted double-exponential. Currents were elicited by depolarizing pulses from –80 mv to +60 mV in 1s duration. τ_1 is the inactivation time constant, $RA_{(\tau1)}$ is the relative amplitude of fast component of decay, τ_2 is a slow inactivation time constant. I_{1s}/I_{peak} represents percentage current amplitude remaining after 1s. $V_{0.5}$ is voltage of half-maximal activation, **Ks** is the slope-factor for voltage-dependent activation.

3.2.2.3 Correlation of the effect of NADPH binding mutants and catalytic site mutants

In order to investigate the effect of prevention of the fast inactivation by point mutations at the catalytic site and mutations in NADPH binding sites, the double mutant β subunit, Kvβ1.1D119AQ248R was constructed. If oxidoreductase activity is coupled to inactivation in Kvβ1.1, the way of potential disruption of the Kvβ1.1 enzymatic activity should not change its effect on inactivation. If the D119A and Q248R mutation prevent fast inactivation of Kvβ1.1 by the same mechanism, then this effects should not be additive. If inactivation prevention is caused by different mechanisms, it is expected that the effect of D119A,Q248R double point mutation would be more pronounced, than the effect of both point mutations taken separately. Figure 16 shows example of normalized traces for Kv1.5 alone, and in combination with different Kvβ1.1 subunits (wild type, single point mutations, double point mutation). Table 7 summarizes the corresponding kinetic parameters of inactivation. The inactivation seen with the double mutant

Kvβ1.1D119AQ248R were identical with Kvβ1.1Q248R. Inactivation parameters of Kv1.5 in combination with Kvβ1.1Q248R were quite similar to once observed with Kvβ1.1D119A. However, Kvβ1.1D119A caused slightly slower inactivation at the second and third phase of the exponential decay.

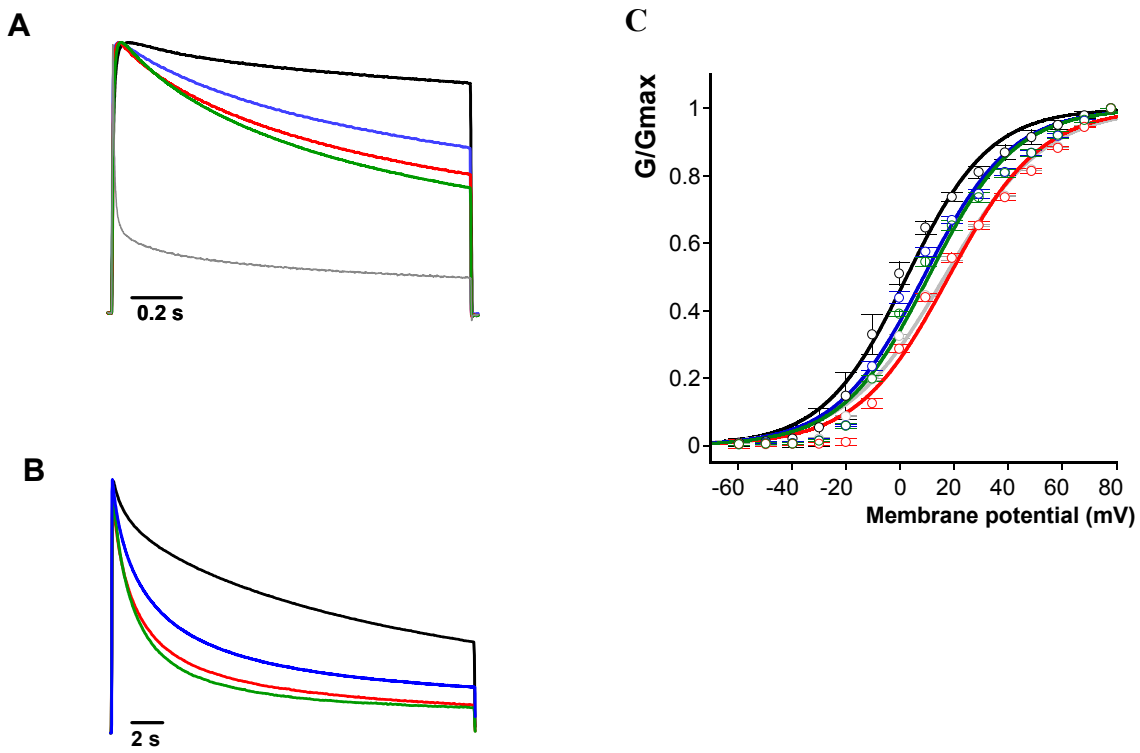

Figure 16. Comparison of inactivating activity of mutant beta subunits: ***A*** **-** inactivating activity of Kvβ1.1Q248R **(red*)***, Kvβ1.1D119A **(blue*)*** and double point-mutant Kvβ1.1D119AQ248R **(green)** is shown**.** Black curve represents current from homomeric Kv1.5 channels. Current traces elicited by depolarizing pulse from holding potential of –80 mV to +60 mV are represented as normalized curves. Leak currents have been subtracted. *Bars* indicate time calibrations. ***B*** **-** GV-curves of corresponding channel-complexes. The colours are the same as for *A*. Injected cRNA amounts were 0.1ng/oocyte for Kv1.5 alpha subunit and 2.5ng/oocyte for beta subunits correspondingly. The injected alpha to beta cRNA ratio was 1 to 25.

Comparing the current amplitudes remaining after 1 s and 15 s depolarizing pulses to +60 mV, showed that Kvβ1.1D119A changed the slow inactivation of Kv1.5 mediated currents slightly less effectively than the double mutant Kvβ1.1D119AQ248R. However, the important observation is, that the double mutant did not further slow inactivation, indicating that the effects of Kvβ1.1D119A and Kvβ1.1Q248R are not additive.

Subunits **(ratios are 1:25)**	τ_1 (ms)	**RA (τ_1) %**	τ_2 (ms)	**RA (τ_1) %**	τ_2 (ms)	**I_{1s}/I_{peak} %**	**I_{15s}/I_{peak} %**	**n**
Kv1.5	583±86	24±1.2	10177±496	-	-	82.9±1.3	37.2±1.3	5
Kv1.5+Kvβ1.1wt	5.4±0.3	95.5	299±19.4	-	-	13.0±2.9	-	5
Kv1.5+Kvβ1.1Q248R	76.1±9.4	19.1±2.6	677±20.2	56±3	4212±295	49.4±1.5	10.9±2.7	5
Kv1.5+Kvβ1.1D119A	126±61.9	19.4±8.6	614±53,5	33.8±2	6288±299	57.3±5.0	20.5±4.1	5
Kv1.5+Kvβ1.1D119A Q248R	125.9±38.7	19.1±1.5	751±24.5	60.2±1.5	3670±411	45.5±4.6	8.4±1.7	6

Table 7. Inactivation kinetics of Kv1.5 with and without Kvβ1.1 subunits. Curves (1s, +60mV) were fitted to double- and triple-exponential. τ_1 is the time constant of fast exponential decay, $RA_{(\tau_1)}$ is the relative amplitude of fast component in percentage. τ_2 is time constant of second component, $RA_{(\tau_2)}$ is relative amplitude of second component in percentage, I_{1s}/I_{peak}, I_{15s}/I_{peak} show percentage current amplitude remaining after 1 and 15 second depolarizing pulse at +60 mV.

3.3 Role of expression system

3.3.1 Kvβ3 confers rapid inactivation to Kv1 channels in CHO and HEK 293 cells.

As mentioned previously, Kvβ3 possesses a functional N-terminal "ball"-domain capable of mediating N-type inactivation. In mammalian cell-lines it has been shown, that co-expression of Kv1.5 with Kvβ3 leads to A-type currents (Leicher et al., 1998), although Kvβ3 failed to inactivate Kv1.5 in Xenopus oocytes. To investigate if Kvβ3-mediated rapid inactivation is specific to Kv1.5 or if it is generally applicable to all Kv1 channels, Kv1α subunits were co-expressed with Kvβ3 in CHO cells. Kv1.4 wild type channels possess an intrinsic auto-inhibitory domain, which causes a fast N-type inactivation of the channel upon depolarization (Jan and Jan 1996). In order not to confuse Kv1.4 autoinhibition and the Kvβ3-mediated inactivating on Kv1.4 channels, the first 110 amino acids were deleted from Kv1.4, which resulted in slowly inactivating Kv1.4Δ110 channels. The gating parameters for the Kv1 channels in absence and presence of Kvβ3 were compared. Currents mediated by a homomeric Kv1.1, Kv1.2, Kv1.3, Kv1.4Δ110, Kv1.5 and Kv1.6 channels, respectively, were measured in the whole-cell patch-clamp configuration in CHO cells. The currents showed slow and incomplete inactivation, described also as C-type inactivation (Rasmusson et al., 1998). Current decay of all channels, except of Kv1.4Δ110, could be fitted by a single exponential function. Kv1.4Δ110 was fitted by a double-exponential function. All Kv1 channels showed rapid N-type inactivation with Kvβ3, except Kv1.3. Kvβ3 conferred fast inactivation even to Kv1.6, which possesses an N-type inactivation prevention (NIP) domain for Kvβ1.1 within its N-terminal part (Roeper et al., 1998). The inactivation time constants ranged from 6-15 ms for the fast component, which accounted for 78-95% of the total decay (Table 7). Current decay of all Kv1/Kvβ3 channel complexes except of Kv1.4Δ110/Kvβ3, were fitted by a double-exponential function. Kv1.4Δ110/Kvβ3

currents were fitted using a triple-exponential function. Kvβ3 co-expression did not confer rapid inactivation to Kv1.3 channels. However, it caused a biphasic decay of the currents not seen with Kv1.3 in the absence of Kvβ3. Kv1.3 was co-expressed with both Kvβ3 and Kvβ1.1. Neither Kvβ3 nor Kvβ1.1 conferred a rapid inactivation to the Kv1.3. Moreover, both β subunits did interact functionally with Kv1.3 judged from the significant changes in inactivation gating. Inactivation parameters for all Kv1 channels are summarized in Table 8.

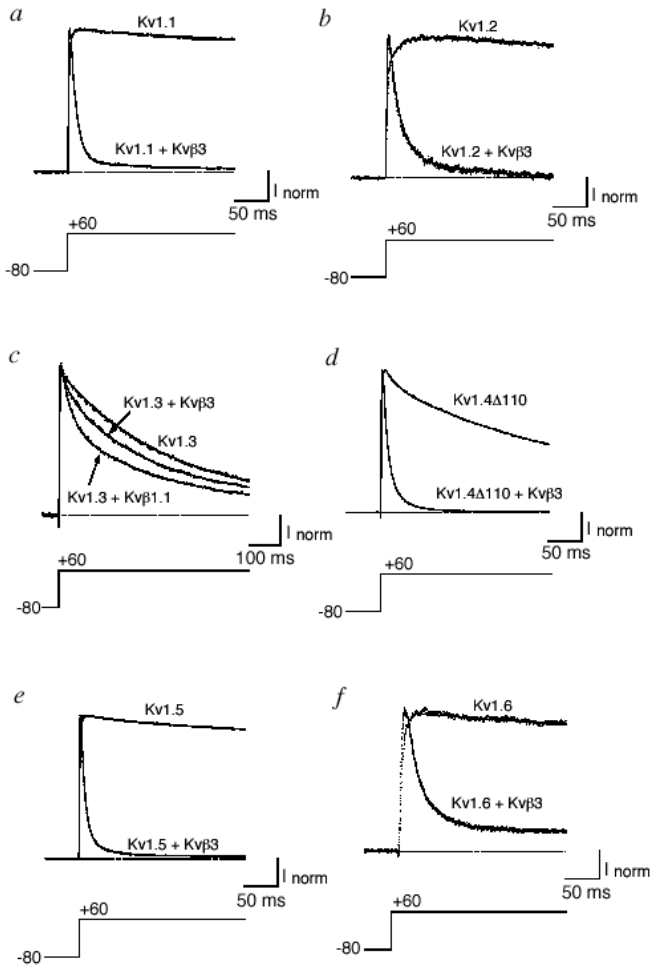

Figure 17. Normalised current traces of Kv1 channels alone and co-expressed with Kvβ3. Current were elicited by depolarizing the CHO cell membrane from –80 mV to +60 mV. Normalized whole-cell currents traces are shown for Kv1.1 (a), Kv1.2 (b), Kv1.3 (c), Kv1.4Δ110 (d), Kv1.5 (e) and Kv1.6 channels (f) alone and with Kvβ3.1. Kv1.3 was also tested with Kvβ1.1. Note different time scale for Kv1.3-mediated currents. Fitting curves are superimposed on the current traces, and dotted lines represent zero current.

In contrast to Kvβ1.1 and Kvβ2, which can shift the activation curve of channels to more negative potentials (Uebele et al., 1998, Accilli et al., 1997), Kvβ3 did not cause considerable changes in the voltage-dependent activation, as calculated from peak current amplitudes (Figure 15).

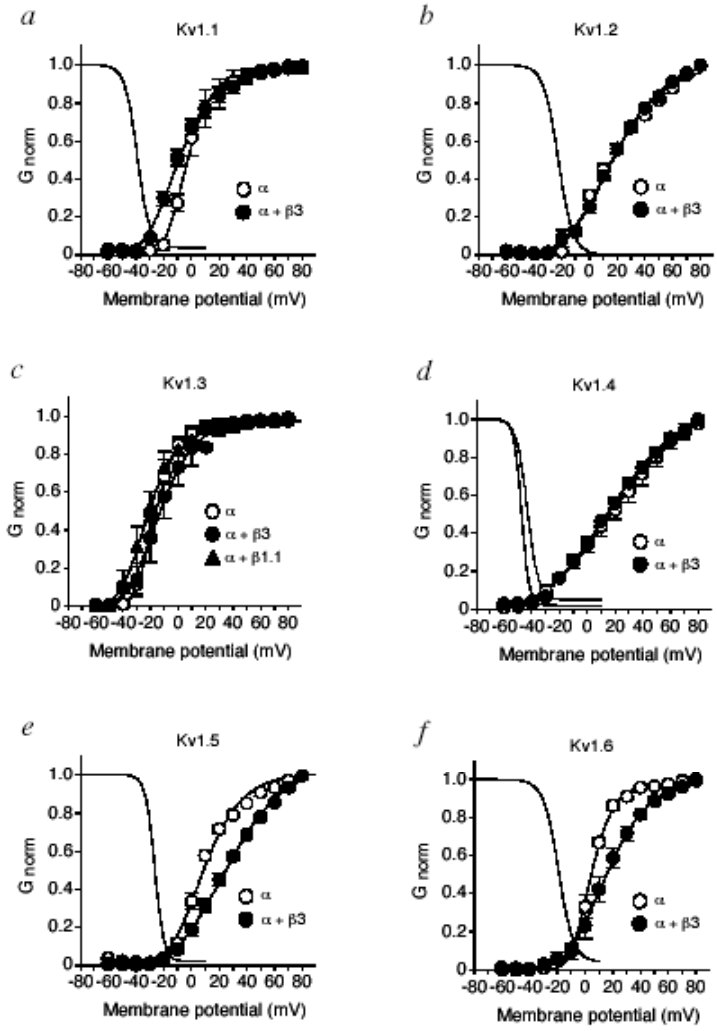

Figure 18. The voltage-dependence of the activation of homomeric Kv1, and heteromeric Kv1/Kvβ3 channels. Normalized GV-curves in the absence and presence of Kvβ3 were calculated from peak currents amplitudes recorded in whole-cell configuration of patch-clamp. CHO cells were transfected with Kv1.1 (a), Kv1.2 (b), Kv1.3 (c), Kv1.4 (d), Kv1.5 (e) or Kv1.6 (f) cDNA alone, and together with Kvβ3 cDNA at 1:10 ratio. A series of test pulses from holding potential -80 mV to different potentials in 10 mV increments were applied to determine the voltage-dependence of activation.

To test whether the expression in other mammalian cell-lines may also allow Kvβ3-mediated fast inactivation, K1.5 was co-expressed with Kvβ3 in HEK 293 cells and whole-cell currents were measured. Figure 19 shows N- type inactivation of the Kv1.5/Kvβ3 channels expressed in HEK 293 cells. In the HEK 293 expression system, similar to CHO expression system, co-expression of Kvβ3 conferred rapid inactivation to Kv1.5. However decay kinetics in HEK 293 cells were

Channel	τ_1 (ms)	$RA_{(\tau 1)}$ (%)	τ_2 (ms) [(iii)] τ_3 (ms)	$\tau_{f\,OFF}$ (ms)	$RA\tau_{f\,OFF}$ (%)	$\tau_{s\,OFF}$ (ms)
Kv1.1	582 ± 72 (n=3)	-	-	*n.d*	-	-
Kv1.2	1242 ± 202 (n=8)	-	-	*n.d.*	-	-
Kv1.3	382 ± 22 (n=6)	-	-	9.0 ± 2.0 (n=4)	-	-
Kv1.4	25.4 ± 7.2 (n=7)	93 ± 2	131 ± 22	14.8 ± 2.8 (n=5)	-	-
Kv1.4Δ110	86 ± 18 (n=5)	30 ± 7	619 ± 206	*n.d.*	-	-
Kv1.5	635 ± 65 (n=7)	-	-	*n.d.*	-	-
Kv1.6	666 ± 45 (n=4)	-	-	*n.d.*	-	-
Kv1.1 + Kvβ3	5.7 ± 1.3 (n=3)	95 ± 1	59 ± 18 -	389 ± 57 (n=3)	-	-
Kv1.2 + Kvβ3	6.2 ± 0.4 (n=5)	85 ± 6	74 ± 23 -	171 ± 40 (n=4)	63 ± 7	1.8 ± 4.1
Kv1.3 + Kvβ3	104 ± 28 (n=7)	20 ± 2	436 ± 67 -	-	-	10.1 ± 1.5 (n=5)
Kv1.3 + Kvβ1.1	37 ± 6 (n=6)	32 ± 5	294 ± 17 -	-	-	9.4 ± 0.6 (n=3)
Kv1.4 + Kvβ3	8.1 ± 0.5 (n=4)	89 ± 2	34 ± 6 [(iii)] 359 ± 81	-	-	n.d.
Kv1.4Δ110 + Kvβ3	7.1 ± 0.7 (n=11)	78 ± 4	28 ± 3 [(iii)] 279 ± 30	-	-	4.8 ± 0.7 (n=5)
Kv1.5 + Kvβ3	5.6 ± 0.5 (n=10)	91 ± 1	44 ± 8 -	445 ± 107 (n=3)	14 ± 2	2.8 ± 4.8
Kv1.6 + Kvβ3	15.3 ± 1.7 (n=14)	90 ± 2	249 ± 36 -	435 ± 41 (n=4)	72 ± 3	7.0 ± 5.2

Table 8. Gating parameters of different Kv1 channels in absence and presence of Kvβ3. Curves were fitted single-exponential for Kv1, and double-exponential in the case of Kv1/Kvβ3 combinations. Current of both Kv1.4wt and Δ110Kv1.4 could be adequately fitted by double-exponential function. Currents from co-expressed Kv1.4/Kvβ3 channel complexes were fitted to triple-exponential. Current were elicited by depolarizing pulse from holding potential of –80 mV to +60 mV. τ_1 is the time constant of fast exponential decay, **RA(τ_1)** is the relative amplitude of fast component, τ_2 and τ_3 are the time constants of second and third components, correspondingly. $\tau_{f\,OFF}$ and $\tau_{s\,OFF}$ are fast and slow time constants of recovery of the channels from inactivation at –80 mV. **n.d**.- indicates that values are not determined.

almost two times slower than in CHO cells (Table 9, for comparison see Table 8). Current traces of homomeric Kv1.5 channels could be only adequately fitted with two exponential function, albeit the first component contributed only 37% to the total current decay.

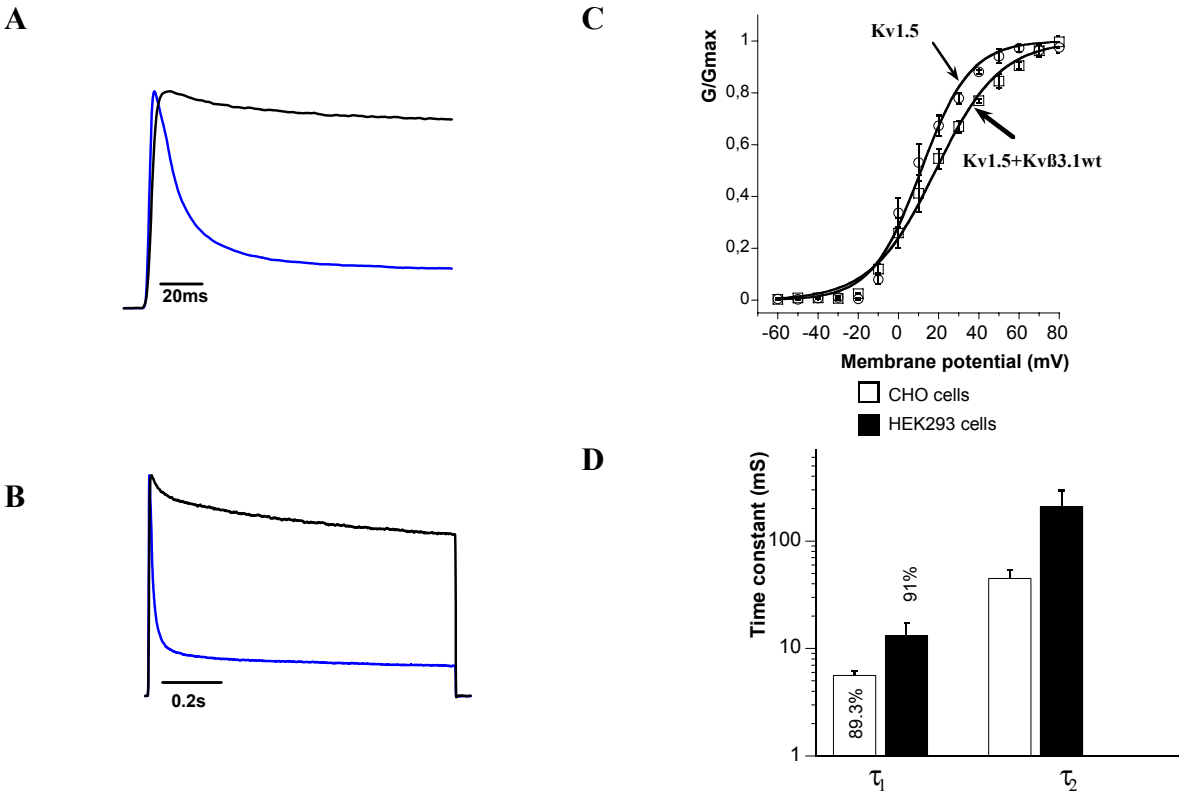

Figure 19. Fast inactivation of Kv1.5 upon co-expression with Kvβ3 subunit in HEK 293 cells. ***A and B.*** Whole-cell currents were recorded from HEK 293 cells transfected with Kv1.5 alone **(black)**, and with Kvβ3 **(blue)** shown in 150 ms and 1s time scales. Current were elicited by depolarising the membrane from –80 mV to +60 mV. ***C*** – The normalized conductance-voltage relationship for Kv1.5 (n=5) and Kv1.5/Kvβ3 (n=6) are shown. ***D*** **-** Comparison of inactivation time constants in HEK 293 (**filled bars,** n=5) and in CHO (**empty bars,** n=10) cell-lines. τ_1 is the fast, and τ_2 is the slow inactivation time constant of double-exponential fit. Numbers above the bars show the relative amplitude of the corresponding fast component.

Subunits	τ_1 (ms)	RA (τ_1) (%)	τ_2 (ms)	I_{1s}/I_{peak} (%)	$V_{1/2}$ (mV)	Ks (mV)
Kv1.5	39.6± 12,3 (n=4)	37±15 (n=4)	689±198 (n=4)	68.8±7.4 (n=4)	11.1±4.0 (n=3)	11.9±0.45 (n=3)
Kv1.5 + Kvβ3	13.2±4.12 (n=9)	89 ± 4 (n=9)	209 ± 85 (n=9)	12.5±5.64 (n=9)	18.5±6.37 (n=5)	15.6±1.17 (n=5)

Table 9. Inactivation kinetics of Kv1.5 channel alone, and in presence of Kvβ3 subunit. Curves were fitted with a single-exponential function for Kv1.5, and with double-exponential function for Kv1/Kvβ3 combinations. Current were recorded by depolarising the membrane from a holding potential of –80 mV to +60 mV. τ_1 is time constant of fast exponential decay, $RA_{(\tau_1)}$ is the relative amplitude of fast component. τ_2 is the time constant of second component. **n.d.** – not determined.

3.3.2 Effect of mutations in the nucleotide coenzyme binding sites and hydride transfer residues on the Kvβ1.1-mediated inactivating activity in mammalian cells.

To investigate if the prevention or impairment of the nucleotide coenzyme binding in Kvβ1.1 affects the Kvβ1.1-medited inactivation in CHO cells, corresponding mutant subunits were functionally co-expressed with Kv1.5 and whole-cell current were recorded. Wild type Kvβ1.1, which served as a control, conferred a rapid inactivation to Kv1.5 channels. These data corresponded well with previously reported results (Leicher et al., 1996). However, both Kvβ1.1 mutant subunits with compromised nucleotide coenzyme binding affinity caused inactivation with significantly slow kinetics (two times larger time-constants) than Kvβ1.1wt (Figure 20). Also the relative amplitude of the fast components of current decays was lower than Kvβ1.1 subunits with Kv1.5. These effects were slightly more pronounced for Kvβ1.1R298E than for Kvβ1.1Q248R (Table 10). However, both Kvβ1.1Q248R and Kvβ1.1R298E were able to confer N-type inactivation to Kv1.5 channels in CHO cells.

Similar to the nucleotide coenzyme binding mutants, the putative oxidoreductase catalytic site mutants, Kvβ1.1D119A and Kvβ1.1Y124F were co-expressed with Kv1.5 in CHO cells and

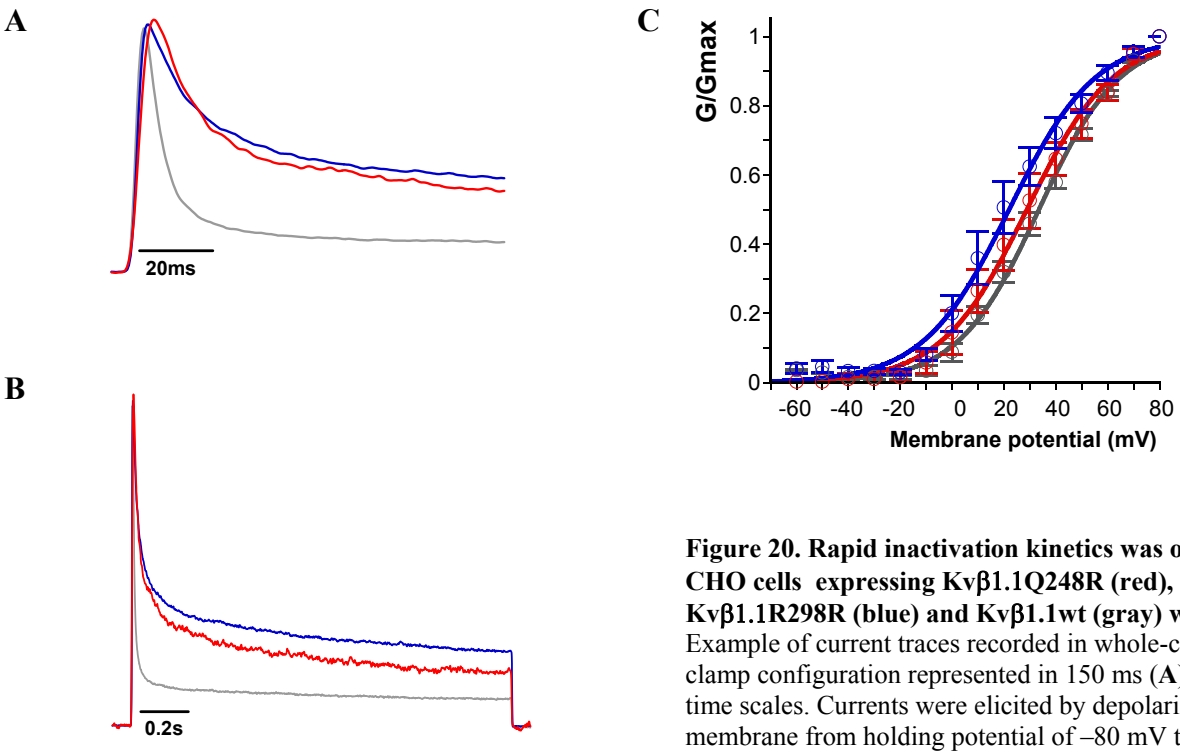

Figure 20. Rapid inactivation kinetics was obtained in CHO cells expressing Kvβ1.1Q248R (red), Kvβ1.1R298R (blue) and Kvβ1.1wt (gray) with Kv1.5. Example of current traces recorded in whole-cell patch-clamp configuration represented in 150 ms (**A**), and 1s (**B**) time scales. Currents were elicited by depolarization of the membrane from holding potential of –80 mV to +60 mV. ***C*** **–**Corresponding conductance-voltage relationship of co-expressed channels. The transfected cDNA ratio for different channels was always α:β=1:10. Number of experiments and kinetic parameters are shown in Table 10.

Subunits	τ_1 (ms)	RA (τ_1) (%)	τ_2 (ms)	I_{1s}/I_{peak} (%)	$V_{1/2}$ (mV)	Ks (mV)	n
Kv1.5+Kvβ1.1wt	5.98±0.83	95.7±2.8	208±43.5	8.02±5.14	33.5±1.4	15.7±2.2	8
Kv1.5+Kvβ1.1Q248R	14.3±2.8*	81.6±6.8	345±104	17.5±4.46*	27.2±3.9	16.5±1.3	6
Kv1.5+Kvβ1.1R298E	12.5±2.5*	83.7±9.2	362±71.7	19.9±14.4*	26.4±8.7 (n=3)	16.4±1.4 (n=3)	7
Kv1.5+Kvβ1.1D119A	11.2±3.7*	76.4±10.7	400±142	31.3±13.2 *	n.d.	n.d.	5
Kv1.5+Kvβ1.1Y124F	9.67±6.01	90.1±8.66	241±139	17.7±13.5	n.d.	n.d.	3

Table 10. Inactivation parameters for Kv1.5 in presence of different Kvβ1.1 subunits in CHO cells. Curves were fitted with double-exponential function. τ_1 is the time constant of fast component of the double-exponential decay, **RA**$_{(\tau_1)}$ is the relative amplitude of fast component. τ_2 is the time constant of slow component, respectively. With asterisk are shown the values that are significantly different form Kv1.5/Kvβ1.1 at 0.05 level (Students T-test). **n.d.** - indicated that values are not determined.

kinetic parameters of inactivation were analysed. Kvβ1.1D119A co-expression conferred rapid inactivation to the Kv1.5, which was significantly slower than the Kvβ1.1wt-mediated inactivation (Figure 21). Its effect was very similar to the inactivating effect of the NADPH defective subunits. By contrast, Kvβ1.1Y124F co-expression with Kv1.5 resulted in currents that were not significantly different from Kv1.5/Kvβ1.1wt mediated once (Table 10).

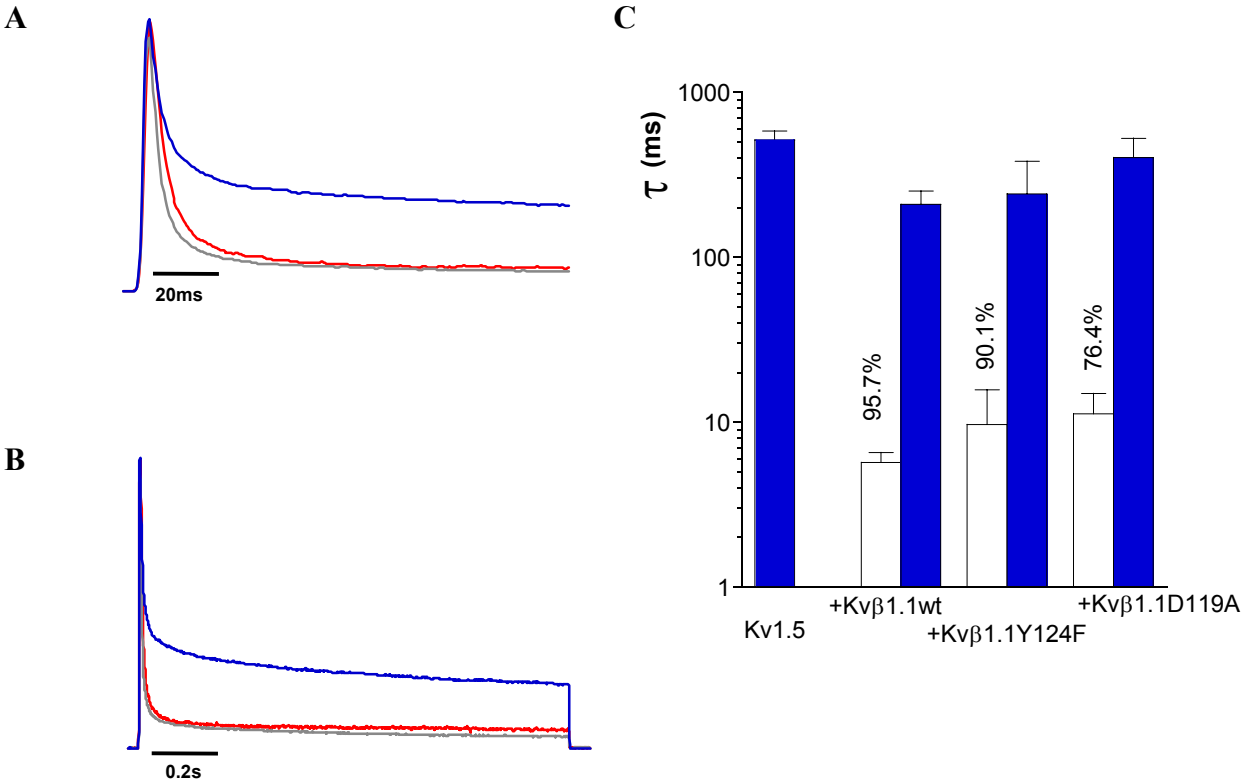

Figure 21. Catalytic site mutant subunits of Kvβ1.1 confer fast inactivation to Kv1.5 in CHO cells. Example of whole-cell current traces of co-expressed Kv1.5/Kvβ1.1wt **(gray,** n=8**)**, Kv1.5/Kvβ1.1Y124F **(red,** n=3**)** and Kv1.5/Kvβ1.1D119A **(blue,** n=4**).** cDNA ratio in transfection mixture was α:β=1:10 for all combinations. Current were elicited by depolarizing pulse from –80 mV to +60 mV with 150 ms **(*A*)** and 1s **(B)** durations.
***C*-** comparison of inactivation time constants. Empty bars represent the fast components, and the blue ones the slow components of current decay, respectively. The numbers above the bars represent the relative amplitude of corresponding fast component in percents.

In terms of technical approach, one main difference between measurements in two-electrode voltage-clamp and patch-clamp is, that in the first case the cellular cytoplasm remains unaffected, whereas in the second case, intracellular components are washed out. In our

experiments, dilution of the intracellular nucleotide coenzymes and/or substrate of the β subunits could have an effect on Kvβ-mediated N-type inactivation. To avoid a dilution of intracellular factors, recordings were performed using the perforated-patch method. For this purpose, a porous antibiotic Amphotericin B was added to the patch-pipette solution. For these experiments Kvβ1.1Q248R, with a decreased nucleotide binding affinity was chosen. Series resistance (Rs) values were critical factors for these measurements, which required a proper voltage clamp of the cell membrane in whole cell configuration. Current traces from cells with Rs values above 12 MΩ were not analysed. To account for possible effects of Amphotericin B and membrane clamp artefacts during recording, experiments were also performed in whole-cell mode and with Amphotericine B in the pipette. Experimental artefacts could be excluded during recording from Amphotericin B perforated CHO cells, because the current traces, recorded in the whole-cell and the perforated-patch configurations were identical (Figure 22A,B).

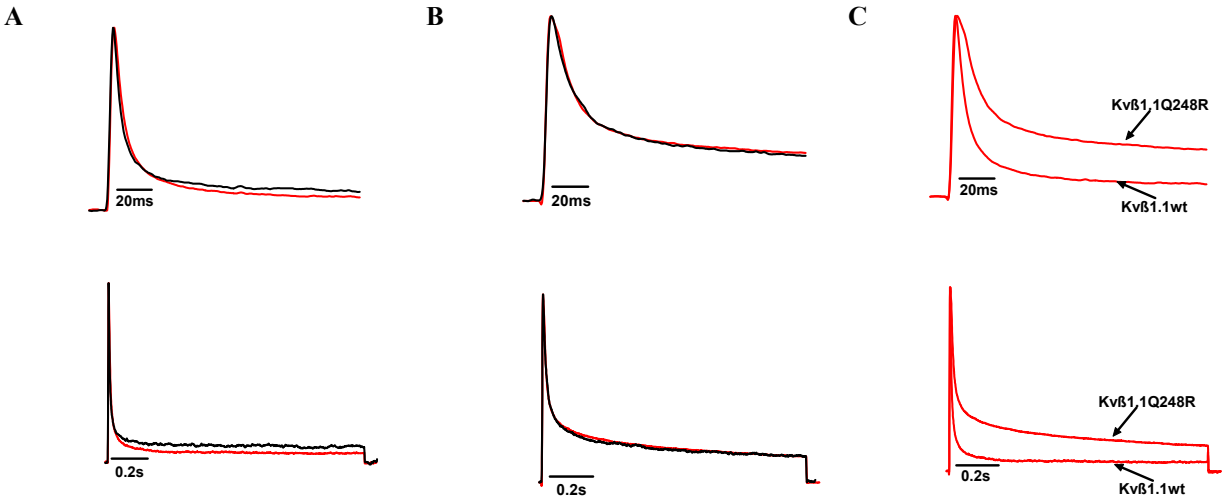

Figure 22. Example of current traces recorded in whole-cell and perforated-patch configuration of patch-clamp technique from CHO cells co-transfected with Kv1.5 and with different Kvβ1.1 subunits. Whole-cell recordings are shown in black, the perforated-patch ones in **red.** Concentration of Amphotericin B in the patch-pipette was 0.2 - 0.4 µg/µl.
***A* -** Comparison of Kvβ1.1wt-mediated inactivation in whole-cell and perforated-patch recordings.
B- Comparison of Kvβ1.1Q248R-mediated inactivation recorded in whole-cell and perforated-patch modes.
C- Comparison of inactivating activity of Kvβ1.1wt and Kvβ1.1Q248R in perforated-patches.
CHO cells were transfected with appropriate α:β cDNA ratio of 1:10. Current were elicited by depolarizing pulse from –80 mV to +60 mV.

Subunits	τ_1 (ms)	RA (τ_1) (%)	τ_2 (ms)	I_{1s}/I_{peak} (%)	$V_{1/2}$ (mV)	Ks (mV)	n
Kv1.5+Kvβ1.1wt whole- cell	4.16±0.46	94.4±1.3	121±39.8	5.95±0.35	31.4±2.7	18.4±3.2	3
Kv1.5+Kvβ1.1wt Perforated patch	5.48±0.30	93.2±0.36	147±19.5	7.08±1.79	30.3±1.7	17.9±0.9	4
Kv1.5+Kvβ1.1Q248R whole-cell	14.1±1.32	76.6±2.19	305±26.6	19.4±1.	21.0±1.6	16.8±0.5	7
Kv1.5+Kvβ1.1Q248R Perforated patch	15.3±1.61	78.2 ±3.27	322.8±32.7	18.1±3.93	21.9±1.2	16.5±0.5	5

Table 11. Inactivation parameters of Kv1.5 co-transfected with different Kvβ1.1 subunits in whole-cell and perforated-patch configurations of patch-clamp technique. Currents, elicited by 1s depolarizing pulse from –80 mV to +60 mV, were fitted to double exponential function. τ_1 is the time constant of fast exponential component of decay, $RA_{(\tau_1)}$ is the relative amplitude of fast component, τ_2 is the time constant of second component, I_{1s}/I_{peak} is the fraction of remaining current after the 1s depolarizing pulse. $V_{1/2}$ is the voltage of half-maximal activation, **Ks** is the slope of activation curve. **n** is the number of experiments.

The comparison of data obtained from perforated-patch recording of transfected CHO cells shows, that inactivation parameters for both Kv1.5/Kvβ1.1wt and Kv1.5/Kvβ1.1Q248R are correspond well with those recorded in whole-cell mode (Table 11).

4. Discussion

In the present study the permissive structural determinants in Kvα and the role of the oxidoreductase features of the Kvβ subunits in Kvβ-mediated inactivation was investigated. Our experimental results show following functional aspects: 1) non-cytoplasmatic domains of potassium channels can dramatically influence the Kvβ-mediated inactivating activity; 2) Kvβ3 inactivating function is regained by replacement of homologous Kvβ1.1 regions from C-terminus. These regions overlap with NADPH binding domains of Kvβ subunits; 3) Kvβ1.1 is able to bind reversibly nucleotide coenzymes with high affinity; 4) NADPH binding properties of Kvβ1.1 are important for its inactivating activity when co-expressed with Kv1 channels; 5) This correlation varies depending on heterologous expression system.

4.1 Permissive and non-permissive structures for N-type inactivation

The mechanism of the fast inactivation of potassium channels has been intensively investigated during the past five decades (Aldrich 2002). The crystal structure of KscA potassium channel in the presence of pore blocking ion tetra-butyl-ammonium (TBA), and the double mutant-cycle analysis of interaction between inactivation gate of the Kvβ1.1 and its receptor site in S6 elucidated the important details of N-type inactivation (Zhou et al., 2002). The first 4-6 amino acid residues in the Kvβ1.1 N-terminus represent the inactivation gate of Kvβ1.1, which sneaks its way into the pore of the channel through so-called "lateral windows" (Sokolova et al., 2001, Kobertz et al., 2000), constituted by connections between the transmemrane segments and the cytoplasmic tetramerization domain via the T1-S1 linker (Figure 1B). The T1 domain of Shaker-related potassium channels represents the interaction site for beta subunits

(Gulbis et al., 2000). Kv2.1 do not interact with Kvβ subunits (Nakahara et al., 1996), apparently due to differences in T1 domain (Bixby et al., 1999). The Kv2.1 N-terminus contains a putative Zn^{2+} binding motive (Bixby et al., 1999). Mutations of protein residues, that are assumed to coordinate the Zn^{2+}, influenced the gating of Kv2.1 (not shown). However, the replacement of Kv2.1 N-terminus by respective part of the Kv1.2 did not rescue inactivating function of Kvβ1.1. One can argue that the structure of whole T1-Linker-S1 region is completely different in Kv2.1, because it possesses a Zn^{2+} binding motif (Bixby et al., 1999), and this could change the topology of lateral windows in Kv2.1, as well as in ChimA. However, ChimC contain the Kv1.2 sequence up to S4, but do not show Kvβ1.1-mediated rapid inactivation either.

Apparently, the receptor site of Kv2.1 in S6 region has a lower affinity for the Kvβ1.1 inactivating domain than the Kv1.2 receptor, but comparison of Kvβ1.1-mediated inactivation of ChimA and ChimB (Figure 4C; Figure 5) suggests, that these slight differences of affinity are not responsible for absence of rapid inactivation in Kv2.1. Comparison of Kvβ1.1-mediated inactivation of ChimB with those of Kv1.2 or ChimG shows, that the slight increase in current decay in presence of Kv1.2 receptor site can not explain attenuation of Kvβ1.1-induced inactivation of chimeras ChimA. These data suggest, that differences in receptor site account only mildly for Kvβ-mediated inactivation of channels.

However, increasing amount of evidence about the influence of other parts of the channel on Kvβ-mediated fast inactivation is being collected. For example, the distal N-terminal domain (NIP domain) can prevent Kvβ1.1-mediated fast inactivation in Kv1.6 (Röper et al., 1998). Only complete replacement of Kv1.5 N-terminus can rescue the fast inactivation of the Kv1.3 channel in the presence of Kvβ1.1 (not shown). Kv2.1 is closely related to Kv1 subfamily members, and, therefore, it is assumed that these channels have similar topological structure. However, our results, obtained by recordings from chimeric Kv1.2/Kv2.1 channels co-expressed with Kvβ1.1, showed that the large region including the S1-S5 and P-loop in Kv2.1 may eliminate the process

of Kvβ1.1-induced N-type inactivation. Surprisingly, cytoplasmatic linkers S2-S3 (L_{S2-S3}) and S4-S5 (L_{S4-S5}) alone play a minor role, as co-expression experiments of ChimC and ChimG with Kvβ1.1 showed (Figure 7), since replacement of these linkers by Kv1.2 homologous regions did not rescue Kvβ1.1-mediated inactivation of Kv2.1 (Figure 7A, E).

The structure of the cytoplasmatic C-terminus of mammalian Kv1 channels is largely unknown. It is assumed, that Kvβ-mediated inactivation is not interfered by the topology of the C-terminus and other cytoplasmic elements. Kv2.1 possesses a large cytoplasmic C-terminus, which does not interfere with Kvβ1.1-mediated inactivation, as co-expression of ChimF (Figure 7D) and C-terminally truncated ChimA (not shown) with Kvβ1.1 indicate.

Based on our data with chimeric channel investigations, we propose, that the S1-S5-Ploop region, in interplay with the pore of the channel may play a role in preventing the Kvβ1.1-mediated inactivation. How the membrane imbedded segments influence the process of inactivation is not yet clear. One possibility is, that the transmembrane segments can influence the topology of the cytoplasmic structures, which may affect the path, which inactivating gate passes to reach its receptor site.

Our data show, that Kvβ1.1 inactivating gate and its receptor site lying deep in the pore of channel are necessary but not sufficient for fast inactivation. Kvβ1.1-mediated inactivation could be prevented or permitted by as yet unknown structure(s) in potassium channels α subunits.

4.2 Kvβ subunits and redox-regulation of membrane excitability

The regulation of membrane excitability may be achieved by direct modulation of membrane embedded ion channels based on different cytoplasmic mechanisms. In paricular, it has been shown, that potassium channels may be candidate molecules for oxygen sensing Haddad and Liu 2000, Patel and Honore 2001, Coppock et al., 2001). It has been proposed also,

that in hypoxia-resistance pulmonary arterial smooth muscle cells (PASMC), the upregulation of Kvβ subunits may play a crucial role (Coppock and Tamkun 2001). In HEK 293 cells, co-expression of Kvβ2 confers O_2 sensitivity to Kv2.1 channels (Coppock and Tamkun 2001). Since it is known, that Kvβ2 does not interact with Kv2.1 to form α4/β4 complexes (Nakahira et al., 1996), Kvβ2 may somehow indirectly be involved in O_2 sensing. The molecular mechanism of this processes is not known. On the other hand, Kvβ subunits are the members of the aldo-keto reductase (AKR) superfamily of enzymes that catalyze the reduction or oxidation of different small molecular weight carbonyl substrates (Jez et al., 1997). Most of these substrates are involved in the protection of cells by detoxification of reactive oxygen countering molecules (Kubiseski et all., 1992), that may cause an inhibition of various membrane transport mechanisms (Grimshaw et al., 1990). Kvβ subunits play a role in connecting the cellular redox state to membrane excitability. As Figure 11 shows, NADPH binding properties of Kvβ subunits may determine the inactivation properties of heteromeric Kv1.5/Kvβ1.1 channels. It is possible, that Kvβ subunits sense the redox state of the cell, and accordingly modulate ion channel properties. Table 4 gives the nucleotide coenzyme binding affinities for Kvβ1.1 and Kvβ2. Which coenzyme nucleotide could be bound to the Kvβ1.1 will depend on the concentration of oxidized nucleotides coenzyme, such as: $NADP^+$, NAD^+ and reduced NADPH, NADH. This is given by following equation:

$$Y_{\mathrm{NADPH}} = \left(1 + \left\{\frac{K_d^{\mathrm{NADPH}}}{[\mathrm{NADPH}]}\right\} + \left\{\frac{K_d^{\mathrm{NADPH}}[\mathrm{NADP^+}]}{\mathrm{K_d}^{\mathrm{NADP^+}}[\mathrm{NADPH}]}\right\}\right)^{-1}$$

(Liu et al., 2001)

where Y_{NADPH} is the fraction of the enzyme that has bound NADPH, K_D^{NADPH} and K_D^{NADP+} are the dissociation constant for NADPH and $NADP^+$ -enzyme complex, respectively, [] – refer to the intracellular concentration of corresponding nucleotides.

Despite the lower affinity of Kvβ subunits for NAD^+ and NADH, they may also play a role by competing with NADPH and $NADP^+$, because it is known that the concentrations of NAD^+ and NADH are in order of magnitude higher than $NADP^+$ and NADPH concentration in the cell (Hoek and Rydstrom 1988). The relative concentrations of nucleotide coenzymes change during the oxidative stress occurring in stroke, Parkinson's disease, Alzheimer's disease (Adams et a., 2001). In these conditions, Kvβ subunits may play a crucial role in developing defense mechanism for cell survival.

Among Kvβ1.1 catalytic site mutations, the most pronounced effect on the Kvβ1.1-mediated inactivation in Xenopus oocytes was obtained with D119A. Like in other AKR family members, D119A together with the conserved lysine (Figure 20) forms hydrogen-bond/salt-bridge network in Kvβ2 (Gulbis et al., 1999). This arrangement of catalytic residues in AKR enzyme decreases pK_a of catalytic tyrosine (Y124 in Kvβ1.1), which is necessary for the proton donation by hydroxyl group of tyrosine (Jez et al., 1997). However, the aspartic acid residue at the catalytic site may also have a role in coordination of NADPH molecule (Figure 23). Whether the D119A mutation disrupts Kvβ1.1-mediated inactivation through affecting NADPH binding, or directly eliminating putative catalytic activity of protein is arguable. Further investigations of NADPH binding properties of Kvβ1.1D119A could elucidate this issue. The Y124F mutation had less pronounced influence on Kvβ1.1-induced rapid inactivation than D119A (Figure 9). However, the corresponding tyrosine mutation in the other members of AKR superfamily completely

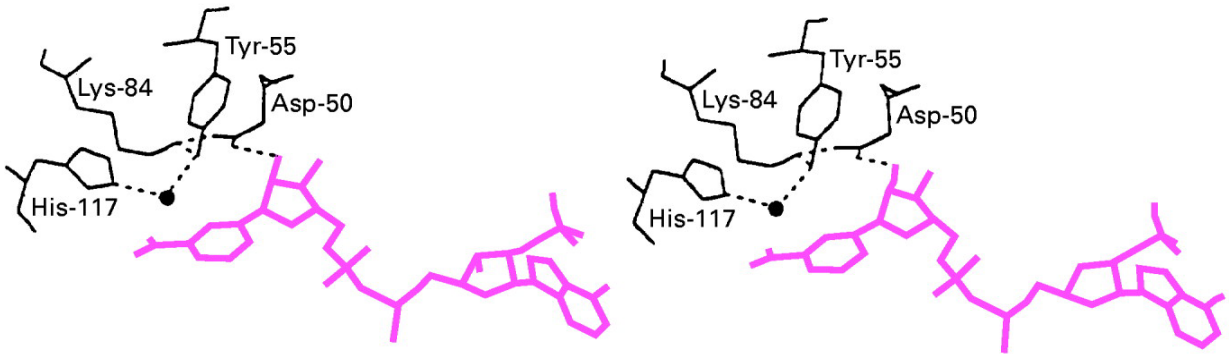

Figure 23. Steriovіew into the 3D structure of 3a-HSD–NADPH complex representing typical architecture of the active site of AKR superfamily. The side-chains of tyrosine and aspartic acid residues form hydrogen-bond/salt-bridge complex. The hydrogen bond is also formed between the groups of ribose -OH in NADPH and CO^- group of ASP-50. NADPH molecule is depicted in rose color, the protein residues are black (Jez et al, 1997).

abolished their catalytic activity (Tartle et al., 1993, Pawlowski and Penning 1994). The effect Kvβ1.1K152A on Kvβ1.1-mediated inactivation of Kv1.5 was quite similar to the one of Kvβ1.1Y124F. As two of three catalytic site mutations of Kvβ1.1 influenced only modestly the Kvβ1.1-induced inactivation, it is likely, that Kvβ1.1-mediated inactivation is modulated mainly, or exclusively, by the nucleotide coenzyme binding, and not primarily by the putative catalytic activity of Kvβ1.1. As mentioned above, the D119A mutation may change NADPH binding properties of Kvβ1.1, which was shown to eliminate Kvβ1.1-induced inactivating activity (see Kvβ1.1Q248R and Kvβ1.1R298E). This hypothesis would be in agreement with the investigation, showing that Kvβ2Y90F-expressing mice had no overt phenotype, whereas Kvβ2-null mice had occasional seizures, reduced life span, cold swim-induced tremors (McCormack et al., 2002). This means that, Kvβ1.1Y124F may still be able to catalyze the enzymatic reaction, like the corresponding mutant members of AKR. The modest effect of Kvβ1.1Y124F on Kvβ1.1-mediated inactivation in Xenopus oocyte (Figure 6) indicates that this mutant may retain partial catalytic activity.

4.3 Changeable Kvß-mediated inactivation between expression systems

In contrast to the Xenopus oocyte expression system, Kvβ3 co-expression confers fast N-type inactivation to most Kv1 channels in mammalian cell-line like CHO and HEK cells . This confirmed the previous results, that Kvβ3.1 possesses functional inactivation domain. Kvβ3 apparently, requires certain physiological conditions in order to be "active" (cause fast inactivation). This means, that its function may be physiologically regulated as described above. The cytoplasmic concentration of nucleotide coenzymes and/or putative substrate molecules, as well as the character of putative substrate(s) may vary in different cell types. This could explain the observed differences in inactivating activity of Kvβ3 in the Xenopus oocyte and in the CHO cell expression systems, respectively. In HEK 293 cells Kvβ3 co-expression conferred fast inactivation to Kv1.5 channels, which was almost 2 times slower than in CHO cells. This implies that in HEK 293 cells Kvβ3-mediated inactivation regulation so that, non-inactivating mode of Kv1.5/Kvβ3 is favored.

Although in their core domains Kvβ1.1 and Kvβ3 have 86 % amino acid identity, our data indicate, that two domains determine the different inactivating properties in Xenopus oocytes. The distinct amino acid sequence with Domain I and Domain II (Figure 9) in Kvβ3.1 may disrupt enzymatic activity or change its substrate-specificity.

Kvβ1.1 loss of function mutants (NADPH binding and catalytic site mutants) when co-expressed with Kv1.5 in CHO and HEK 293 cells do show significant changes in inactivation kinetics as compared to the Kvβ1.1 wild type. However, Kvβ-mediated N-type inactivation still accounted for 70-90% of the current decay. Apparently, in contrast to the Xenopus oocyte expression system, in CHO and HEK 293 cells, changing the nucleotide coenzyme binding properties does not dramatically influence inactivating activity of Kvβ1.1. The data obtained by recordings in perforated-patches configurations from CHO cells transfected with Kv1.5/Kvβ1.1

and Kv1.5/Kvβ1.1Q248R indicate, that intracellular factors of the cells (nucleotide coenzymes, putative substrate molecules of Kvβ subunits) do not play a role for mentioned discrepancies in Kv1.5/Kvβ1.1Q248R inactivation kinetics in mammalian cells and Xenopus oocytes. Apparently, some other unknown factors may influence the Kvβ-mediated inactivation in mammalian cell lines.

The regulation of expression and trafficking of ion channels represents another way of "fine tuning" of membrane excitability (Yellen 2002). If enzymatic features of the Kvβ subunits can affect the membrane trafficking of the Kvα/Kvβ complexes (Campomanes et al., 2002), it seems possible that in our co-expression experiments NADPH binding mutants, did not express or properly trafficked to the membrane. This could lead to the expression of large number of Kvα homomeric channels, due to insufficient availability of Kvβ subunits. In this case, two different channel populations could be present in plasma membrane of Xenopus oocytes. I consider the possibility that currents recorded by co-expression of Kv1.5 with NADPH-binding mutant Kvβ1.1 (no fast inactivation) could be due to the summation of two different current fractions: one mediated by homomeric Kv1.5, and the other mediated by Kv1.5/Kvβ1.1Q248R, that shows Kvβ1.1-mediated inactivation features similar to Kv1.5/Kvβ1.1wt. Is it possible, that the summation of these two current components results in a non-inactivating current, which shows similar kinetic properties as recorded for Kv1.5/Kvβ1.1Q248R currents after injection of cRNA into Xenopus oocytes? To answer this question, a mathematical simulation has been performed by adding a different fractions of Kv1.5/Kvβ1.1wt current to Kv1.5 currents. Resulting simulated curves (Figure 24 green) were normalized and plotted together with measured Kv1.5/Kvβ1.1Q248R current trace (24A red). This stimulation shows that Kv1.5/Kvβ1.1Q248R-mediated current curves have completely different activation (Figure 24A) and inactivation (Figure 24B) kinetics than simulated ones. We conclude that inactivation

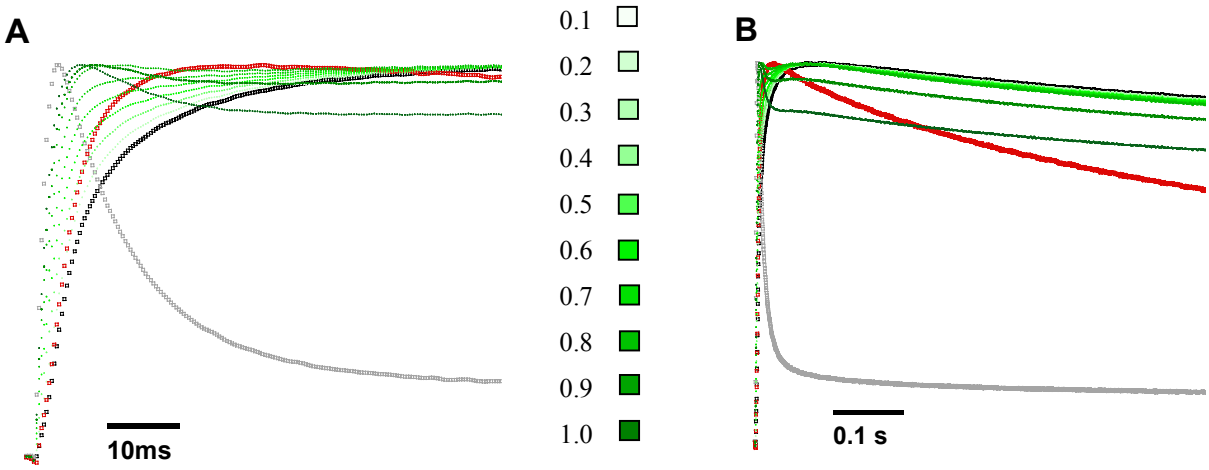

Figure 24. Comparison of simulated (green) and recorded normalized curves. The inactivation pattern of recorded Kv1.5/Kvβ1.1Q248R (red) trace could not be obtained by summation of Kv1.5 and different fractions (0.1 - 1) of Kv1.5/Kvβ1.1wt rapidly inactivating currents. Simulated curves were normalized and depicted in the graph together with Kv1.5 (black), Kv1.5/Kvβ1.1wt (gray), Kv1.5/Kvβ1.1Q248R (red) currents traces. ***A-*** comparison of activation of the stimulated and recorded currents. ***B-***comparison of the inactivation of simulated and recorded currents. The simulated currents can represent neither activation nor inactivation of recorded Kv1.5/Kvβ1.1Q248R currents.

kinetics of measured channels Kv1.5/Kvβ1.1Q248R could *not* be stimulated by summation of two different current "populations", namely Kv1.5 and Kv1.5/Kvβ1.1wt.

Furthermore, the impairment of NADPH binding, apparently is *not* interfering with the trafficking of mutant channel complexes to the plasma membrane, as co-expression of Kvβ1.1Q248R did not influence current amplitudes in Xenopus oocytes (Figure 14).

Immunostaining studies would directly show the expression patterns of mutant channel subunits both in Xenopus oocytes and in CHO cell expression systems. This will reveal the quantitatively the subunit expression in above mentioned heterologous expression system.

5. Summary

The accessory β-subunits of Shaker-related voltage-dependent potassium channels (Kv1) form tetramers arranged with 4-fold rotational symmetry, like the membrane-integral and pore-forming alpha subunits (Gulbis et al., 1999). The crystal structure of the conserved Kvβ2 core domain shows that Kvβ subunits are potentially oxidoreductase enzymes containing an active site composed of conserved catalytic residues, a nicotinamide cofactor ($NADP^+$) and a substrate-binding site. At the other hand Kvβ subunits with an N-terminal inactivating domain like Kvβ1.1 (Rettig et al., 1994) and Kvβ3.1 (Heinemann et al., 1996) confer a rapid N-type inactivation to otherwise non-inactivating Kv1 channels. By a combination of structural modelling and electrophysiological characterization of structure-based mutations, as well as by direct measurement of nucleotide coenzyme binding, it is shown, that changes in Kvβ oxidoreductase activity may markedly influence the gating mode of Kv1 channels: Kvβ1.1 subunit reversibly binds different nucleotide coenzymes. Mutating the residues, that make direct contact with the $NADP^+$ molecule, can attenuate the nucleotide coenzymes binding of Kvβ1.1. These mutants of Kvβ1.1 are no more able to confer rapid inactivation to Kv1 upon their co-expression in Xenopus oocytes. Similarly, amino acid substitutions at the putative catalytic residues in the Kvβ1.1 attenuate the inactivating activity of Kvβ1.1. I propose that Kvβ oxidoreductase activity couples Kv channel inactivation to cellular redox regulation. The sensitivity of this kind of regulation is dependent on cell type. In CHO and HEK 293 expression systems, the effect of oxidoreductase features of Kvβ subunits on Kvβ-mediated rapid inactivation is less pronounced.

The molecular aspects of N-type inactivation have been recently elucidated in unprecedented details (Zhou et al. 2001). A small domain composed of several amino acids at the N-terminus of Kvβ1.1 blocks the channel by binding to its receptor site in the pore. By co-expression of

Kvβ1.1 with chimeric channels, made between Kv1.2 and Kv2.1 it is shown, that, as yet unknown structural elements in the transmembrane region of Kv2.1 can prevent the Kvβ1.1-mediated rapid inactivation. We conclude that the presence of N-terminal inactivating domain and an appropriate receptor site in the pore of the channel are necessary but not sufficient for rapid N-type inactivation of the channel.

6. References

Accili EA, Kiehn J, Yang Q, Wang Z, Brown AM, Wible BA. 1997. Separable Kvbeta subunit domains alter expression and gating of potassium channels. J Biol Chem 272: 25824-31. K^+

Adams JD, Jr., Klaidman LK, Chang ML, Yang J. 2001. Brain oxidative stress--analytical chemistry and thermodynamics of glutathione and NADPH. Curr Top Med Chem 1: 473-82.

Aldrich RW. 2001. Fifty years of inactivation. Nature 411: 643-4.

Antz C, Bauer T, Kalbacher H, Frank R, Covarrubias M, et al. 1999. Control of K^+ channel gating by protein phosphorylation: structural switches of the inactivation gate. Nat Struct Biol 6: 146-50.

Bahring R, Milligan CJ, Vardanyan V, Engeland B, Young BA, et al. 2001. Coupling of voltage-dependent potassium channel inactivation and oxidoreductase active site of Kvbeta subunits. J Biol Chem 276: 22923-9.

Berneche S, Roux B. 2001. Energetics of ion conduction through the K^+ channel. Nature 414: 73-7.

Bezanilla F. 2002. Voltage sensor movements. J Gen Physiol 120: 465-73.

Bixby KA, Nanao MH, Shen NV, Kreusch A, Bellamy H, et al. 1999. Zn^{2+}-binding and molecular determinants of tetramerization in voltage-gated K^+ channels. Nat Struct Biol 6: 38-43.

Cahalan MD, Wulff H, Chandy KG. 2001. Molecular properties and physiological roles of ion channels in the immune system. J Clin Immunol 21: 235-52.

Campomanes CR, Carroll KI, Manganas LN, Hershberger ME, Gong B, et al. 2002. Kv beta subunit oxidoreductase activity and Kv1 potassium channel trafficking. J Biol Chem 277: 8298-305.

Castellino RC, Morales MJ, Strauss HC, Rasmusson RL. 1995. Time- and voltage-dependent modulation of a Kv1.4 channel by a beta-subunit (Kv beta 3) cloned from ferret ventricle. Am J Physiol 269: H385-91.

Cooper EC, Jan LY. 1999. Ion channel genes and human neurological disease: recent progress, prospects, and challenges. Proc Natl Acad Sci U S A 96: 4759-66.

Coppock EA, Martens JR, Tamkun MM. 2001. Molecular basis of hypoxia-induced pulmonary vasoconstriction: role of voltage-gated K^+ channels. Am J Physiol Lung Cell Mol Physiol 281: L1-12.

Coppock EA, Tamkun MM. 2001. Differential expression of K(V) channel alpha- and beta-subunits in the bovine pulmonary arterial circulation. Am J Physiol Lung Cell Mol Physiol 281: L1350-60.

del Camino D, Holmgren M, Liu Y, Yellen G. 2000. Blocker protection in the pore of a voltage-gated K^+ channel and its structural implications. Nature 403: 321-5.

Demo SD, Yellen G. 1991. The inactivation gate of the Shaker K^+ channel behaves like an open-channel blocker. Neuron 7: 743-53.

Doyle DA, Morais Cabral J, Pfuetzner RA, Kuo A, Gulbis JM, et al. 1998. The structure of the potassium channel: molecular basis of K^+ conduction and selectivity. Science 280: 69-77.

Dubois JM, Rouzaire-Dubois B. 1993. Role of potassium channels in mitogenesis. Prog Biophys Mol Biol 59: 1-21.

England SK, Uebele VN, Kodali J, Bennett PB, Tamkun MM. 1995. A novel K^+ channel beta-subunit (hKv beta 1.3) is produced via alternative mRNA splicing. J Biol Chem 270: 28531-4.

Grimshaw CE, Shahbaz M, Putney CG. 1990. Mechanistic basis for nonlinear kinetics of aldehyde reduction catalyzed by aldose reductase. Biochemistry 29: 9947-55.

Gulbis JM, Mann S, MacKinnon R. 1999. Structure of a voltage-dependent K^+ channel beta subunit. Cell 97: 943-52.

Gulbis JM, Zhou M, Mann S, MacKinnon R. 2000. Structure of the cytoplasmic beta subunit-T1 assembly of voltage-dependent K^+ channels. Science 289: 123-7.

Haddad GG, Liu H. 2000. Different O2-sensing mechanisms by different K^+ channels. Adv Exp Med Biol 475: 441-52.

Hanlon MR, Wallace BA. 2002. Structure and function of voltage-dependent ion channel regulatory beta subunits. Biochemistry 41: 2886-94.

Heginbotham L, Abramson T, MacKinnon R. 1992. A functional connection between the pores of distantly related ion channels as revealed by mutant K^+ channels. Science 258: 1152-5.

Heinemann SH, Rettig J, Graack HR, Pongs O. 1996. Functional characterization of Kv channel beta-subunits from rat brain. J Physiol 493: 625-33.

Heinemann SH, Rettig J, Wunder F, Pongs O. 1995. Molecular and functional characterization of a rat brain Kv beta 3 potassium channel subunit. FEBS Lett 377: 383-9.

Hille B, 2001. *Ion channels of excitable membranes*. Sunderland, MA: Sinauer Associates, Inc.

Hodgkin AL, Huxley AF. 1952. A quantitative description of membrane current and its application to conduction and excitation in nerve. J. Physiol 117: 500-544

Horn R. 2002. Coupled movements in voltage-gated ion channels. J Gen Physiol 120: 449-53.

Hoshi T, Zagotta WN, Aldrich RW. 1990. Biophysical and molecular mechanisms of Shaker potassium channel inactivation. Science 250: 533-8.

Hoshi T, Zagotta WN, Aldrich RW. 1991. Two types of inactivation in Shaker K^+ channels: effects of alterations in the carboxy-terminal region. Neuron 7: 547-56.

Isacoff EY, Jan YN, Jan LY. 1991. Putative receptor for the cytoplasmic inactivation gate in the Shaker K^+ channel. Nature 353: 86-90.

Jan LY, Jan YN. 1997. Cloned potassium channels from eukaryotes and prokaryotes. Annu Rev Neurosci 20: 91-123.

Jez JM, Bennett MJ, Schlegel BP, Lewis M, Penning TM. 1997a. Comparative anatomy of the aldo-keto reductase superfamily. Biochem J 326: 625-36.

Jez JM, Flynn TG, Penning TM. 1997b. A new nomenclature for the aldo-keto reductase superfamily. Biochem Pharmacol 54: 639-47.

Jiang Y, Lee A, Chen J, Cadene M, Chait BT, MacKinnon R. 2002. The open pore conformation of potassium channels. Nature 417: 523-6.

Jiang Y, Pico A, Cadene M, Chait BT, MacKinnon R. 2001. Structure of the RCK domain from the E. coli K^+ channel and demonstration of its presence in the human BK channel. Neuron 29: 593-601.

Johnston D, Hoffman DA, Magee JC, Poolos NP, Watanabe S, et al. 2000. Dendritic potassium channels in hippocampal pyramidal neurons. J Physiol 525: 75-81.

Keynes RD, Elinder F. 1999. The screw-helical voltage gating of ion channels. Proc R Soc Lond B Biol Sci 266: 843-52.

Kobertz WR, Williams C, Miller C. 2000. Hanging gondola structure of the T1 domain in a voltage-gated K($^+$) channel. Biochemistry 39: 10347-52.

Kreusch A, Pfaffinger PJ, Stevens CF, Choe S. 1998. Crystal structure of the tetramerization domain of the Shaker potassium channel. Nature 392: 945-8.

Kubiseski TJ, Hyndman DJ, Morjana NA, Flynn TG. 1992. Studies on pig muscle aldose reductase. Kinetic mechanism and evidence for a slow conformational change upon coenzyme binding. J Biol Chem 267: 6510-7.

Kurachi Y, Ishii M. 2003. Cell signal control of the G protein-gated potassium channel and its subcellular localization. J Physiol 15: 15

Larsson HP. 2002. The search is on for the voltage sensor-to-gate coupling. J Gen Physiol 120: 475-81.

Larsson HP, Elinder F. 2000. A conserved glutamate is important for slow inactivation in K^+ channels. Neuron 27: 573-83.

Lee TE, Philipson LH, Nelson DJ. 1996. N-type inactivation in the mammalian Shaker K^+ channel Kv1.4. J Membr Biol 151: 225-35.

Leicher T, Bahring R, Isbrandt D, Pongs O. 1998. Coexpression of the KCNA3B gene product with Kv1.5 leads to a novel A-type potassium channel. J Biol Chem 273: 35095-101.

Leicher T, Roeper J, Weber K, Wang X, Pongs O. 1996. Structural and functional characterization of human potassium channel subunit beta 1 (KCNA1B). Neuropharmacology 35: 787-95.

Li M, Unwin N, Stauffer KA, Jan YN, Jan LY. 1994. Images of purified Shaker potassium channels. Curr Biol 4: 110-5.

Liu SQ, Jin H, Zacarias A, Srivastava S, Bhatnagar A. 2001. Binding of pyridine nucleotide coenzymes to the beta-subunit of the voltage-sensitive K^+ channel. J Biol Chem 276: 11812-20.

Loots E, Isacoff EY. 1998. Protein rearrangements underlying slow inactivation of the Shaker K^+ channel. J Gen Physiol 112: 377-89.

Lu Z, Klem AM, Ramu Y. 2002. Coupling between voltage sensors and activation gate in voltage-gated K^+ channels. J Gen Physiol 120: 663-76.

MacKinnon R. 1991. Determination of the subunit stoichiometry of a voltage-activated potassium channel. Nature 350: 232-5.

McCormack K, Connor JX, Zhou L, Ho LL, Ganetzky B, et al. 2002. Genetic analysis of the mammalian K^+ channel beta subunit Kvbeta 2 (Kcnab2). J Biol Chem 277: 13219-28.

McCormack K, McCormack T, Tanouye M, Rudy B, Stuhmer W. 1995. Alternative splicing of the human Shaker K^+ channel beta 1 gene and functional expression of the beta 2 gene product. FEBS Lett 370: 32-6.

McCormack T, McCormack K. 1994. Shaker K^+ channel beta subunits belong to an NAD(P)H-dependent oxidoreductase superfamily. Cell 79: 1133-5.

Meir A, Ginsburg S, Butkevich A, Kachalsky SG, Kaiserman I, et al. 1999. Ion channels in presynaptic nerve terminals and control of transmitter release. Physiol Rev 79: 1019-88.

Morales MJ, Castellino RC, Crews AL, Rasmusson RL, Strauss HC. 1995. A novel beta subunit increases rate of inactivation of specific voltage-gated potassium channel alpha subunits. J Biol Chem 270: 6272-7.

Murrell-Lagnado RD, Aldrich RW. 1993. Energetics of Shaker K channels block by inactivation peptides. J Gen Physiol 102: 977-1003.

Nakahira K, Shi G, Rhodes KJ, Trimmer JS. 1996. Selective interaction of voltage-gated K^+ channel beta-subunits with alpha-subunits. J Biol Chem 271: 7084-9.

Nerbonne JM. 2000. Molecular basis of functional voltage-gated K^+ channel diversity in the mammalian myocardium. J Physiol 525: 285-98.

Niemeyer MI, Cid LP, Barros LF, Sepulveda FV. 2001. Modulation of the two-pore domain acid-sensitive K^+ channel TASK-2 (KCNK5) by changes in cell volume. J Biol Chem 276: 43166-74.

Nishida M, MacKinnon R. 2002. Structural basis of inward rectification: cytoplasmic pore of the G protein-gated inward rectifier GIRK1 at 1.8 A resolution. Cell 111: 957-65.

Noulin JF, Brochiero E, Coady MJ, Laprade R, Lapointe JY. 2001. Molecular identity and regulation of renal potassium channels. Jpn J Physiol 51: 631-47.

Orlova EV, Papakosta M, Booy FP, van Heel M, Dolly JO. 2003. Voltage-gated K^+ channel from mammalian brain: 3D structure at 18A of the complete (alpha)4(beta)4 complex. J Mol Biol 326: 1005-12.

Papazian DM. 1999. Potassium channels: some assembly required. Neuron 23: 7-10.

Papazian DM, Shao XM, Seoh SA, Mock AF, Huang Y, Wainstock DH. 1995. Electrostatic interactions of S4 voltage sensor in Shaker K^+ channel. Neuron 14: 1293-301.

Parcej DN, Scott VE, Dolly JO. 1992. Oligomeric properties of alpha-dendrotoxin-sensitive potassium ion channels purified from bovine brain. Biochemistry 31: 11084-8.

Patel AJ, Honore E. 2001. Molecular physiology of oxygen-sensitive potassium channels. Eur Respir J 18: 221-7.

Pawlowski JE, Penning TM. 1994. Overexpression and mutagenesis of the cDNA for rat liver 3 alpha-hydroxysteroid/dihydrodiol dehydrogenase. Role of cysteines and tyrosines in catalysis. J Biol Chem 269: 13502-10.

Penning TM. 1999. Molecular determinants of steroid recognition and catalysis in aldo-keto reductases. Lessons from 3alpha-hydroxysteroid dehydrogenase. J Steroid Biochem Mol Biol 69: 211-25.

Pluger S, Faulhaber J, Furstenau M, Lohn M, Waldschutz R, et al. 2000. Mice with disrupted BK channel beta1 subunit gene feature abnormal $Ca(2^+)$ spark/STOC coupling and elevated blood pressure. Circ Res 87: E53-60.

Pongs O. 1999. Voltage-gated potassium channels: from hyperexcitability to excitement. FEBS Lett 452: 31-5.

Rettig J, Heinemann SH, Wunder F, Lorra C, Parcej DN, et al. 1994. Inactivation properties of voltage-gated K^+ channels altered by presence of beta-subunit. Nature 369: 289-94.

Rhodes KJ, Strassle BW, Monaghan MM, Bekele-Arcuri Z, Matos MF, Trimmer JS. 1997. Association and colocalization of the Kvbeta1 and Kvbeta2 beta-subunits with Kv1 alpha-subunits in mammalian brain K^+ channel complexes. J Neurosci 17: 8246-58.

Röper J, Sewing S, Zhang Y, Sommer T, Wanner SG, Pongs O. 1998. NIP domain prevents N-type inactivation in voltage-gated potassium channels. Nature 391: 390-3.

Ruppersberg JP, Frank R, Pongs O, Stocker M. 1991. Cloned neuronal IK(A) channels reopen during recovery from inactivation. Nature 353: 657-60.

Sackmann B, Neher E. 1995. *Single-channel recordings*. Plenum Publishing Corp.

Sanli G, Blaber M. 2001. Structural assembly of the active site in an aldo-keto reductase by NADPH cofactor. J Mol Biol 309: 1209-18.

Sato Y, Sakaguchi M, Goshima S, Nakamura T, Uozumi N. 2003. Molecular dissection of the contribution of negatively and positively charged residues in S2, S3, and S4 to the final membrane topology of the voltage sensor in the K^+ channel, KAT1. J Biol Chem 278: 13227-34.

Schlegel BP, Jez JM, Penning TM. 1998. Mutagenesis of 3 alpha-hydroxysteroid dehydrogenase reveals a "push-pull" mechanism for proton transfer in aldo-keto reductases. Biochemistry 37: 3538-48.

Schlegel BP, Ratnam K, Penning TM. 1998. Retention of NADPH-linked quinone reductase activity in an aldo-keto reductase following mutation of the catalytic tyrosine. Biochemistry 37: 11003-11.

Schmitt N, Schwarz M, Peretz A, Abitbol I, Attali B, Pongs O. 2000. A recessive C-terminal Jervell and Lange-Nielsen mutation of the KCNQ1 channel impairs subunit assembly. Embo J 19: 332-40.

Scott VE, Parcej DN, Keen JN, Findlay JB, Dolly JO. 1990. Alpha-dendrotoxin acceptor from bovine brain is a K^+ channel protein. Evidence from the N-terminal sequence of its larger subunit. J Biol Chem 265: 20094-7.

Scott VE, Rettig J, Parcej DN, Keen JN, Findlay JB, et al. 1994. Primary structure of a beta subunit of alpha-dendrotoxin-sensitive K^+ channels from bovine brain. Proc Natl Acad Sci U S A 91: 1637-41.

Seoh SA, Sigg D, Papazian DM, Bezanilla F. 1996. Voltage-sensing residues in the S2 and S4 segments of the Shaker K^+ channel. Neuron 16: 1159-67.

Sewing S, Roeper J, Pongs O. 1996. Kv beta 1 subunit binding specific for shaker-related potassium channel alpha subunits. Neuron 16: 455-63.

Shen NV, Chen X, Boyer MM, Pfaffinger PJ. 1993. Deletion analysis of K^+ channel assembly. Neuron 11: 67-76.

Sokolova O, Kolmakova-Partensky L, Grigorieff N. 2001. Three-dimensional structure of a voltage-gated potassium channel at 2.5 nm resolution. Structure (Camb) 9: 215-20.

Tarle I, Borhani DW, Wilson DK, Quiocho FA, Petrash JM. 1993. Probing the active site of human aldose reductase. Site-directed mutagenesis of Asp-43, Tyr-48, Lys-77, and His-110. J Biol Chem 268: 25687-93.

Uebele VN, England SK, Gallagher DJ, Snyders DJ, Bennett PB, Tamkun MM. 1998. Distinct domains of the voltage-gated K^+ channel Kv beta 1.3 beta-subunit affect voltage-dependent gating. Am J Physiol 274: C1485-95.

Urlaub G, Chasin LA. 1980. Isolation of Chinese hamster cell mutants deficient in dihydrofolate reductase activity. Proc Natl Acad Sci U S A 77: 4216-20.

Vartanov SS, Pavlov AR, Iaropolov AI. 1992. [Aldose reductase: physiological role, properties and prospects for regulating activity]. Biokhimiia 57: 323-41.

Vergara C, Latorre R, Marrion NV, Adelman JP. 1998. Calcium-activated potassium channels. Curr Opin Neurobiol 8: 321-9.

Watanabe S, Hoffman DA, Migliore M, Johnston D. 2002. Dendritic K^+ channels contribute to spike-timing dependent long-term potentiation in hippocampal pyramidal neurons. Proc Natl Acad Sci U S A 99: 8366-71.

Weinreich F, Jentsch TJ. 2000. Neurological diseases caused by ion-channel mutations. Curr Opin Neurobiol 10: 409-15.

Xu J, Li M. 1997. Kvbeta2 inhibits the Kvbeta1-mediated inactivation of K^+ channels in transfected mammalian cells. J Biol Chem 272: 11728-35.

Xu J, Yu W, Jan YN, Jan LY, Li M. 1995. Assembly of voltage-gated potassium channels. Conserved hydrophilic motifs determine subfamily-specific interactions between the alpha-subunits. J Biol Chem 270: 24761-8.

Yang J, Yu M, Jan YN, Jan LY. 1997. Stabilization of ion selectivity filter by pore loop ion pairs in an inwardly rectifying potassium channel. Proc Natl Acad Sci U S A 94: 1568-72.

Yellen G. 2002. The voltage-gated potassium channels and their relatives. Nature 419: 35-42.

Yifrach O, MacKinnon R. 2002. Energetics of pore opening in a voltage-gated $K(^+)$ channel. Cell 111: 231-9.

Yu W, Xu J, Li M. 1996. NAB domain is essential for the subunit assembly of both alpha-alpha and alpha-beta complexes of shaker-like potassium channels. Neuron 16: 441-53.

Zagotta WN, Hoshi T, Aldrich RW. 1990. Restoration of inactivation in mutants of Shaker potassium channels by a peptide derived from ShB. Science 250: 568-71.

Zhou M, Morais-Cabral JH, Mann S, MacKinnon R. 2001. Potassium channel receptor site for the inactivation gate and quaternary amine inhibitors. Nature 411: 657-61.

7. Attachments

7.1 Abbreviations

A	Ampere (electric current unit)
BK	big conductance Ca^{2+} -activated potassium channels
C	electric capacitance
Cav	voltage activated calcium channels
Chim	chimera
CHO	Chinese hamster ovary (cells)
ClC	chloride channels
CO_2	carbon dioxide
DMSO	dimethylsulphoxide
DOPE	dioleoyl phosphatidylethanole-amine
E	electric potential
Eag	ether-a-go-go potassium channel
EGTA	(ethylene glycol-bis(2-aminoethyl-ether) -N,N,N',N'-tetracetic acid
Exp	exponent
G	conductance
GV	conductance voltage relationship
h	hour
HEK 293	Human embryonic kidney cell-line
HEPES	N-(2-hydroxyethyl)piperazine-N'-(2-ethanesulfonic acid)
I	electric current
I_{1s}	electric current value at the 1s depolarization
I_{peak}	electric current value at the peak of trace
KCl	potassium chloride (salt)
KcsA	potassium selective channel from *Streptomyces lividans*
K_d	dissociation constant
K_s	slope factor for conductance-voltage curve
Kv	voltage activated potassium channel
Kvβ	beta subunits of Shaker-related potassium channels
LQT	Long Q-T syndrome
MthK	*Methanobacter thermoautotropium* potassium channel
NAB	N-terminal association domain for potassium channels
NAD^+	nicotinamide adenine dinucleotide (oxidised form)
NADH	nicotinamide adenine dinucleotide (reduced form)
$NADP^+$	nicotinamide adenine dinucleotide phosphate (oxidised form)

NADPH	nicotinamide adenine dinucleotide phosphate (reduced form)
Nav	voltage activated sodium channels
^{o}C	degree of Celsius
OR2	oocyte Ringer 2
PCR	polymerase chain reactions
RA	relative amplitude (of decay components in exponential fits)
Rs	series resistance
t	time
TBA	tetra-butyl-ammonium ion
V	voltage
Ω	Ohm (electric resistance unit)

7.2 Nicotinamid nucleotide coenzymes

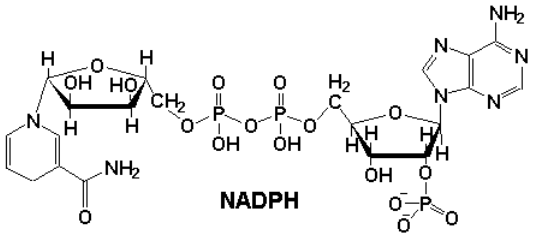

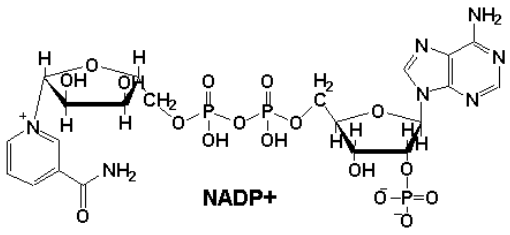

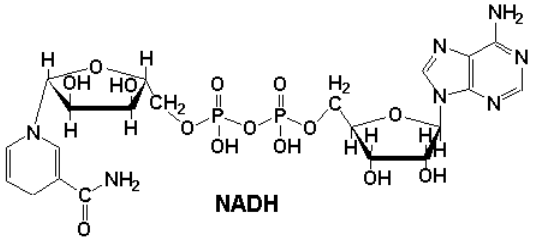

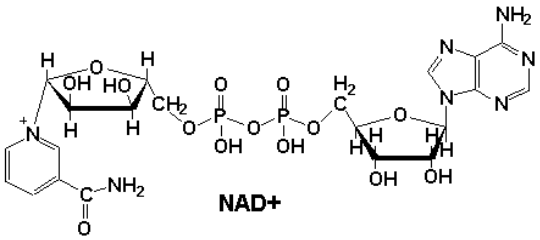

7.3 Clone-cards of used constructs.

7.3.1 Clone-cards for Kv1.2/Kv2.1 chimeric channels.

The definitions KCNB1 and KCNA2 on circular DNA maps refer to the human Kv2.1 and rat Kv1.2 genes, respectively. Numbers indicate amino acids sequences of the corresponding proteins. The changeover is the site where the green arrows end. The red colored arrow shows the multi-component DNA. Frequently used single cutting restriction enzymes are shown with red lines, the multiple-cutting ones with blue lines correspondingly. The T7 and SP6 promotors are also indicated on maps. "1240s" is the binding site for the appropriate sense-primer on the T7 promotor. With the "Poly A" is signed the binding region for anti-sense primer used for sequencing the antisense DNA.

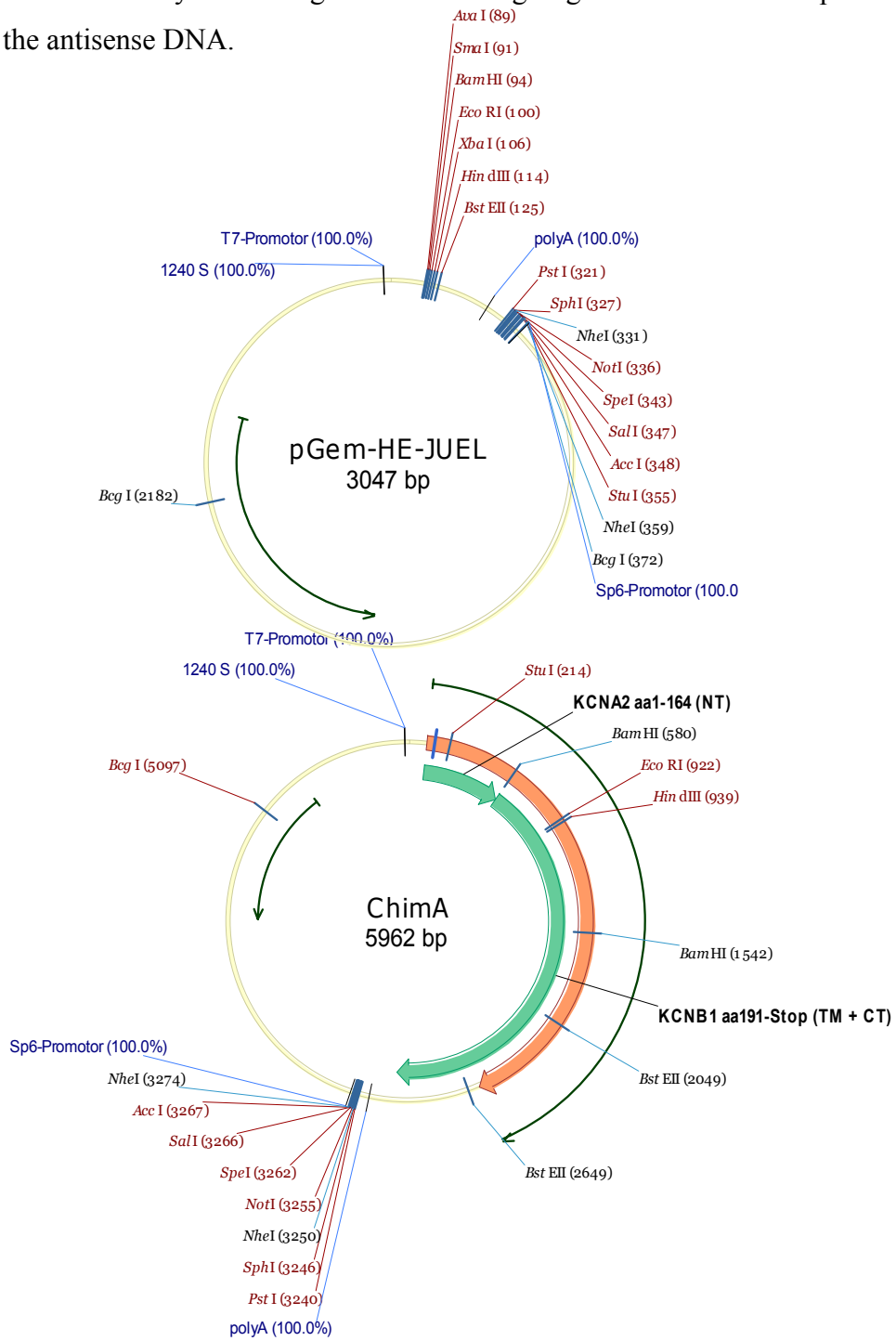

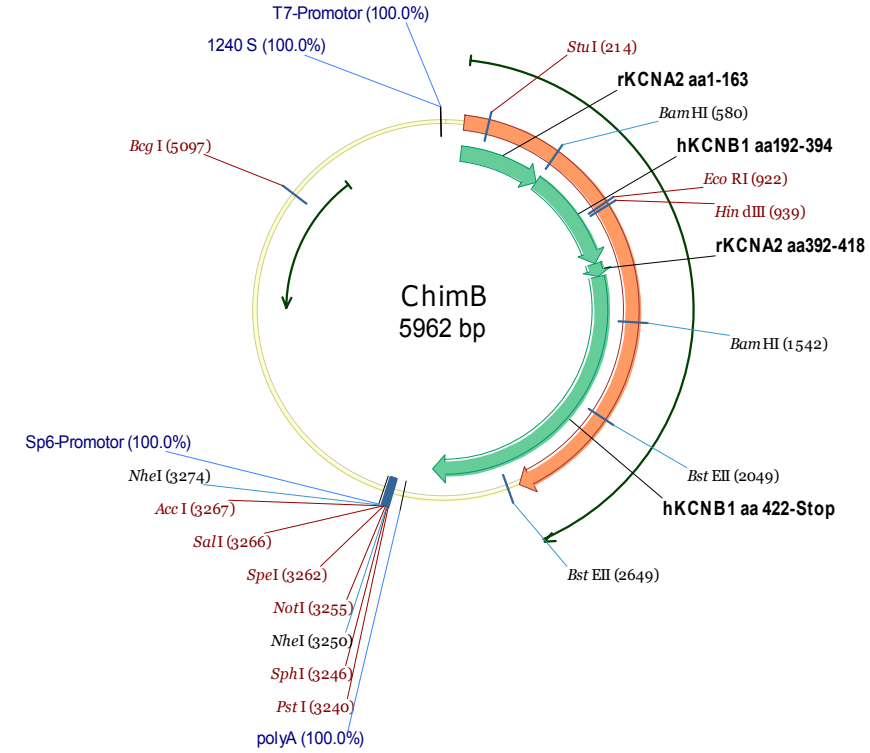
T7-Promotor (100.0%)
1240 S (100.0%)
StuI (214)
rKCNA2 aa1-163
BamHI (580)
hKCNB1 aa192-394
Bcg I (5097)
Eco RI (922)
Hin dIII (939)
rKCNA2 aa392-418
ChimB
5962 bp
BamHI (1542)
Sp6-Promotor (100.0%)
BstEII (2049)
NheI (3274)
hKCNB1 aa 422-Stop
Acc I (3267)
SalI (3266)
BstEII (2649)
SpeI (3262)
NotI (3255)
NheI (3250)
SphI (3246)
Pst I (3240)
polyA (100.0%)

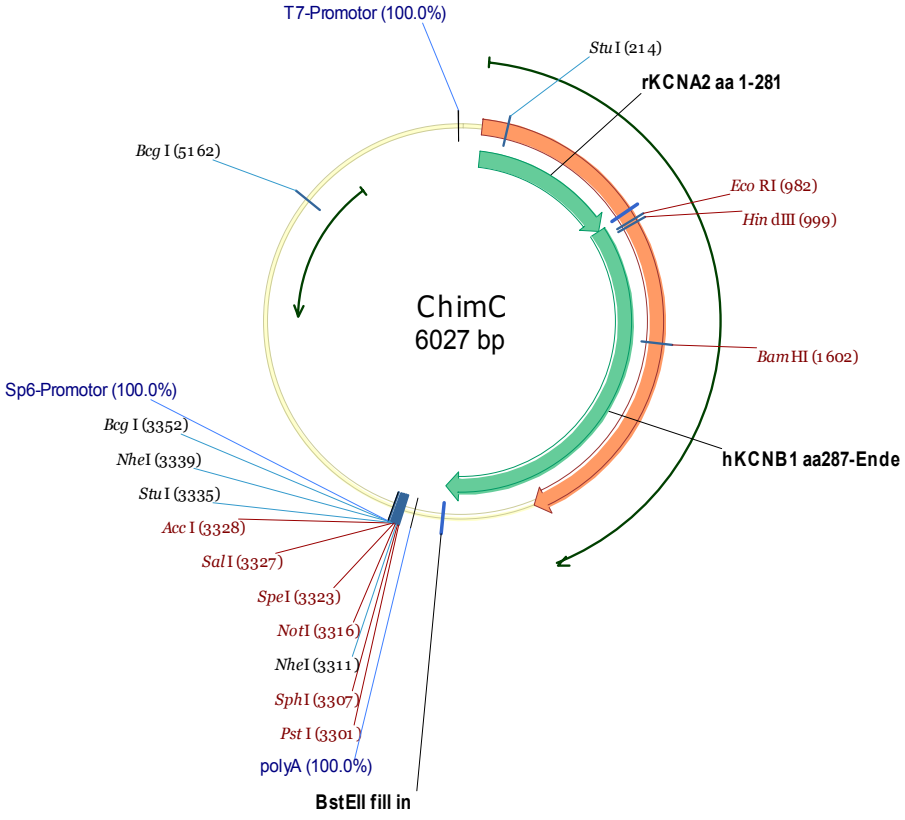
T7-Promotor (100.0%)
StuI (214)
rKCNA2 aa 1-281
Bcg I (5162)
Eco RI (982)
Hin dIII (999)
ChimC
6027 bp
BamHI (1602)
Sp6-Promotor (100.0%)
hKCNB1 aa287-Ende
Bcg I (3352)
NheI (3339)
StuI (3335)
Acc I (3328)
SalI (3327)
SpeI (3323)
NotI (3316)
NheI (3311)
SphI (3307)
Pst I (3301)
polyA (100.0%)
BstEII fill in

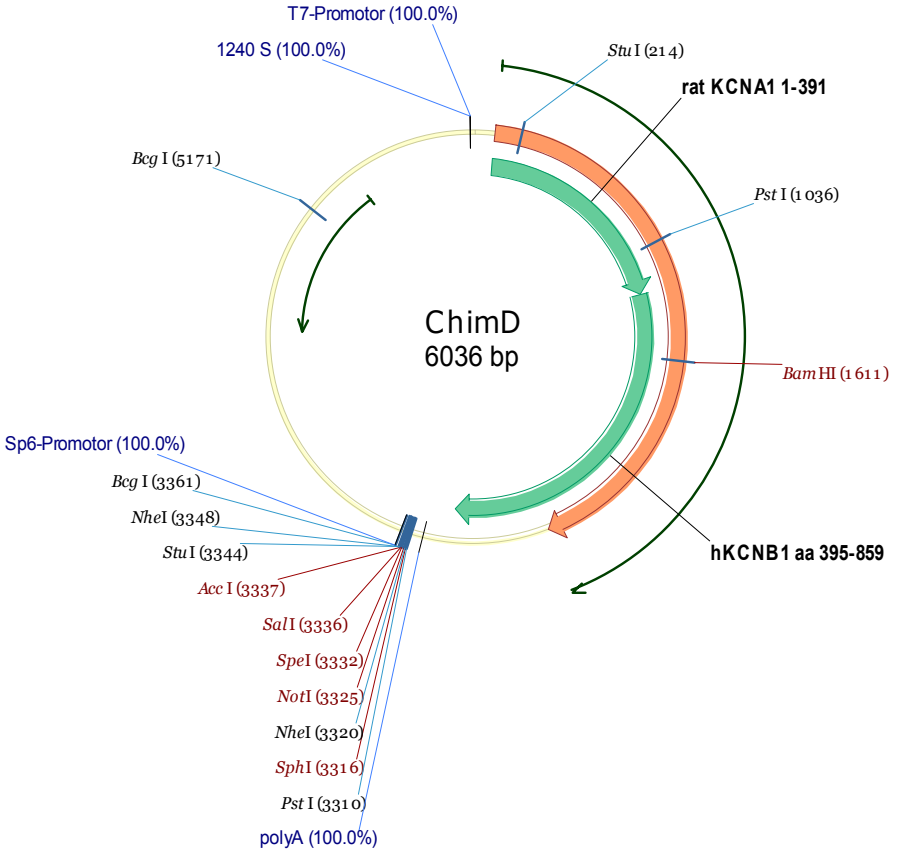
T7-Promotor (100.0%)
1240 S (100.0%)
StuI (214)
rat KCNA1 1-391
Bcg I (5171)
PstI (1036)
ChimD
6036 bp
BamHI (1611)
Sp6-Promotor (100.0%)
Bcg I (3361)
NheI (3348)
StuI (3344)
hKCNB1 aa 395-859
Acc I (3337)
SalI (3336)
SpeI (3332)
NotI (3325)
NheI (3320)
SphI (3316)
PstI (3310)
polyA (100.0%)

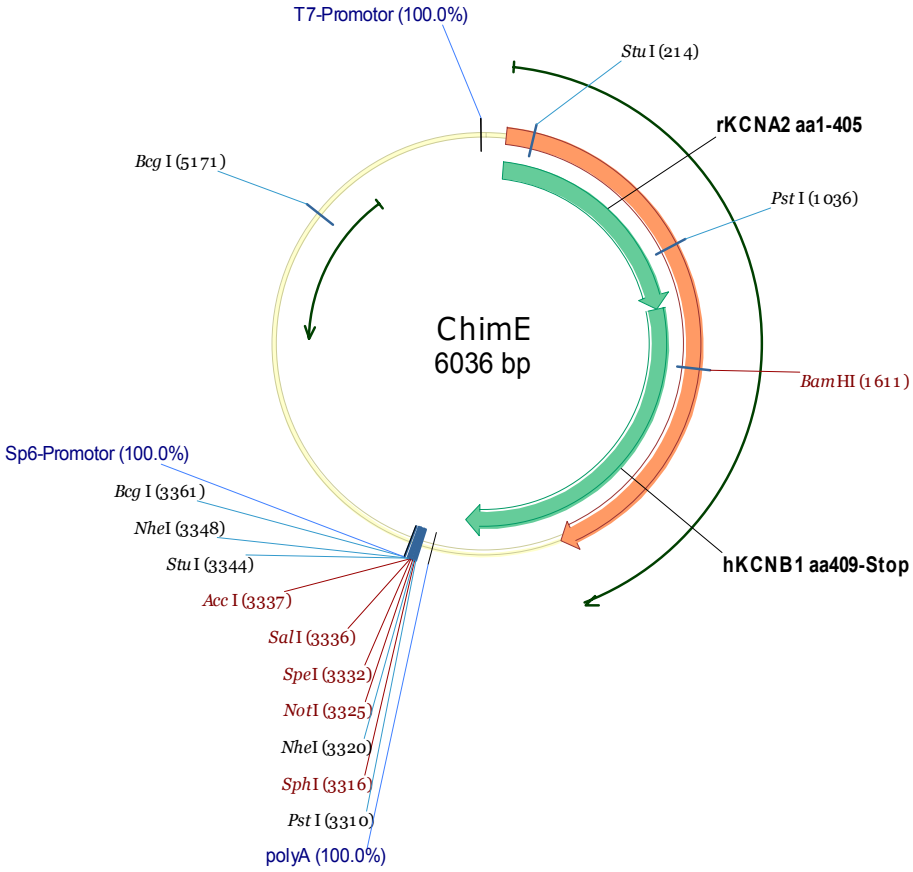
T7-Promotor (100.0%)
StuI (214)
rKCNA2 aa1-405
Bcg I (5171)
PstI (1036)
ChimE
6036 bp
BamHI (1611)
Sp6-Promotor (100.0%)
Bcg I (3361)
NheI (3348)
StuI (3344)
hKCNB1 aa409-Stop
Acc I (3337)
SalI (3336)
SpeI (3332)
NotI (3325)
NheI (3320)
SphI (3316)
PstI (3310)
polyA (100.0%)

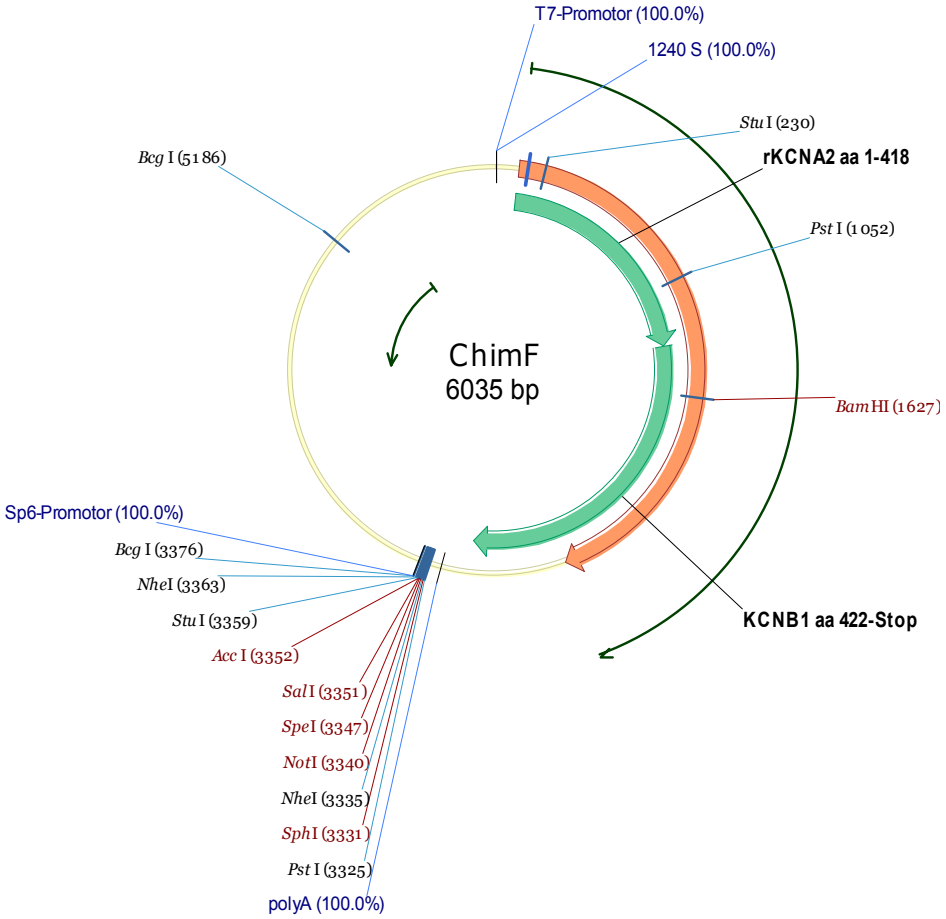
T7-Promotor (100.0%)
1240 S (100.0%)
Stu I (230)
rKCNA2 aa 1-418
Bcg I (5186)
Pst I (1052)
ChimF
6035 bp
Bam HI (1627)
Sp6-Promotor (100.0%)
Bcg I (3376)
Nhe I (3363)
Stu I (3359)
KCNB1 aa 422-Stop
Acc I (3352)
Sal I (3351)
Spe I (3347)
Not I (3340)
Nhe I (3335)
Sph I (3331)
Pst I (3325)
polyA (100.0%)

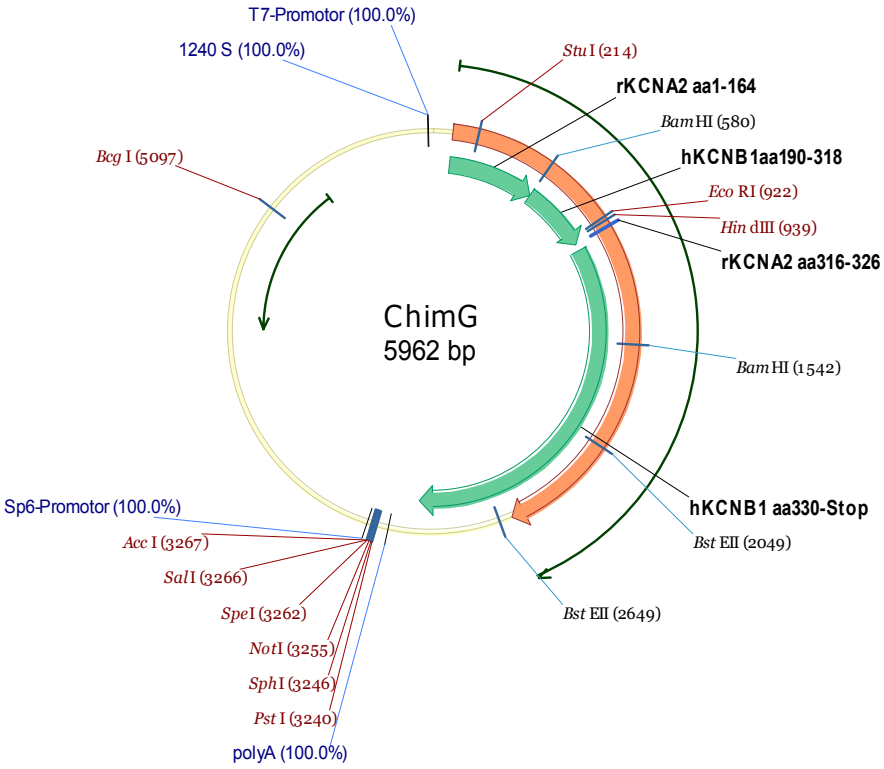
T7-Promotor (100.0%)
1240 S (100.0%)
Stu I (214)
rKCNA2 aa1-164
Bam HI (580)
hKCNB1aa190-318
Bcg I (5097)
Eco RI (922)
Hin dIII (939)
rKCNA2 aa316-326
ChimG
5962 bp
Bam HI (1542)
hKCNB1 aa330-Stop
Sp6-Promotor (100.0%)
Bst EII (2049)
Acc I (3267)
Sal I (3266)
Bst EII (2649)
Spe I (3262)
Not I (3255)
Sph I (3246)
Pst I (3240)
polyA (100.0%)

7.3.2 Examples of the clone-cards for used plasmids for transfection and cRNA synthesis for mutant Kvβ1.1 subunit. D119A point-mutation in Kvβ1.1 is shown in pGEM-HE-JUEL **(A)** and in pcDNA 3 **(B)** vectors.

A

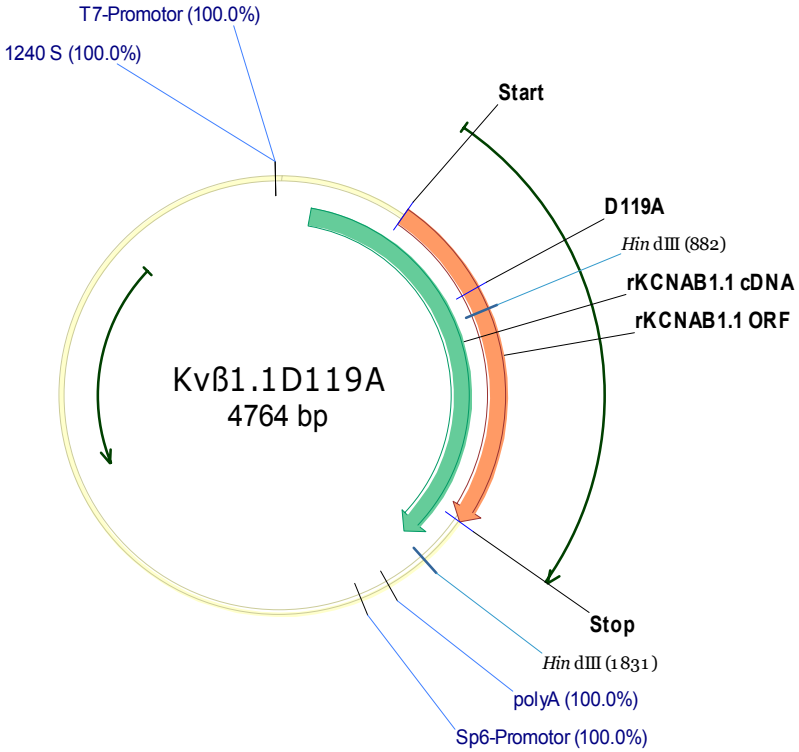

B

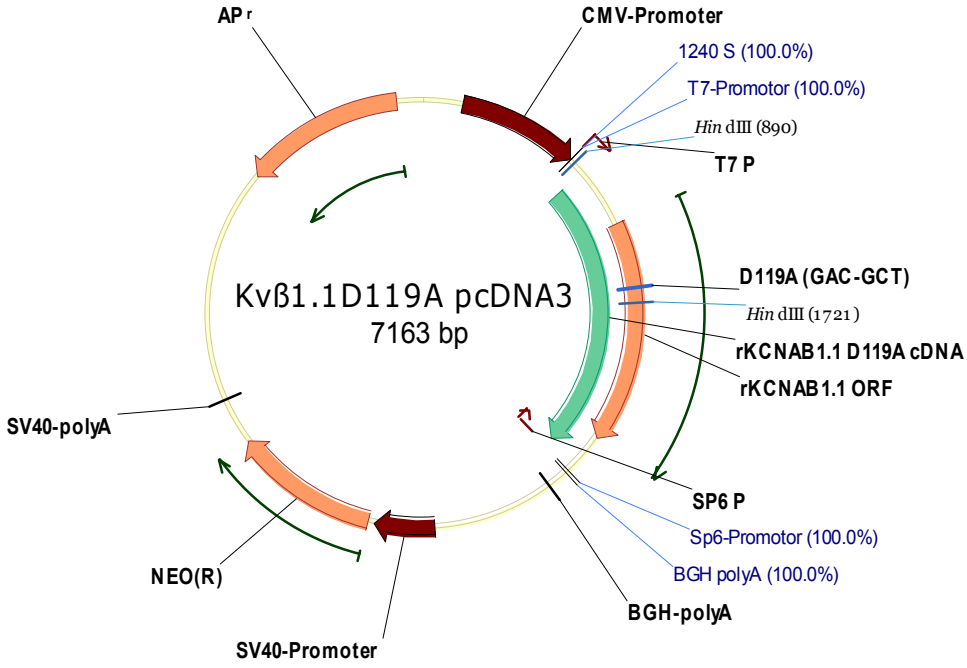

Large part of this work is included in following publications:

Bahring R, Milligan CJ, Vardanyan V, Engeland B, Young BA, Dannenberg J, Waldschutz R, Edwards JP, Wray D, Pongs O. Coupling of voltage-dependent potassium channel inactivation and oxidoreductase active site of Kvbeta subunits. *J. Biol. Chem.* 276, 22923-9 (2001).

Bahring, R., Vardanyan, V., Pongs, O. Differential modulation of Kv1 channel-mediated currents by coexpression of Kvβ3 subunit in a mammalian cell-line. *Mol. Memebr. Biol.* **21,** 19-25 (2004).

Acknowledgements

I would like to thank Prof. O. Pongs for giving me an opportunity to work in his internationally famous and state-of-the-art equipped institute and on such an up-to-date and exciting topic.

My special thanks go to Dr. Robert Bähring for inviting me to his electrophysiology lab thousand miles away from my homeland, for helping me accommodate at the beginning of my work. Thanks also for supervision at the first two years, and cooperativeness in many questions. I am grateful also for critical reading of the manuscript of dissertation.

I thank Dr. Engeland and Dr. Dannenberg for help and collaboration in molecular biological experiments. I appreciate help of Dr. M. Schwartz in experiments with Xenopuss oocyte at the beginning of my work.

My thanks go to all co-workers of the Institute of Neural Signal transduction for cooperation and friendly atmosphere. Special thanks go to the members of our electrophysiology team, to all technical personal of institute.

I am grateful to my family in Armenia for support in difficult days of my life that made my current work possible.

CURRICULUM VITAE

VARDANYAN Vitya

PERSONAL

Date of birth: 07 Jan 1973
Citizenship: Republic of ARMENIA

EDUCATION

1990-1995	Yerevan State University Department of Biophysics
1995-1998	Center of Biophysics, Armenian NAS Aspirantura
1999-2003	University of Hamburg Centre for Molecular Neurobiology (PhD study)

RESEARCH AND LABORATORY EXPERIENCE

1993-1995	Laboratory of Membrane Biophysics Department of Biophysics, Yerevan State University Subject: ***Regulation of H^+- K^+ exchange in anaerobically grown E.coli***.
1995-1999	Aspirantura at the Biophysics Center of Armenian NAS Laboratory of Membrane Biology Subject: ***Decreased contractility and acetylcholine-sensitivity in hyperosmotic medium in isolated perfused snail (Helix pomatia) heart.***
1999-2003	Subject: PhD at the Center for Molecular Neurobiology Hamburg, Institute of Neural Signal Transduction Subject: ***Structural requirements and role of oxidoreductase features for Kvβ-mediated potassium channel inactivation.***
2003-present	Postdoctoral study at the Center for Molecular Neurobiology Institute of Molecular Neurophathobiology.

LANGUAGES

Armenian (native), Russian, English, German.

PUBLICATIONS

Bahring, R., Vardanyan, V., Pongs, O. Differential modulation of Kv1 channel-mediated currents by coexpression of Kvβ3 subunit in a mammalian cell-line. *Mol. Memebr. Biol.* 2004 **21**, 19-25 (2004).

Teng, S., Ma, L., Zhen, Y., Lin, C., Bahring, R., Vardanyan, V., Pongs, O., Hui, R. Novel gene hKCNE4 slows the activation of the KCNQ1 channel. *Biochem. Biophys. Res. Commun*. **303**, 808-813 (2003).

Bahring R, Milligan CJ, Vardanyan V, Engeland B, Young BA, Dannenberg J, Waldschutz R, Edwards JP, Wray D, Pongs O. Coupling of voltage-dependent potassium channel inactivation and oxidoreductase active site of Kvbeta subunits. *J. Biol. Chem.* 276, 22923-9 (2001).

Vardanian, V.A., Ayrapetyan, S.N. On the effect of hyperosmotic shock on isolated snail (*Helix pomatia*) heart contraction. *Biol. J. Armenia* **50**, 134-39 (1999), (in Russian).

Trchounian, A., Ohanjanyan, Y., Bagramyan, K., Vardanian, V., Zakharyan, E., Vassilian, A., Davtian, M. Relationship of the Escherichia coli TrkA system of potassium ion uptake with the F_0F_1-ATPase under growth conditions without anaerobic or aerobic respiration. *Biosci. Rep.* **18,** 143-54 (1998).

Vardanian, V.A., Trchunian, A.A,. Effect of temperature on H^+-K^+ exchange in Escherichia coli bacteria during their anaerobic growth. *Biofizika* **43,** 1026-9 (1998), (in Russian).

Trchunian, A.A., Vardanian, V.A., Vasilian A.V. Role of Arc-system for the control of synthesis of respiratory enzymes in regulation of K+-transporting system in glycolysing Escherichia coli. *Biofizika* **43,** 470-4 (1998), (in Russian).